ISOLATION AND CHARACTERIZATION OF ANTIBACTERIAL COMPOUNDS FROM AERIAL PARTS OF CLAVILLIA *(MIRABILIS JALAPA* LINN)

BY

MAS'UD ENEJI SADIQ

DEPARTMENT OF BIOCHEMISTRY, FACULTY OF LIFE SCIENCES,
AHMADU BELLO UNIVERSITY, ZARIA
NIGERIA

AUGUST, 2017

ISOLATION AND CHARACTERIZATION OF ANTIBACTERIAL COMPOUNDS FROM AERIAL PARTS OF CLAVILLIA *(MIRABILIS JALAPA* LINN)

By

Mas'ud Eneji SADIQ, B.Sc. (Maiduguri) 2004, M.Sc. (Zaria), 2011
PhD/SCI/4638/2011-2012

A THESIS SUBMITTED TO THE SCHOOL OF POSTGRADUATE STUDIES, AHMADU BELLO UNIVERSITY, ZARIA

IN PARTIAL FULFILLMENT OF THE REQUIREMENTS FOR THE AWARD OF DOCTOR OF PHILOSOPHY IN BIOCHEMISTRY

DEPARTMENT OF BIOCHEMISTRY, FACULTY OF LIFE SCIENCES
AHMADU BELLO UNIVERSITY, ZARIA
NIGERIA

AUGUST, 2017

DECLARATION

I hereby declare that the work in this thesis titled "**Isolation and Characterization of Antibacterial Compounds from Aerial Parts of Clavillia (*Mirabilis jalapa* Linn)**" was performed by me in the Department of Biochemistry under the supervision of Professor H. M. Inuwa, Professor K.M. Anigo and Professor D. A. Ameh. The information derived from the literature has been duly acknowledged in the text and a list of references provided. No part of this work has been presented for another degree or diploma at any institution.

Masud Eneji SADIQ _____ _____

Signature Date

CERTIFICATION

This thesis titled "**Isolation and Characterization of Antibacterial Compounds from Aerial Parts of Clavillia (*Mirabilis jalapa* Linn)**" by Mas'ud Eneji SADIQ meets the regulations governing the award of the degree of Doctor of Philosophy of Ahmadu Bello University, and is approved for its contribution to knowledge and literary presentation.

_____ Date_____
Prof. H.M Inuwa
Chairman, Supervisory Committee

_____ Date_____
Prof. K. M. Anigo
Member, Supervisory Committee

_____ Date_____
Prof. D. A. Ameh
Member, Supervisory Committee

_____ Date_____
Prof. M. N. Shuaibu
Head of Department

_____ Date_____
Prof. K. A. Bala
Dean, School of Postgraduate Studies

DEDICATION

This work is dedicated to all my teachers.

ACKNOWLEDGEMENTS

In the name of Allah, The Gracious, Ever Merciful.

I wish to use this medium to acknowledge, appreciate and say thank you to all those who made the compilation of this work a success.

Firstly my sincere gratitude goes to my supervisors Prof. H. M. Inuwa, Prof. K. M. Anigo and Prof. D. A. Ameh for their guide and support. I am indebted also to Prof. I. A. Umar for mentoring me, my wife and colleagues right from our days as graduate students. The indelible mark you've left in us shall be fondly remembered. To all staff and research students of Biochemistry Department, ABU, Zaria, I remain grateful.

I must also extend my gratitude to Prof Atta-ur-Rahman and Prof. Iqbal M. Choudhary, my host supervisors and founding fathers of International Centre for Chemical and Biological Sciences (ICCBS), University of Karachi, Karachi, Pakistan for providing me hospitable and conducive environment during my stay as a visiting research fellow in their institute. I look forward to meeting such great scientists of our time. And to Prof. Goran, Prof. Khalilu-Rahman, Dr. Adhikari, Dr. Waqqar and a host of others for their advice and guidance in my research. I must not forget to appreciate and say thank you to Third World Academy of Science (TWAS) for making this work and my dream a reality. The sponsorship offered me would remain fresh in my memories.

My profound gratitude also goes to staff of Abdullahi Fodiyo Library, Usmanu Danfodiyo University for their enviable kindness and providing me access to reference materials. I acknowledge the contributions of Simulations plus Inc. especially Dr. Michael Lawless for assisting me with softwares and technical support during the course of my research. I am grateful indeed.

Finally, I wish to extend my heartfelt gratitude to all my friends and family for the sacrifice, patience, good times and hard times. You all stood by me, encouraged me and made the whole ordeal a success. To my friends – El-Tayyib, Mujeeb-ur-Rahman, Osas, Dr. Irfan, Emmanuel, Ajapmoh, Zafar, Ali, Farah, Zaheen, Farouk, Cao, Sajjad, Gulnaz, Aliya and so many others I cannot forget - to you all I say thank you. My mum and Uncle, my wife and son, my siblings, I remain grateful for your love and prayers. Indeed it was a time well spent.

ABSTRACT

This study examined the antibacterial effects of some compounds present in the medicinal plant *Mirabilis jalapa*. Extracts of the aerial parts were obtained by soxhlet extraction using organic solvents in increasing order of polarity. Each extract was subsequently screened for bactericidal activity against clinical isolates of selected entero-pathogenic bacteria. Active fractions were subjected to several steps of chromatography techniques resulting in isolation of four compounds. The structure of each compound was elucidated using data obtained from 1D and 2D Nuclear Magnetic Resonance (NMR), Fourier Transform Infra Red (FTIR) and Ultraviolet (UV) spectroscopic techniques. Molecular masses of the compounds were also determined by Electron Impact ionization-Mass Spectrometry (EI-MS) and Electrospray Ionization-Mass Spectrometry (ESI-MS). Administration, Distribution, Metabolism and Toxic (ADMETox) properties of each isolated compound was evaluated by *in silico* methods while *in-vitro* antimicrobial assay was conducted on compounds predicted to possess drug-like properties suitable for oral route administration. The methanol extract showed Minimum Inhibitory Concentration (MIC) values of 2.5 mg/ml against *Bacillus cereus, Eschericia coli, Salmonella typhi* and *Shigella dysentariea* while 10 mg/ml was the Minimum Bactericidal Concentration (MBC) required to completely kill the organisms. Trolline (compound **1)**, isorhamnetin (compound **2)**, and tryptophan (compound **3)** were isolated from methanol extract while β-sitosterol (compound **4)** was isolated from dichloromethane extract. Compound **1** was selected for bioassay based on cumulated results on *in silico* evaluation and ADMET risk-codes generated from Admet predictor software used. Antimicrobial screening of compound **1** against selected enteropathogenic bacterial cells described showed MIC values in the range 57 µM - 114 µM while MBC values recorded were within the range 114 µM – 228 µM. The findings

of this research identified trolline, isolated for the first time from *M. jalapa* as bioactive chemical entity present in methanol extract of aerial parts of *M. jalapa*.

TABLE OF CONTENTS

LIST OF TABLES

LIST OF FIGURES

LIST OF PLATES

LIST OF APPENDICES

ABBREVIATIONS, DEFINITIONS AND SYMBOLS

TLC:	Thin Layer Chromatography
HPLC:	High Pressure Liquid Chromatography
GC:	Gas Chromatography
MS:	Mass Spectroscopy
NMR:	Nuclear Magnetic Resonance
RIA:	Radio Immunological Assay
HTS:	High Throughput Screening
NCE:	New Chemical Entities
FTIR:	Fourier Transform Infra Red
TMS:	Tetramethyl silane
DEPT:	Distortionless Enhancement of Proton Transfer
DOSY:	Diffusion Ordered Spectroscopy
COSY:	Proton-proton Homonuclear Correlation Spectroscopy
HETCOR:	Heteronuclear Correlation Spectroscopy
TOCSY:	Total Correlation Spectroscopy
HOHAHA:	**Ho**monuclear **Ha**rtmann **Ha**hn
HMQC:	Heteronuclear Multiquantum correlation
HSQC:	Heteronuclear Single quantum correlation
HMBC:	Heteronuclear Multi-Bond Coherence
ADME:	Administration, Distribution, Metabolism, Elimination
QSAR:	Quantitative Structure Activity Relationship
MIC:	Minimum Inhibitory Concentration
MBC:	Minimum Bactericidal Concnetration
ICCBS:	International Center for Chemical and Biological Sciences

***J*:** Coupling Constant

***δ*:** Chemical shift

ppm: parts per million

CHAPTER ONE

1.0 INTRODUCTION

Diseases related to the gastrointestinal tract are a major cause of morbidity or stunted growth amongst children especially in developing countries. It is estimated that more than 10 million children below the age of five years die each year worldwide with pneumonia and diarrhea as predominant causes (Petri *et al.*, 2008). Of this figure, more than half of these deaths occur in six countries including Nigeria (Black *et al*., 2003). The Child Health Epidemiology Research Group (CHERG) created by WHO in 2001 estimated that the syndrome of diarrhea accounted for 18% of deaths in children less than five years, with malnutrition as a comorbid condition in 53% of all deaths (Petri *et al.*, 2008).

Most diarrhoeal related diseases in developing countries have an infectious origin. A wide array of microbes is responsible for the cycle of bouts that may be experienced by immunocompetent and immunocompromised individuals. Commonly encountered entero-pathogenic organisms include parasites like *Ascaris lumbricoides*, *Cryptosporidium spp*., *Giardia lamblia, Entamoeba histolytica* and *Trichuris trichiura*; and bacteria like *Vibrio cholera*, *Shigella spp*., *Salmonella spp*., and Enteropathogenic *E. coli* (EPEC). Viruses like the rotavirus are also known to cause enteric disturbances. The pathophysiologic mechanism associated with these enterpathogens are diverse, however, a common symptom exhibited in most cases involve loss of body fluids causing an imbalance of body water and electrolytes (Hodges and Gill 2010).

A growing concern in recent times with respect to enteropathogenic diseases is the emergence of drug resistant microbes. The widespread use of antimicrobial agents in animal husbandry and the food chain constitute an important source of microbial resistance thus the threat of zoonotic complications become imminent. Resistance

against drugs which were previously efficacious like the cephalosporins have been reported to be related to acquired resistance among eneterobactericeae. Surveillance studies relating antimicrobial resistance and antibiotic consumption have drawn attention to the development and spread of drug resistant infectious organisms (Okeke *et al.,* 2007).The threat of exposures to these organisms poses a risk to proper growth and development in the formative years of a child thus a lasting impact may be experienced due to poor nutrient absorption, frequent diarrhea and malnutrition.

Substances that are taken for their intended pharmacologic properties either as drugs, stimulants, etc usually undergo biotransformation. The transformation of chemical substances in the body may result in metabolites that are more biologically active than the parent compound or are made less biologically active in the process of making the compound more hydrophilic for easy elimination from the body (Lin and Lu, 1997). An understanding of the metabolic fate of a compound provides insights to predicting its therapeutic outcome, toxicity effects and its suitability for use in the treatment of diseases.

Many studies have reported the therapeutic potentials of compounds present in crude plant extracts in the treatment of diseases. The primary health care needs of many rural populations, especially in the developing world, largely depend on medicinal herbs. The therapeutic potential of these herbs probably depends on several constituents of unpurified plant extracts. Interactions between these various compounds that constitute the mixture as well as the possibility of a multi-target outcome among others, are evidences put forward supporting the use of crude plant extracts (WHO, 2002; Ahmad *et al.,* 2013). Indeed certain compounds improve the absorption and subsequent bioavailability of other compounds which may or may not necessarily result in an increased therapeutic effect.

Mixtures of many constituents of medicinal plant extracts are very variable and difficult to characterize. Botanical extracts made directly from crude plant material may also show substantial variation in composition, quality, and therapeutic effects (Kunle *et al.,* 2012). It is also very tasking to maintain standardized extracts of high-quality with consistent levels of specified compounds. There are also problems associated with microbiological contamination, presence of foreign materials, such as heavy metals, pesticide residues and phytotoxins (Bent, 2008; Kunle *et al.,* 2012). Other major drawbacks in the use of crude extracts include the lack of specificity in drug target and difficulty in associating therapeutic property to particular compound(s) in the mixture (EMEA, 2005).

Individuals exposed to the frequent use of herbal mixtures run the risk of developing highly sensitized and activated cytochrome P-450 enzyme systems, a phenomenon known as enzyme induction (Zhang *et al.,* 2003; Leucuta and Vlase, 2006). These enzymes known for their broad substrate specificities transform drugs and other compounds to their more soluble forms thus are easily eliminated from the body. This may result in a shortened half life ($t_{1/2}$) of expected therapeutic response of drugs metabolized by similar routes and the possibilities of having several metabolites for a single drug compound due to the versatilities of cytochrome P-450s (Gupta and Atul, 2000) and other drug metabolizing enzymes (Qiao *et al.,* 2012). Research findings in drug metabolism have shown species-related drug toxicities resulting from differences in enzyme systems and metabolic pathways (Lin, 1995; Lin *et al.,* 1996; Mehrotra *et al.,* 2007; Berry *et al.,* 2011). Similarly, evidences from pharmacogenetics and pharmacogenomics (Kim *et al.,* 2008; Holstein *et al.,* 2012; Kadiyala and Tan, 2013) show that humans have the tendency to react differently to the same drug component. It is important therefore, to know the composition and possibly the structures of the

constituents of drugs and other formulations. This would guarantee relevant criteria for uniformity and safety of chemical substances relevant to healthcare delivery (EMEA, 2005).

Modern equipment and techniques have encouraged rapid advancements in natural products research development. Various *in-vitro* methods have been developed for elucidating pathways, enzymes involved and major metabolites (Zhang *et al.*, 2003) in drug development strategies (Brandon *et al.*, 2003; Brennan, 2012; Holstein *et al.*, 2012; Kim *et al.*, 2012). Available *in-vitro* metabolism technologies that utilize microsomes, liver slices (Brandon *et al.*, 2003), tissue banks, CYP enzyme expression systems, and recently, the use of computer softwares in silico simulations and predictions among others have allowed for high throughput metabolism assessments, reduced cost and time expended and complete avoidance or reduction in number of animal models normally required in traditional *in-vivo* methods (Brunner and Langer, 2006). For example, precision-cut liver slices have been shown to reflect a complete *in-vitro* metabolite profile of a compound since this system retains the physiological conditions of enzymes and co-factors of both phase I and phase II reactions, therefore simulates the *in-vivo* situation (van de Kerkhof *et al.*, 2006). However, *in-vitro* and *in-silico* bioassays generally serve as a link or a means to predict the outcomes of, or reject completely, a given drug candidate before being subjected to *in-vivo* studies (Jacob and Ahmad, 2003; Eikel *et al.*, 2011; Solon, 2012). Thus a balanced *in-vitro/in-vivo* approach coupled with high sensitive quantitation techniques (Krajcsi *et al.*, 2012) contribute significantly in the quality and reliability of data obtained within a given time frame on the fate of bioactive compounds in biological systems.

1.1 STATEMENT OF RESEARCH PROBLEM

Many plants indigenous to the West African sub region have been studied and shown to have various therapeutic properties. A significant proportion of these researches unfortunately terminate at the level of whole crude plant extracts. A major limiting factor is poor access to standard research environment or underfunded projects. Medicinal plants with promising economic importance as a result become underutilized thus poorly harnessed in meeting the health care needs of the populace. Elswhere like China, India and other Asian countries, progress have been recorded in the development of local traditional medicinal practice refined to promote safe, acceptable and marketable products.

Child mortality resulting from preventable diseases in developing nations like Nigeria is a major source of concern. An estimated 1.87 million deaths from diarrhoea of children aged less than 5 years was observed globally. WHO African and South-East Asia Regions combined accounted for 78% (1.46 million) of all diarrhoea deaths occurring among children in the developing world while 73% of these deaths are concentrated in just 15 developing countries including Nigeria (Boschi-Pinto *et al.,* 2008). Poverty, lack of access to quality health facilities and good portable drinking water further worsens the situation in a region where climatic factors favours growth and proliferation of pathogens. Treatment of recurrent cases of infections and exposure of infectious organisms to antimicrobial agents has led to emergence of organisms resistant to cheap available drugs. The need to search for new lead compounds to augment or totally replace drugs that are losing their potency and effectiveness as a result of emergence of evidences linking such to severe adverse effects or microbial resistance becomes imperative.

1.2 JUSTIFICATION OF THE STUDY

A reservoir of knowledge on medicinal plants exists in many African societies. The plant *Mirabilis jalapa* selected for this study is based on its trado-medicinal uses (Singh *et al.,* 2010) and antimicrobial activities especially those relating to enteric infections (Oladunmoye, 2007; Muthumani *et al.,* 2010; Nath *et al.,* 2010; Eneji *et al.,* 2011, Shaik *et al.,* 2012).

1.3 AIM OF THE RESEARCH

The aim of this research is to isolate and characterize compounds from aerial parts of *M. jalapa* against some enterobacteria.

1.4 OBJECTIVES

The objectives of this research are as follows:

1. Anti-bacterial screening of extracts of aerial parts of *M. jalapa*
2. Isolation of pure compounds from selected extracts with potential activity.
3. Characterization and structural elucidation of isolated compounds
4. *in-silico* physico-chemical evaluation of isolated compounds
5. Antibacterial screening of characterized compounds

CHAPTER TWO

2.0 LITERATURE REVIEW

2.1 Natural Products and Drug Discovery

Natural products are chemical compounds or substances produced by living organisms possessing bioactive properties that are pharmacologically useful in drug discovery (Lahlou, 2013). Medicinal plants over the years have been recognized as major sources of natural products especially in the treatment of various diseases. The attractiveness of natural products as varied source of lead compounds with drug-like properties has historical roots. For example, about 60% of cancer drugs and 75% of infectious disease drugs are derived from natural products (Boldi, 2004). The stereochemical architecture, chirality and unique carbon skeletons of natural products traverse a large expanse of diversity yet to be explored. Thus screening natural products have so far been a successful strategy for the discovery of medicines.

The decline in the interest on natural products in the past 20 years has not led to a significant improvement in the discovery of new drug components by synthetic means which gained in popularity within this period (Harvey, 2008). From an economic perspective, natural products constitute the best selling non-protein drugs. The combined proceeds from sales of natural products derived drugs – sinvastatin, lovastatin, enalapril, pravastatin, atorvastatin, augmentin, ciprofloxacin, clarithromycin and cyclosporine – amount to over $16 billion (Harvey, 2000; Bendseil *et al.*, 2001). More recent natural product based developed drugs include the anti malarial drug artemisinin and the anticancer drugs taxol, docitaxel and camptothecin.

Advancements in chromatography purification and spectroscopy techniques (NMR, MS FTIR) and the more recent computer in silico techniques have led to a more efficient

approach in natural products isolation and characterization, eliminating much of the technical difficulties in traditional isolation and screening methods.

2.2 *Mirabilis Jalapa* Plant

Taxonomy

Kingdom:	Plantae
Sub kingdom:	Tracheobionta
Division:	Angiosperms
Class:	Dicotyledons
Sub class:	Caryophylidae
Order:	Caryophyllales
Family:	Nyctaginaceae
Genus:	Mirabilis
Species:	M. jalapa L

The plant *M. jalapa* belongs to the *Nyctaginaceae* family. It is a perennial herbaceous plant that grows to a height of 50cm to 100cm (Lim, 2014). It has an extensive network of branches with pointed leaves stemming from a tuberous root. The yellow, pink or purple coloured flowers are funneled shaped while the seeds are usually spherical, wrinkled and appear black upon maturity (Eneji *et. al.,* 2011). Phytochemical constituents of the roots, leaves, stem and seeds reveal the plant to contain alkaloids, flavonoids, phenols, steroids, triterpenes, glycosides, amino acids, tannins and saponins. Quite a number of these phytoconstituents have been demonstrated to possess pharmacologic effects useful in diseases like diabetes, oxidative stress, bacterial infection and inflammation (Nath *et al.,* 2010). As a major constituent of Chinese medicine, some Chinese products include extractive of this plant as part of product formulation for example, the Chinese medicine for treating oesophageal cancer (Tao *et al.,* 2010). The plant has been shown to be effective in phytoremediation by promoting

degradation of total petroleum hydrocarbons (TPH) at a tolerance level of ≤10,000mg/Kg (Peng *et al.*, 2009).

Plate 2.1: *Mirabilis jalapa* plant

2.2.1 Antibacterial Properties of *Mirabilis jalapa*

Extractives of various plant parts of the plant *Mirabilis jalapa* have been in folk medicine across different cultures of the world especially in treatment of diseases that are of bacterial origin (Holdsworth, 1992; Comeford, 1996; Encanacion *et al.*, 1998). Several reports have identified the bactericidal effects of organic solvent extracts of aerial parts (leaves, flowers, seeds stem) and roots of the plant. Meera *et al.*, (2012) reported a broad spectrum antibacterial activity of several organic solvent extracts of the leaves of the plant. Disc diffusion and micro dilution assay methods were used to demonstrate inhibitory and bactericidal effects on selected gram positive (*S. aureus, S. epidermis* and *B. subtilis*) and gram negative (*E. coli, P auringanosa* and *K. pneumonia*)

bacteria. Their findings identified methanol extract to be most effective as an antibacterial. Similar works on aerial parts of the plant reported by Zachariah *et al.,* (2012) identified the methanol extract to be most effective against tested microorganisms *S. aureus, Psuedomonas spp., Bacillus spp.* at MIC values of 1.0mg/ml. They also demonstrated antioxidant activity of the methanol plant extract. Other polar organic solvents used for extraction of the plant parts have been reported. The ethanol extract (70%) was shown to have bactericidal effects against the tested organisms *S. aureus, B. cereus, K. pneumonia* and *E. coli* as well as antioxidant properties (Oladunmoye, 2012). Eneji *et al.,* (2011) in their findings reported ethanol extracts to have bactericidal effects on *S. typhi* and *B. cereus* at MBC of 2mg/ml. The organisms screened using various extracts cut across different species known to cause different diseases ranging from enteric (e.g. *S. typhi, E. coli*) to opportunistic skin infections commonly caused by *S. aureus*. Importantly, claims on the effectiveness of the plant as a treatment for dysentery and diarrhea would best be assessed by screening organisms that are associated with food borne and gastro intestinal tract diseases.

2.2.2 Anti Inflammatory Properties of *Mirabilis jalapa*

Extracts of *Mirabilis jalapa* were experimentally demonstrated by Nath *et al.,* (2010) to have anti inflammatory effects. Carrageenan induced rat paw oedema and cotton pellet granuloma models were used to evaluate the acute and chronic anti inflammatory effects of alcoholic and pet ether extracts of the leaves of the plant. Another study by Singh *et al.,* (2010) suggested the efficacy of the aqueous extract of the plant as having anti inflammatory properties. Carrageenan and formalin induced rat paw oedema were also used to evaluate anti inflammatory properties of the extracts. Such methods as reported normally exhibit their inflammatory response via COX-2 mediated increase in prostaglandin production thus contributing to severity of inflammation and pain (Guay

et al., 2004). These methods however, may be limited in application in relation to inflammatory response triggered by bacterial infection especially those related to diarrhoeal diseases. Central to inflammation mechanisms in diarrhoeal infectious diseases is production of cytokines resulting in stimulation of intestinal mucosa to induce inflammatory reaction involving release of proinflammatory agents like IL-6, IL-8 TNF-α (Navaneethan and Giannella, 2008; Hodges and Gill, 2010). Increased production of proinflammatory agents may result in increase in reactive oxygen species. It is however not clear whether the observed anti inflammatory effects of the extracts is by way of enzyme inhibition or as a free radical scavenger.

2.2.3 Isolated Phytochemicals from *Mirabilis jalapa*

Several literatures have reported the isolation of bioactive compounds from *M. jalapa*. Briefly discussed below are some characterized bioactive phytochemcials from the plant.

2.2.3.1 *Trigonelline*

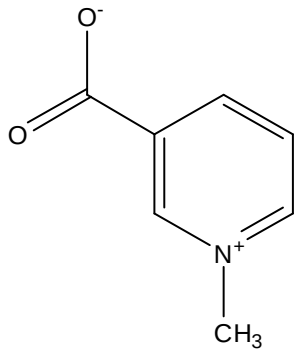

Trigonelline is a major constituent of *Mirabilis jalapa* roots. This compound has been shown to have anti-diabetic properties as reported in the findings of Zhou *et al.,* (2012). They reported trigonelline, has hypoglycemic effects in rats and humans alike. They were able to show the beneficial effects of the compound as a diabetic in decrease in

blood glucose and lipid levels as well as up regulating anti-oxidant enzyme activity (Zhou *et al*., 2013). They also demonstrated the increased serum endogenous glucagon-like peptide-1 (GLP-1) levels and GLP-1R (in rodents) expression which may be attributed to the effects of trigonelline on diabetic peripheral neuropathy (DPN) regulation of GLP-1R/p38 mitogen-activated protein kinases (MAPK) signaling pathways (Zhou *et al.*, 2012).

2.2.3.2 *Cytotoxic Rotenoids*

The ethanolic extract of *Mirabilis jalapa* roots subjected to several chromatographic steps (silica gel 200-300 mesh size, sephadex LH-20) led to the isolation of rotenoid type compounds boeravinone B (1) boeravinone E (2), 9-O-methyl-1-4-hydroxyboeravinone B (3) and mirabijalone B (4) (Xu *et al.*, 2010). Compounds 1-4 basically have same flavonoid skeleton but with differences in side chain substituent.

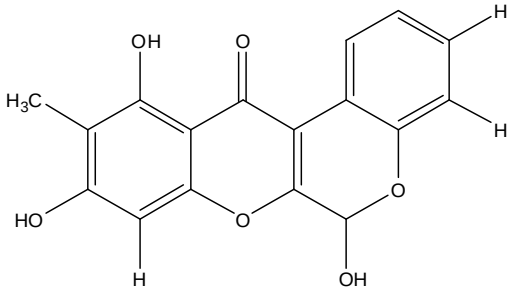

Boeravinone B (1)

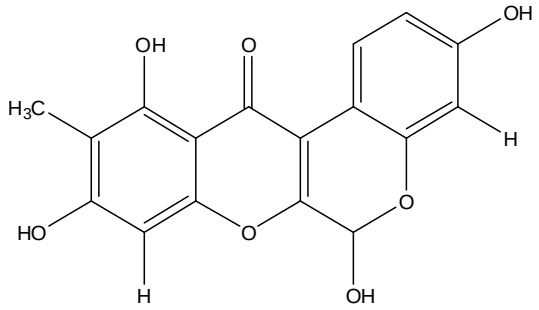

Boeravinone E (2)

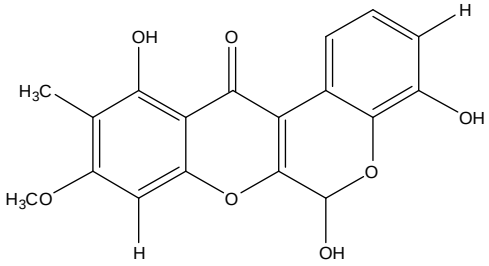

9-O-methyl-1-4-hydroxyboeravinone B (3)

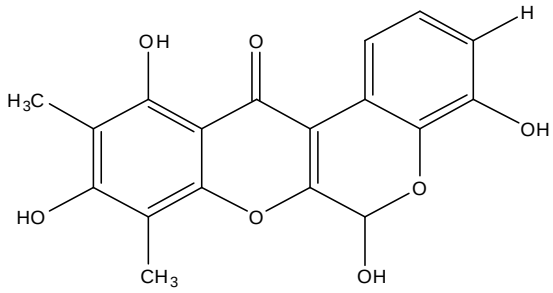

Mirabijalone B (4)

Compounds 3 and 4 were previously isolated and reported in a different study (Yang *et al.,* 2001; Wang *et al.,* 2002) while compounds 1 and 2 were isolated by the authors for the first time from this plant. The microculture tetrazolium (MTT) assay for these compounds 1-4 displayed cytotoxicity against human leukemia cell lines (K562 and HL-60), human lung adenocarcinoma (A549), human hepatoma (BEL-7402) and human stomach cancer (SGC-7901) cell lines.

2.2.3.3 *5, 7-Dihidroxy-2'-methoxy-6-methylisoflavone*

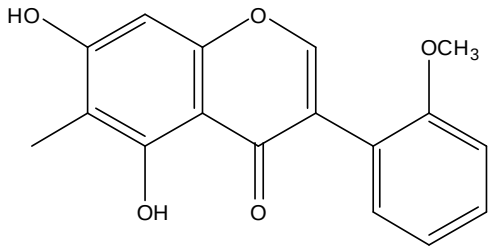

This compound was isolated from a manipulated cell culture of *Mirabiis jalapa* and from roots of *Boerheavia diffusa* both belonging to the *Nyctaginaceae* family. The compound is an amorphous solid with monoisotopic mass of 298.084125. The compound was demonstrated to exhibit muscle relaxing spasmolytic effects (Borelli *et al.,* 2006).

2.2.3.4 *Mirabijalone A*

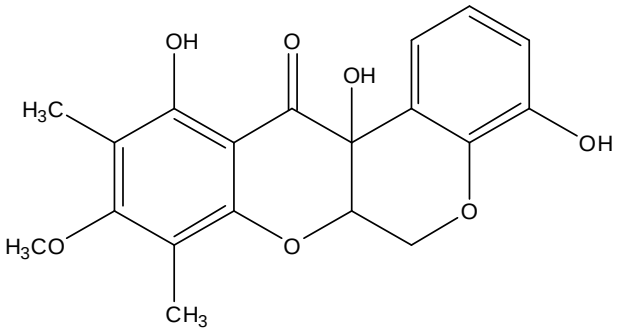

This compound has a yellow like appearance isolated from the roots of *Mirabilis jalapa* (Yi-Fen *et al.,* 2002). The molecular weight is 358.347 with optical rotation [α] 16D of -203.9 (in methanol). It has the basic rotenoid structure with presence of a methoxy group.

2.2.3.5 *N-trans-feruloyl-4-O-methyldopamine*

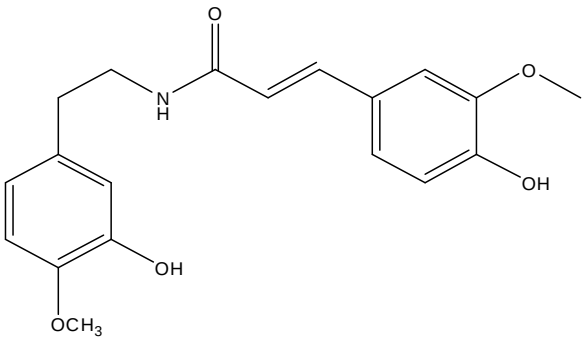

This alkaloid compound was isolated from *Achyranthes ferruginea*, *Mirabilis jalapa* and *Chenopodium album*. The molecular weight is 343.379 with C, H, N and O composition of 66.46%, 6.16% 4.08% and 23.30% respectively. Physically, this compound appears oily and has been shown biologically to have bacterial efflux pump emitter properties (Pedersen *et al.,* 2010).

2.2.3.6 *Mirabilis Antimicrobial Peptides (Mj-AMP)*

Mj-AMP I and II were purified from the seeds of *Mirabilis jalapa* (Cammue *et al.,* 1992). The authors observed Mj-AMPs sequence was unique from all other known plant proteins but showed homology to μ-agatoxins, a neurotoxic peptide isolated from spider venom. The nitrocellulose blots of SDS-PAGE electrophoresis of Mj-AMP I and II suggested molecular masses of 8000Da and 7000Da respectively and a pI value of about 10.5. The cysteine residues in the peptides were involved in disulphide bridges. The peptides were also shown to be non-glycosylated, stable at pH2-11 and not affected by

heat treatment of up to 100^{o}C for 10 minutes. Bioactivity screening of both peptides revealed 50% (IC_{50}) of fungal growth inhibition after 48hours incubation varied from 6 to 300µg/ml for Mj-AMPI and 0.5 to 20 µg/ml for Mj-AMPII. The Mj-AMPs were also demonstrated to inhibit gram positive bacteria *B. megaterium* and *S. lutea* but had no effect on gram-negative *E. coli* and *E. carotovora*. The proteins also did not show any effect on cultured human umbilical vein endothelia cells or human skin muscle fibroblasts even at concentrations of 500 µg/ml. The sequence data shows both peptides to be highly homologous however, their antifungal activity differ markedly.

2.2.3.7 *Trypsin Inhibitors*

Two trypsin inhibitors mirabilis jalapa trypsin inhibitors (MJTI I and II) were isolated by Kowalska and co-workers (2007) from 1Kg *Mirabilis jalapa* seed material. Several chromatographic steps including affinity, ion-exchange as well as preparative gel electrophoresis and reverse phase HPLC on C-18 column were used in obtaining about 20mg of the purified proteins. The authors reported that the isolated inhibitors showed no sequence relationship with any other inhibitor but were homologous to the antimicrobial Mj-AMP peptides isolated from the same plant. Cold ethanol (96%) was used to precipitate the acidic extract (pH4) of *M. jalapa* seeds, followed by affinity chromatography on immobilized catalytically inactive methyl chymotrypsin in presence of 5M NaCl.

2.2.3.8 *Ribosome Inactivating Protein (RIP)-Like Protein*

RIPs are a group of plant enzymes with N-glycosidase activity capable of inactivating ribosomes by modifying 28S rRNA. Also, the ability of the RIPs to cleave supercoiled DNA when incubated together is indicative of its RIP activity. A 30kDa protein with RIP-like properties designated Mj-30 was isolated by Ikawatip (2006). The peptide was

isolated by cationic exchange chromatography on CM sepharose CL-6B column. Mj-30 was shown to have cytotoxic activity against T47D and siHa cell lines but was less toxic (in comparison) to human mononuclear cells.

2.3 In Silico ADME Predictions

In-silico predictions on administration, distribution, metabolism and elimination (ADME) of drugs in modern day research have helped to limit time and reduce cost of searching for NCEs with drug-like potentials (Butina, *et. al.,* 2002; Kapetanovic, 2008). There are different approaches in in-silico modeling of ADME properties. The methods are either data-based such as QSAR, similarity searches, 3D QSAR, structure based methods such as ligand-protein docking and pharmacophore modeling (Yamashita and Hashida, 2004).

Models for in-silico prediction of ADME properties based on the quantitative structure activity relationship (QSAR) approach can be applied to a large number of molecules. The large database of molecular descriptors used in the training of models relies on high quality experimental data relating to the activity which is being predicted. The outcomes of in-silico predictions have been demonstrated to compare favourably with in vitro experimental methods in understanding the pharmacokinetics and dynamics of compounds (Boobis *et al.,* 2002). There are different approaches used in the design of models to predict molecular properties at different pharmacokinetic stages i.e. absorption, distribution, metabolism, excretion and toxicity (ADMET). Examples of such approaches used in model designing include:

- Pattern recognition
- Statistical regression
- Classification
- Artificial neural networks (ANN)

- Genetic algorithms
- Kernel partial Least squares (KPLS)
- Molecular and quantum mechanics
- Support vector machines, etc (Butina *et al.,* 2002).

The Moriguchi model for example is a regression model that describes molecular hydrophobicity (MlogP) based on octanol-water partitioning (Moriguchi *et al.,* 1992). The model was built on a training set of 1230 compounds with a correlation of 0.952. The partial least square (PLS) regression approach published by Crivori *et al.,* (2000) correctly predicted more than 90% of blood-brain-barrier (BBB) data on permeability. Commercially available computer softwares that integrate several of these prediction models include Simulations plus Inc. Lancaster, (USA,) Accelrys Cambridge (UK), Lhasa Ltd Leeds (UK), Comgenex, Budapest (Hungary), etc (Boobis *et al.,* 2002; Butina *et al.,* 2002). The solubility model created by Simulations plus Inc was based on ensembles of artificial neural networks constructed using the ADMET modeler software, with a data set consisting of 3,596 organic compounds (Admet predictor Manual, 2015). Quite a number of software vendors provide the platform for creating compound libraries. Such approach help identify early in time compounds that may satisfy ADMET requirements in drug discovery (Van De Waterbeemd and Gifford, 2003).

The use of computer models in this study serves to provide pharmacokinetic data to complement expectations of compounds as possible lead candidates that may be present in extracts of the plant with potential bioactive properties. It must however be noted that there is no substitute for the actual clinical trials of compounds for their intended use. The dynamics of drug interaction with biological system of diverse complexity can only be well understood when all factors that influence the final outcome are put under thorough investigation. Development or modification of experimental protocols by

combination of techniques in recent times only goes further to revolutionize natural products/medicinal chemistry research in the quest for better health care delivery.

CHAPTER THREE

3.0 MATERIALS AND METHOD

3.1 Materials

3.1.1 Solvents, Chromatography and Bioassay Materials

Solvents used for experimentation included methanol (MeOH), dichloromethane (DCM), ethylacetate (EtAc), hexane (Hex), acetone, butanol (But), and double distilled water (ddH_2O). High Performance Liquid Chromatography (HPLC) grade solvents (Sigma Aldrich, Germany) were used for HPLC purification steps. Chromatography materials included precoated alkylamine (normal phase) and R-18 (reverse phase) TLC plates, silica gel (60-120, 120-230 mesh size), sephadex LH-20 and MCI gels (Sigma Aldrich, USA).

Materials used for antibacterial studies included petri-dishes, micropipette (Ependorff 1-5 µL; 10-100 µL), nutrient agar (Sigma Aldrich, USA). Standard antibiotic drugs used included sparfloxacin, erythromycin and ciprofloxacin supplied by Department of Microbiology, Faculty of Science, Usmanu Danfodiyo University, Sokoto.

3.1.2 Equipment

The following were some equipment used which included Avance AV-600 Cryoporbe, AvanceAV-500 NMR, Electron Ionization Mass spectrometer (EI model no. MAT312 centroid type display), QSTAR Elite ESI-ToF mass spectrometer, Fourier Transform Infra Red (FTIR FTS-65, Biorad), ultraviolet (UV) spectrophotometer (Shimadzu UV-240; Hitachi U3200), Recycling Preparatory HPLC (Reverse phase ODS-H-80, ODS M-80 columns; normal phase ODS-SIL D-60-10 column, Japan Analytical Industries).

3.2 Methodology

3.2.1 Collection, Identification and Processing of Plant Material

The plant material was collected during the rainy season (October 2014) from Rigasa, Igabi Local Government Area of Kaduna State. The plant was identified at the Herbarium unit of the Biological Science Department, Ahmadu Bello University, Zaria with the voucher number 2441deposited. The aerial parts (including leaves, flowers and stems) were carefully collected and air dried under shade. The dried plant material was pulverized, weighed and stored under cool and dry conditions until needed.

3.2.2 Extraction of Plant Material

The pulverized plant material (950 g) was extracted using soxhlet apparatus. Organic solvents were used in increasing order of polarity starting with hexane, dichloromethane and methanol. All extracts were concentrated and weighed. The methanol extract was re-extracted with butanol saturated with water, concentrated and re-dissolved in methanol.

3.2.3 Screening of Extracts for Antibacterial Activity

Standard methods as described by European Committee on Antimicrobial Susceptibility Testing (EUCAST, 2000; 2003) were adopted for all microbiological investigations in this study. Clinical isolates of selected enterobacteria obtained from the Department of Medical Microbiology, Ahmadu Bello University Teaching Hospital, Zaria were screened for susceptibility to the various extracts. The test bacteria used for this screening included *Streptococcus feacalis, Shigella dysenteriae, Salmonella typhi, Salmonella paratyphi, Bacillus cereus, Eschericia coli and Vibrio cholera.*

3.2.3.1 *Preparation of Nutrient Agar*

To exactly 23 g nutrient agar in a conical flask, 1000 ml of distilled water was added. The conical flask was then heated with continuous agitation. This was allowed to boil for 1 minute to ensure complete dissolution of the agar powder and subsequently autoclaved at 121 ºC for 20 minutes. The dissolved sterilized agar was allowed to cool to 45 ºC. This was finally poured into petri dishes and allowed to solidify under sterile conditions.

3.2.3.2 *Nutrient Broth Preparation*

To 1000 ml of distilled water in a conical flask, 25 g of nutrient broth was added and then thoroughly mixed. The mixture was sterilized by autoclaving at 121 ºC for 20 minutes.

3.2.3.3 *Well Diffusion Susceptibility Test*

For each sample, 0.2 g was weighed and dissolved in 10 ml Dimethylsulhoxide (DMSO) to obtain stock concentration of 20 mg/ml. Sterilized media in petri-dishes were then seeded with test bacterial cells. Inoculums were spread by streaking using sterile swab. Seeded plates were allowed to dry after which a cork borer of 5 mm in diameter was used to make wells. Dissolved samples were introduced into the wells of appropriately labeled plates. The plates were then incubated at 37ºC for 24 hours after which the plates were examined for zones of growth inhibition. The diameter of widest points was measured in millimeters using a caliper. Similar preparations were made for positive control (ciprofloxacin, erythromycin and sparfloxacin 20 mg/ml) and negative control containing only solvent of extraction added in the wells (EUCAST, 2000; 2003).

3.2.3.4 *Minimum Inhibitory Concentration (MIC) Determination*

The MICs of the samples were determined using the broth dilution method. Exactly 1.0 ml of prepared nutrient broth was dispensed into 5ml test tubes (pyrex glass) and autoclaved at 121 ºC for 15 minutes. Turbid solutions for each bacterial cell were prepared by dissolving in 0.8 % normal saline. Serial dilutions were made and compared to Mc-Farland's turbidity standard scale of 0.5 with cell concentration of $1.5x10^8$ cfu/ml. Serial dilutions of 10 mg/ml, 5 mg/ml, 2.5 mg/ml and 1.25 mg/ml was done also for each extract from a stock of 20 mg/ml. Cell suspensions were then transferred into the test tubes and incubated at 37 ^oC for 24 hours after which the tubes were inspected for turbidity. Test tube with lowest concentration of sample with turbidity closest to standard represents the MIC for that concentration (EUCAST, 2000; 2003).

3.2.3.5 *Minimum bactericidal concentration (MBC) determination*

The MBC of each sample was determined by using sterilized agar-containing petridishes. The contents of the MIC test tubes were sub-cultured onto the agar plates by dipping a sterile wire loop into each test tube and streaking on the surface of the agar plates. The plates were then incubated at 37 ºC for 24 hours and observed for bacterial growth. The MBC was the plate with lowest sample concentration without any observed growth (EUCAST, 2000; 2003).

3.2.4 Solvent – Solvent Partitioning of DCM and Methanol Crude Extracts

3.2.4.1 *Column Chromatography*

Pyrex glass columns 90 cm by 15 cm, 50 cm by 9 cm and 30 cm by 3 cm columns were variously packed with silica gel (60-120 mesh size). Flash column set up was run using silica gel of mesh size 230-400. Wet packing was done using hexane for all columns.

Crude dichloromethane and methanol extracts were immobilized on silica using solvent of extraction, stirred until a uniformly fine and loose particles were obtained.

Progress of elution was monitored using normal phase silica coated aluminium TLC plates (for non-polar to moderately polar fractions) and reverse phase R-18 ODS glass coated plates (for polar fractions). Developed TLC plates were visualized by spraying with cerric sulphate then heated using a hand held heating gun.

Solvent Partitioning and Column Chromatography of Methanol Extract

The methanol extract (29 g) was first partitioned in a separating funnel with butanol saturated with water. The mixture was allowed to partition and the lower aqueous phase was decanted out to remove extremely polar components. The butanol phase was concentrated using a vacuum rotavapour and subsequently freeze-dried to recover 9g of dry fraction.

The butanol fraction was then introduced into column packed with silica (mesh size 60-120) in the sample : silica ratio of 1 g : 30 g. The column was initially stabilized using hexane. Polarity of the column was gradually increased by eluting with isocratic mixture of 10% methanol : 90% dichloromethane. Fractions F50 to F80 collected using this solvent system were pooled together based on their TLC profiles. Fractions F85 to F98 were eluted using 20 % methanol: 80 % dichloromethane, which were also pooled together.

Fractions F50-80 were subjected to flash column (silica mesh size 230-400) and eluted with 40% acetone : 60% hexane. Fractions F33 to F45 obtained were pooled together and subsequently run on MCI gel column eluted with 60% water : 40% methanol. Fraction F23 was collected while fraction F39 from the same column was eluted using 25% water: 75% methanol.

The fractions F85-98 eluted with 20% methanol : 80% dicholoromethane were also subjected to further chromatography purification steps. Gel filtration using sephadex LH20 was carried out and the column eluted with 40% dichloromethane : 60% methanol to obtain F7.

Column Chromatography of DCM extract

Exactly 46 g of the DCM extract was introduced into the column and stabilized initially with hexane. Isocratic preparation constituting hexane and DCM in the ratio 4:1 respectively was used to elute the column after which polarity of this system was increased to 60% hexane : 40% DCM. Fractions F28-32 obtained were pooled together on the basis of TLC profiles.

Further purification steps on pooled fractions F28-32 involved the use of sephadex LH20 for size exclusion chromatography (gel chromatography). The mobile phase was 50% DCM and 50% MeOH.

3.2.4.2 ***High Performance Liquid Chromatography (HPLC)***

A recycling HPLC instrument (Reverse phase ODS-H-80, ODS M-80 columns; normal phase ODS-SIL D-60-10 column, Japan Analytical Industries) was used to further purify fractions described earlier for the dichloromethane and methanol extracts. Fractions F23 and F29 obtained from acetone : hexane eluted flash column were run separately on HPLC (Reverse phase ODS-H-80 column). The solvent system used for F23 was 60% water : 40% methanol. This was initially sonicated to remove air bubbles and ensure uniform mixture of the solvents. The flow rate was 3 ml/min and 3 mls of 1.5 mg/ml concentration of sample was injected into the machine after base line stabilization of the recorder and refractive index (RI) and UV detectors were set to zero. The retention time observed for the compound **1** (10 mg) obtained was 8 minutes.

Similarly, F29 was eluted using 25% water : 75% methanol and a retention time of 23 minutes was recorded for the compound **2** (7 mg). Reverse phase chromatography (Reverse phase ODS M-80 column) was also carried out on F7 recovered from sephadex LH20 column separation for the fraction F85-98. The flow rate was set at 2.5 ml/minute and sample injection was 1ml of 3 mg/ml. Retention time observed was 20 minutes for the compound **3** (12 mg).

Fraction F28-32 obtained from gel filtration column of the dichloromethane extract (starting material) was subjected to HPLC purification using normal phase ODS-SIL D-60-10 column. The isocratic solvent system used was 30% ethylacetate : 70% hexane. The flow rate was set at 3 ml/min and sample injection volume was 3ml at concentration 5mg/ml. Retention time of 12 minutes was recorded for the compound **4** (9 mg).

Structures of the isolated compounds **1-4** were elucidated by conducting different spectroscopic techniques – NMR, MS, FTIR and UV-Vis.

3.2.5 In Silico Predictions on Physico-Chemical, Metabolic and Toxic Properties of Isolated Compounds

The physico-chemical, metabolic and toxic properties of proposed chemical structures of compounds isolated were predicted using the Admet predictor software, a licensed property of Simulations plus Inc, Lancaster, USA. The programme was used according to license provider guidelines. Simplified Molecular Input Line Entry System (SMILES) notation (Figure 3.1) was generated for each compound which was used to create the input file system for the software. Predictions were calculated using generated two dimensional (2D) structures of the compounds. Risk codes were also generated to assess the drug-like properties for each compound. Compounds with known properties

in literature were also included as test sets to compare prediction output with existing data.

Table 3.1: Input file system for 2D structure generation of compounds

Default S+Peff permeability [cm/s x 10^4] model	
Default Meylan solubility [mg/mL] model	
pH for ionization descriptors = 7.4	
pH for pH-sensitive models = 7.4	
Generic	SMILES
Cimetidine	CNC(NCCSCc1nc[nH]c1C)=NC#N
Ethanol	OCC
Warfarin	c1ccc2C(O)=C(C(c3ccccc3)CC(=O)C)C(=O)Oc2c1
F4 (1)	Oc1cc2C3CCC(=O)N3CCc2cc1O
F5 (2)	Oc1ccc(cc1OC)C=3Oc4cc(O)cc(O)c4C(=O)C=3OC2OC(CO)C(O)C(O)C2O
F7 (3)	O=C(O)C(N)Cc2cnc1ccccc12
F2 (4)	CC(C)C(CC)CCC(C)C1CCC2C3CC=C4CC(O)CCC4(C)C3CCC12C
Ibuprofan	CC(C)CC1=CC=C(C=C1)C(C)C(=O)O

3.2.6 Antimicrobial Susceptibility Test for Isolated Compounds

For pure compounds tested, 1.0 mg of the compound was weighed and dissolved in 10 mls of dimethyl sulphoxide (DMSO) to obtain 100 µg/ml concentration which served as the stock. Serial dilutions of the stock was done to obtain concentrations of 50 µg/ml, 25 µg/ml, 12.5 µg/ml and 6.25 µg/ml. Exactly 0.1ml of prepared solutions were added to wells, 6 mm in diameter in sterilized Mueller Hinton growth medium seeded with microbes previously described. This was incubated at 37 ºC for 24 hours and zones of inhibition were measured in millimetres using a caliper.

3.2.7 Determination of MIC of Isolated Compounds

Dilution of organisms in nutrient broth media described earlier was carried out until, by visual inspection compares favourably to Mc-Farlands turbidity standard scale number 0.5 and at this point the microbial concentration was 1.5 x 10^8 cfu/ml. To each of the

prepared concentration, 0.1 ml of organism was introduced and subsequently incubated at 37 ºC for 24 hours. Concentration of the compound with no turbidity was recorded as the minimum inhibitory concentration (MIC).

3.2.8 Determination of MBC of Isolated Compounds

This assay was carried out to assess bactericidal property of the test compound(s). The contents of each tube from the MIC experiment was sub-cultured on prepared sterile agar and incubated for 24 hours at 37 ºC. Culture plates with lowest concentration of test compound where no growth was observed was recorded as the minimum bactericidal concentration (MBC).

Methods applied for the screening of isolated compounds were as described earlier for the crude extracts.

3.3 Statistics

Results of zones of inhibition of antimicrobial assays were presented as mean ± standard deviations of triplicate determinations while MIC and MBC results were presented as charts and in tabular forms. In silico predictions were also presented as charts and in tabular forms.

CHAPTER FOUR

4.0 RESULTS

4.1 Effect of Plant Extracts on Test Organisms

The Percentage yield of each extract recovered from the plant material was calculated as follows: hexane extract, 3.37%, DCM extract, 4.84% and methanol extract 3.05%. Figure 4.1 presents results on the zones of inhibition of extract against selected enteropathogenic bacteria. The methanol extract had highest zones of inhibition against susceptible organisms when compared to other extracts. *S. dysenteriae* was observed to be the most susceptible organism for all extracts tested (32mm). *S. feacalis* and *V. cholera* were both resistant to all extracts at 20mg/ml. The control drug ciprofloxacin was most active at 5mg/ml concentration but showed no inhibitory effects on *S. feacalis*. Similarly, *S. typhi, S. paratyphi* and *V. cholera* were observed to be resistant to erythromycin while sparfloxacin inhibited growth of all organisms tested.

4.2 Minimum Inhibitory and Minimum Bactericidal Concentrations for Test Organisms

The MIC values in Table 4.1 showed the organisms *B. cereus, E. coli S. typhi* and *S. dysenteriae* were susceptible to the methanol extract at MIC of 2.5 mg/ml. The least active extract was hexane where 10 mg/ml was required to inhibit growth of *B. cereus, E. coli* and *S. typhi*.

The minimum bactericidal concentration (MBC) as shown in Table 4.2 was 10 mg/ml as observed for the methanol extract. The methanol extract also appeared to be most active against *S. dysenteriae* where no bacterial growth was observed at 5 mg/ml.

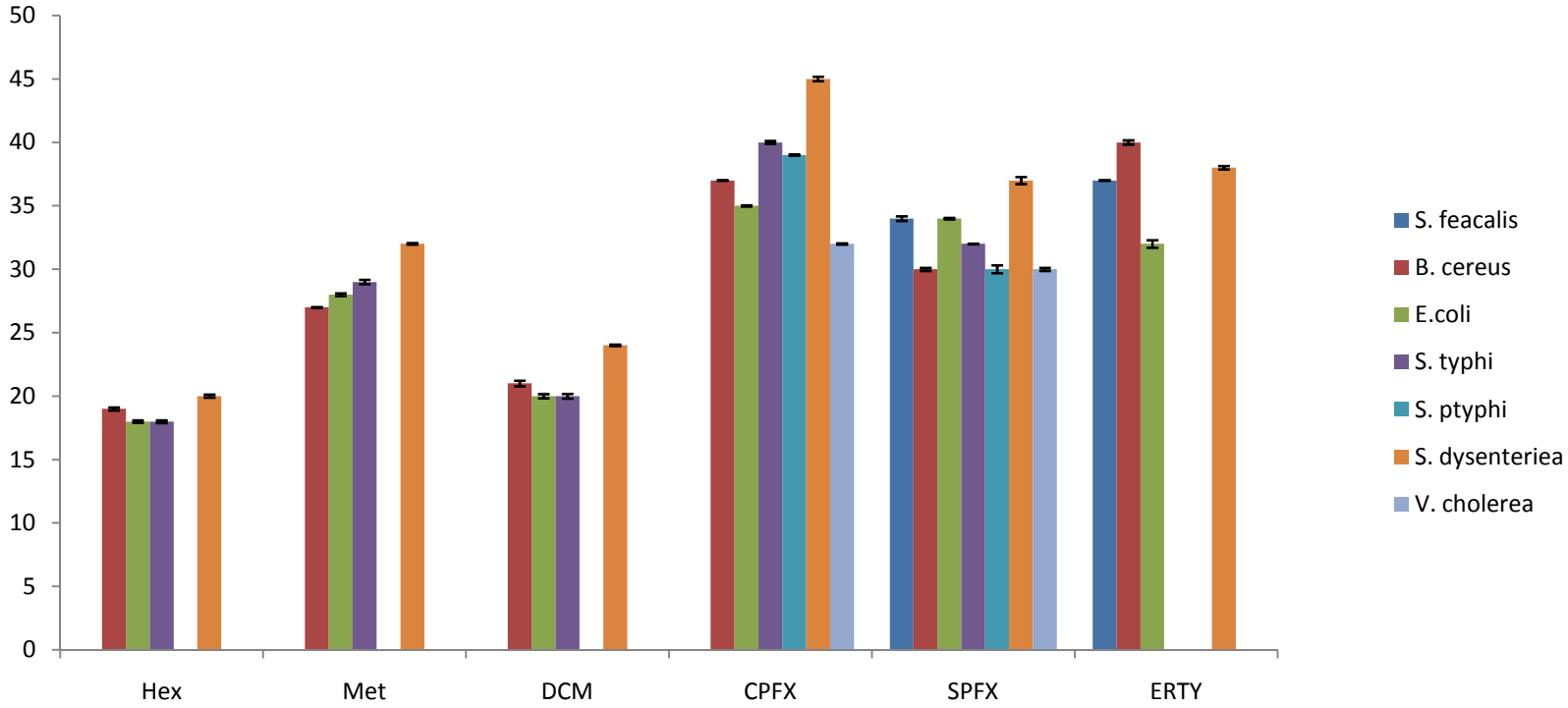

Figure 4.1 Zones of Inhibition of Extracts of Aerial Parts of *M. jalapa* on Test Organisms

Zones of inhibition are presented as mean±standard deviation of triplicate determinations; DCM=Dichloromethane extract; Met=Methanol extract; Hex= Hexane extract; CPFX=ciprofloxacin; SPFX=sparfloxacin; ERTY=erythromycin

Table 4.1: Minimum Inhibitory Concentration (MIC) of Extracts of *M. jalapa* Aerial Parts on Test Organisms

	MIC (mg/ml)		
Organism	Hex	Met	DCM
B. cereus	10.00	2.50	5.00
E.coli	10.00	2.50	5.00
S. typhi	10.00	2.50	5.00
S. dysenteriae	5.00	2.50	5.00

DCM=Dichloromethane extract; Met=Methanol extract; Hex= Hexane extract. Sample concentrations are serial dilutions of 20mg/ml stock solution.

Table 4.2: Minimum Bactericidal Concentration (MBC) of Extracts of *M. jalapa* Aerial Parts on Test Organisms

	MBC (mg/ml)		
Organism	Hex	Met	DCM
B. cereus	20.00	10.00	20.00
E.coli	20.00	10.00	20.00
S. typhi	20.00	10.00	20.00
S. dysenterea	20.00	5.00	10.00

DCM=Dichloromethane extract; Met=Methanol extract; Hex= Hexane extract

4.3 Compounds Isolated From Methanol and DCM Extracts

The methanol and dichloromethane (DCM) extracts which were more active compared to hexane extract against test bacterial organisms were selected for further chromatography purification steps.

Three compounds were isolated from 29 g of methanol extract: compounds **1** (10 mg), **2** (7 mg), and **3** (12 mg). Compound **4** (9 mg) was isolated from 46 g of dichloromethane fraction.

4.4 UV-Visible AND FTIR Spectral Analyses of Compound 1

The UV-visible spectrum showed intense absorbance in the region 229 nm and medium range absorbance at 287 nm which is characteristic of aromatic ring system (Figure 4.2). The FTIR spectrum showed a strong narrow peak at 3425 cm^{-1} in the functional group regions with overtones at 2925 cm^{-1} characteristic of a tertiary amine. The absorbance observed at 1649 cm^{-1} in the finger print region strongly suggests presence of carbonyl group in the compound. The observed peaks are indicative of the presence of an amide type functional group (Figure 4.3).

THERMO ELECTRON ~ VISIONpro SOFTWARE V4.10

Operator Name	ARSHAD ALAM	Date of Report	5/20/2015
Department	Analytical laboratory # 004 TWC	Time of Report	10:59:29AM
Organization	ICCBS.Karachi University.		
Information	Prof Dr. Iqbal/ Masud Sadiq.		

Scan Graph

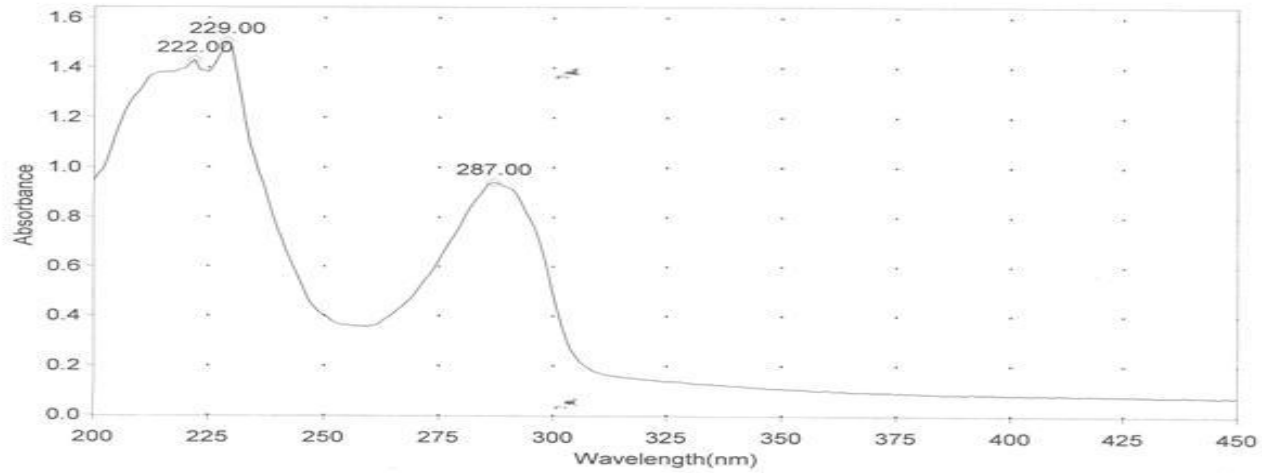

Results Table - MCI- 23.sre,MCI- 23,Cycle01

nm	A
222.00	1.431
229.00	1.506
287.00	0.939
Sensitivity	Medium

Peak Pick Method
Find 8 Peaks Above -3.0000 A
Start Wavelength 200.00 nm
Stop Wavelength 300.00 nm
Sort By Wavelength

Figure 4.2: UV-vis Spectrum of Compound 1

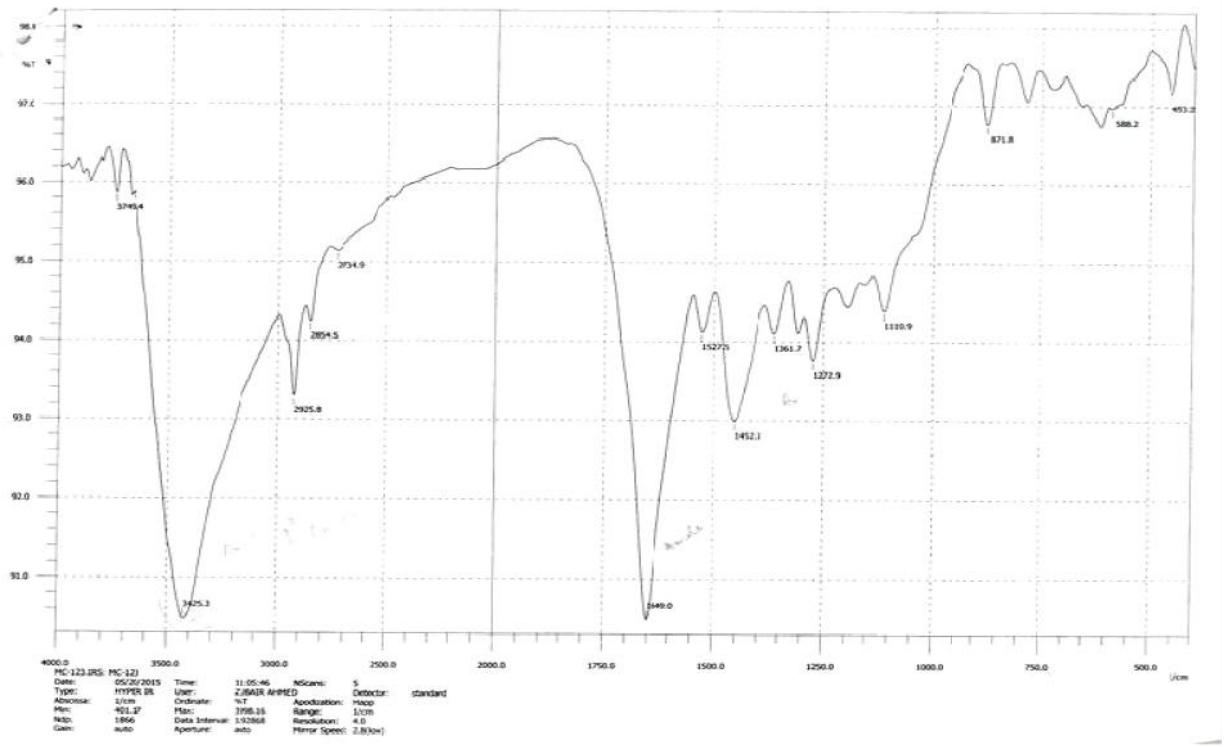

Figure 4.3: FTIR Spectrum of Compound 1

4.5 Nuclear Magnetic Resonance (NMR) Spectral Analyses of Compound 1

4.5.1 Proton (^{1}H) Nuclear Magnetic Resonance of Compound 1

The proton (^{1}H) NMR spectrum of compound **1** revealed signals at chemical shifts 1.76, 2.38, 2.56, 2.63, 2.73, 3.04, 4.08, 4.72 and 6.55 in the aromatic region (Figures 4.4 and 4.5).

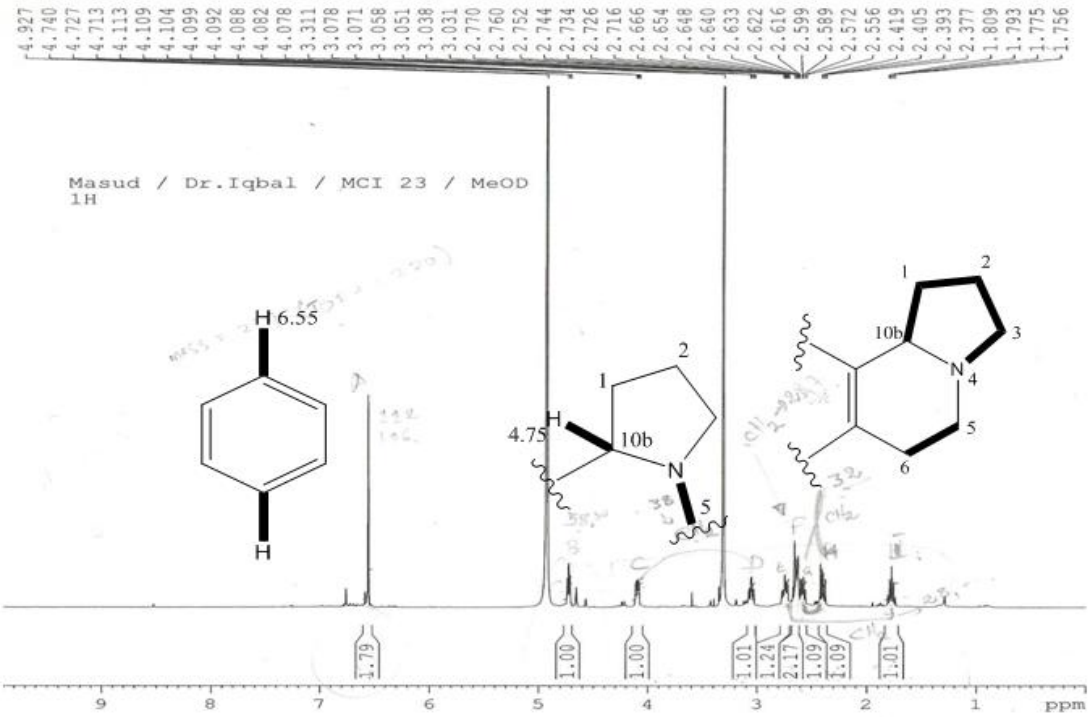

Figure 4.4: ^{1}H NMR (600 MHz, MeOD) of Compound 1

The thick line (▬) indicates the referenced protons

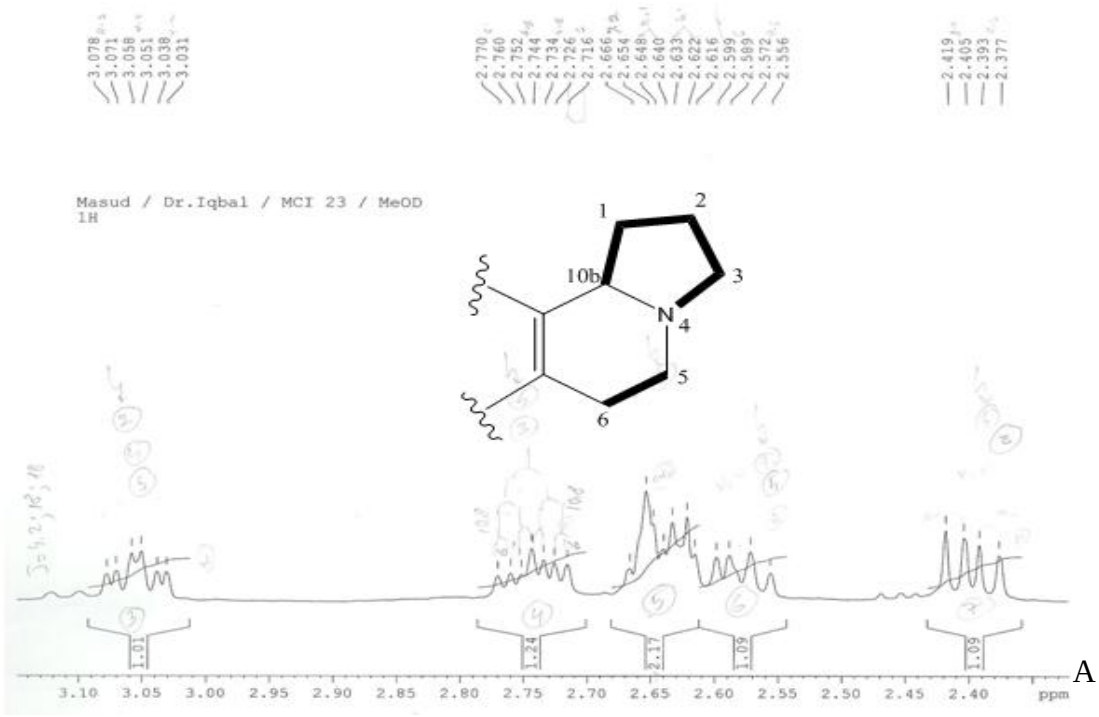

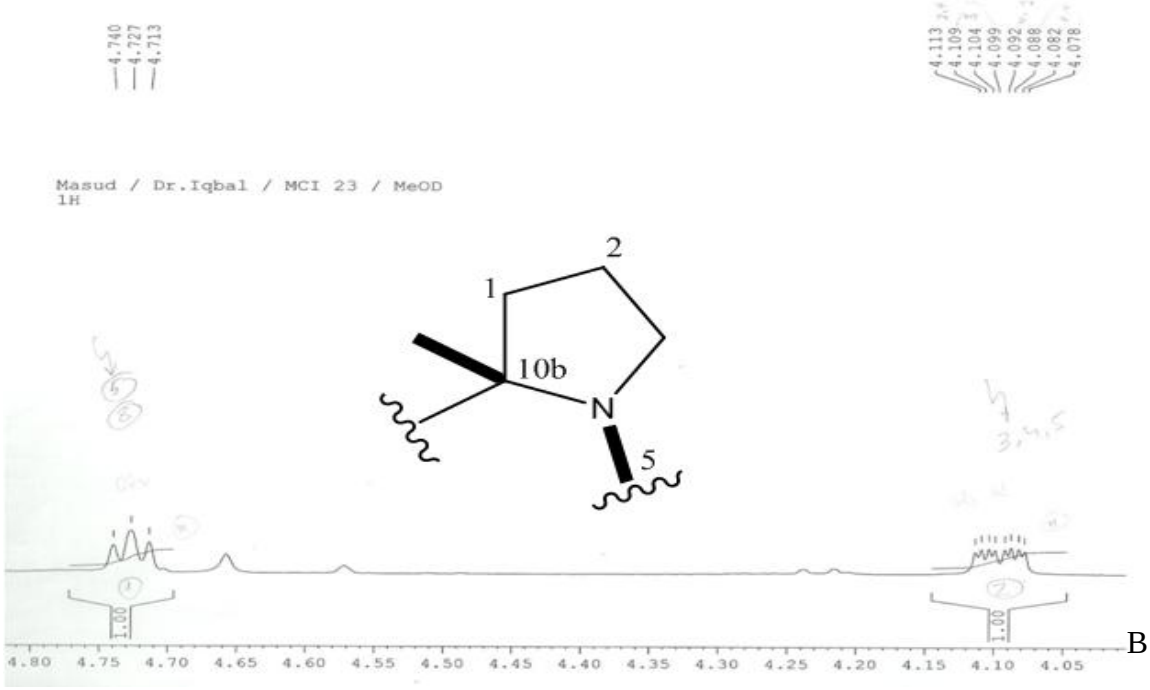

Figure 4.5: Expanded Proton NMR Spectra Showing Regions 2.4-3.10 ppm (A) and 4.05-4.80 ppm (B) for Compound 1

4.5.2 Carbon-13 and DEPT Spectral Analyses of Compound 1

The C-13 broadband spectrum (Figure 4.6) revealed a total of 12 carbons with the following chemical shifts: 28.75 (C-1), 28.82(C-6), 32.70(C-2), 38.64(C-5), 58.30 (C-10b), 112.39(C-10), 116.24(C-7), 125.53 (C-6a), 129.79(C-10a), 145.46(C-8), 145.61(C-9) and 175.86(C-3).

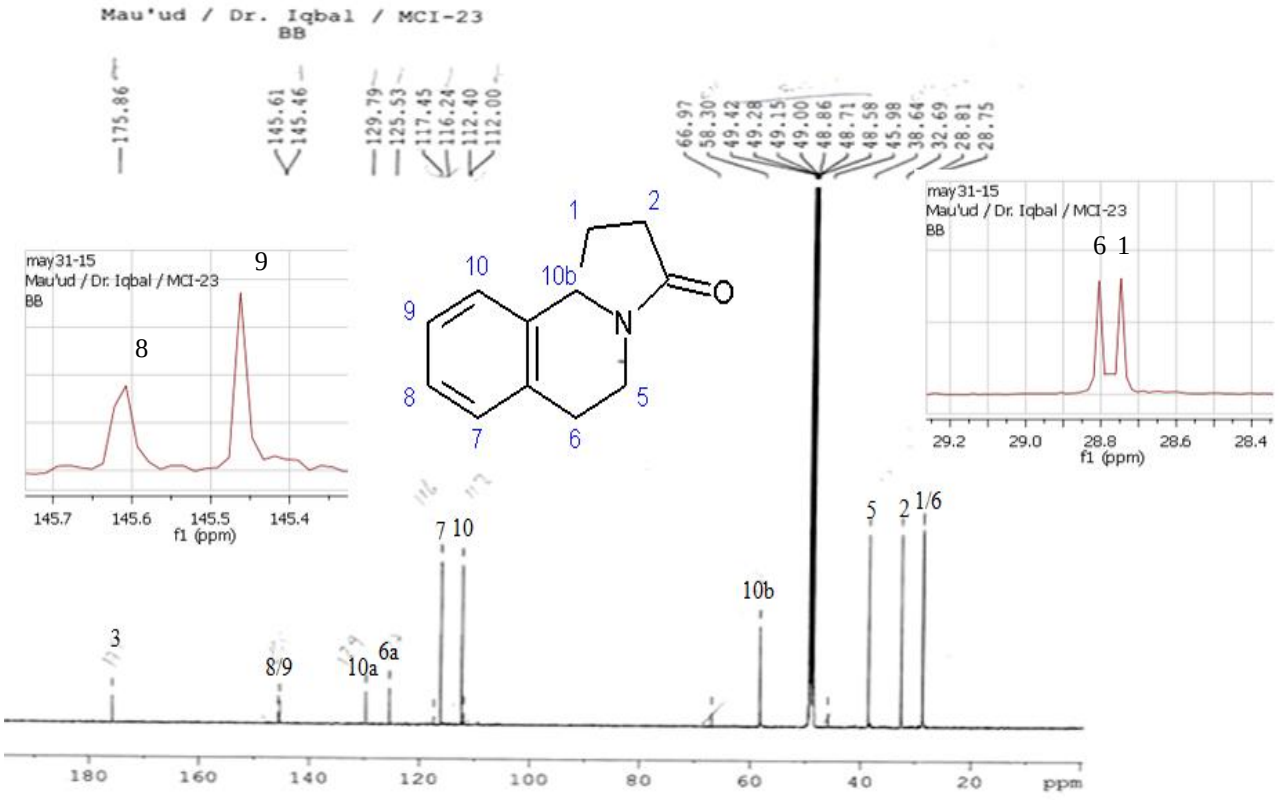

Figure 4.6: C-13 NMR Spectrum for Compound 1

Inserts show expanded regions 28.4-29.2 ppm (C-1 and C-6) and 145.4-145.7 ppm (C-8 and C-9).

DEPT 90 spectral analysis (Figure 4.7) identified three methine carbons: two in the aromatic region and one aliphatic as follows: aliphatic, 58.30(C-10b) and aromatic 112.39(C-10) and 116.24(C-7).

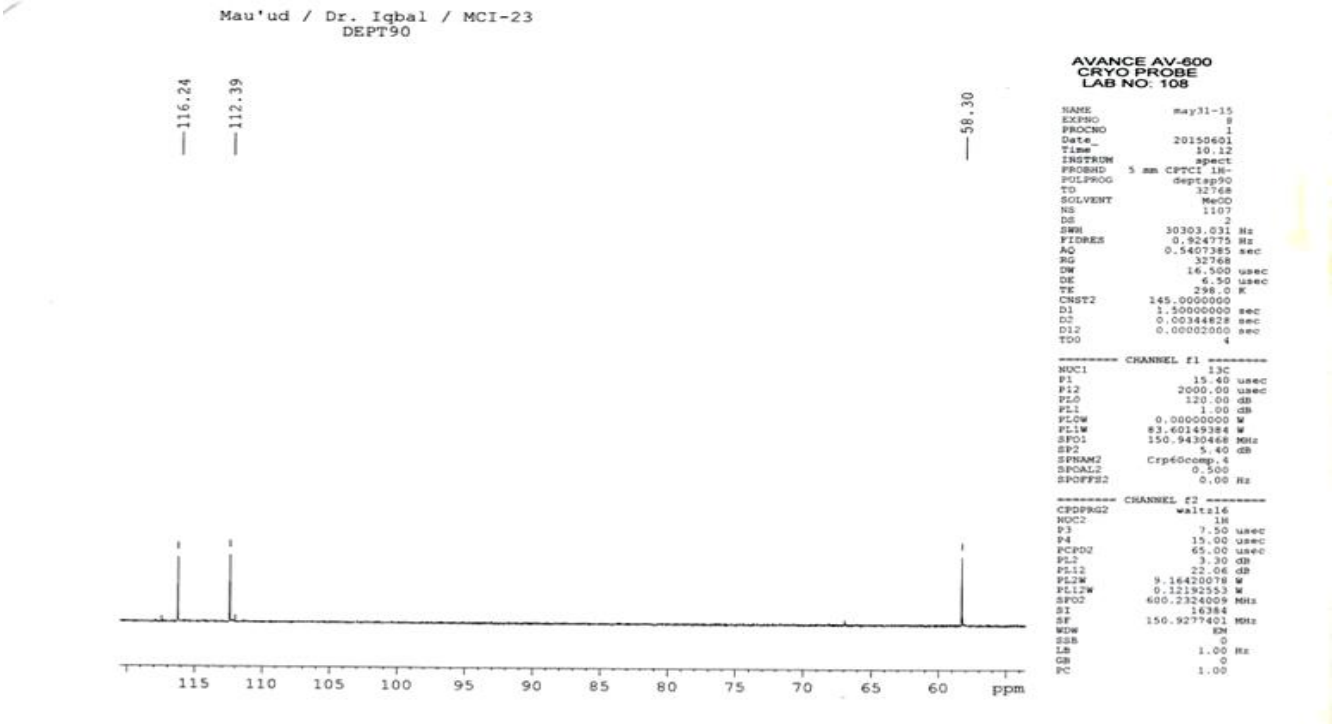

Figure 4.7: DEPT 90 NMR Spectrum for Compound 1

The DEPT 135 spectrum (Figure 4.8) identified methylene carbons (appearing as negative peaks): 28.75 (C-1), 28.82 (C-6), 32.70(C-2), and 38.64(C-5). The aromatic quaternary carbons included those with chemical shifts: 125.53 (C-6a), 129.79(C-10a), while 145.46(C-8) and 145.61(C-9) have hydroxyl (OH) attached. The chemical shifts appearing at 175.86(C-3) is characteristic of carbonyl carbon shift on the C-13 chemical shift scale.

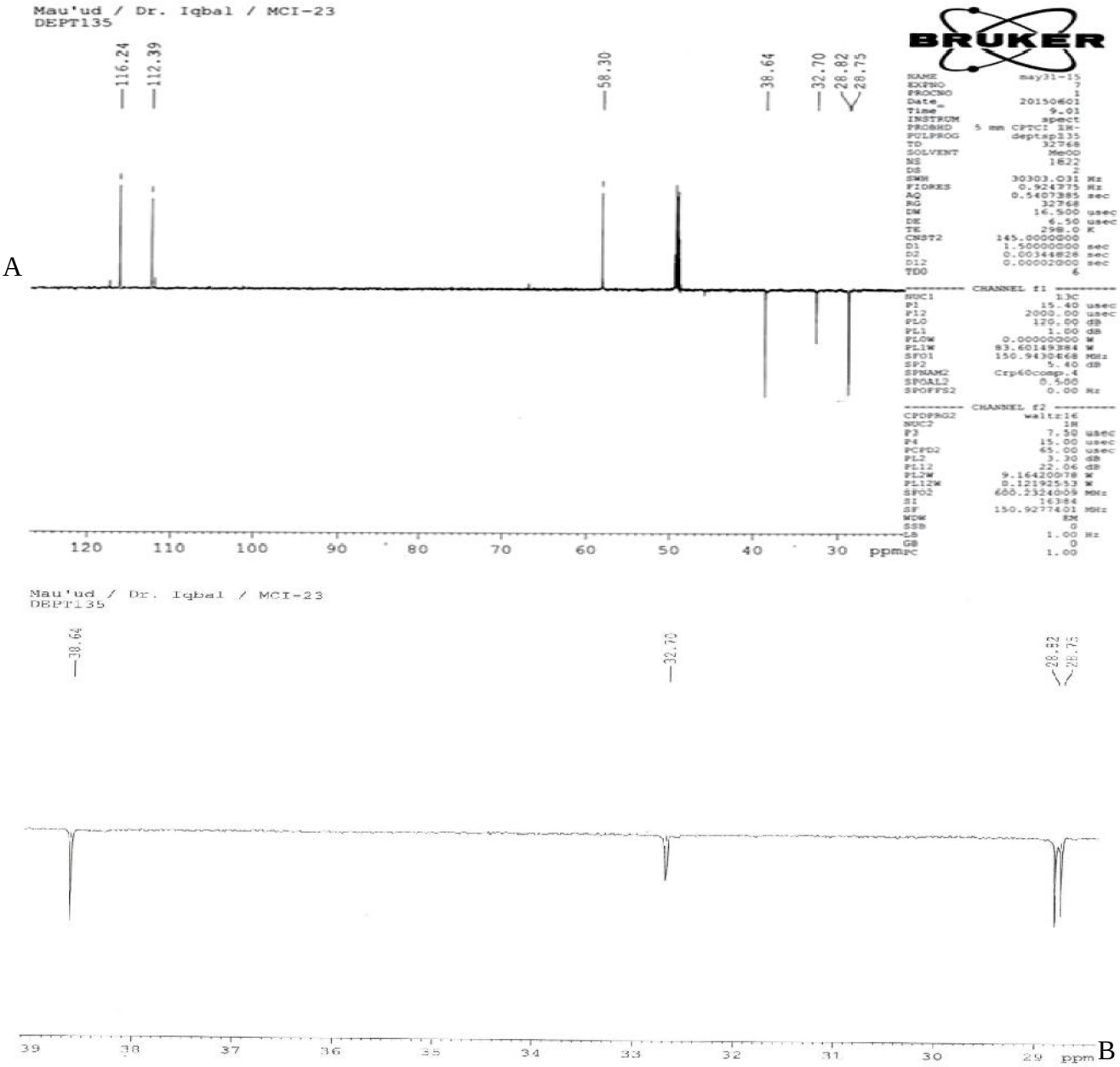

Figure 4.8: DEPT 135 NMR Spectrum of Compound 1

The expanded region 29-39ppm (B) emphasizes the methylene carbons C-1, C-6, C-2 and C-5.

4.6 Two Dimensional (2D) NMR Spectral Analyses of Compound 1

4.6.1 ^{1}H-^{1}H Correlation Spectroscopy (COSY) of compound 1

^{1}H-^{1}H COSY presented in Figures 4.9 and 4.10 revealed correlations between the following protons: H3(4.72)-#H8 (2.66) and #H11 (1.73); H4(4.08)-#H5 (3.04) H6 and H7 (2.66); H9 (2.56)-#10 (2.41) and #H11(1.73); H10 (2.41)-#H11 (1.73).

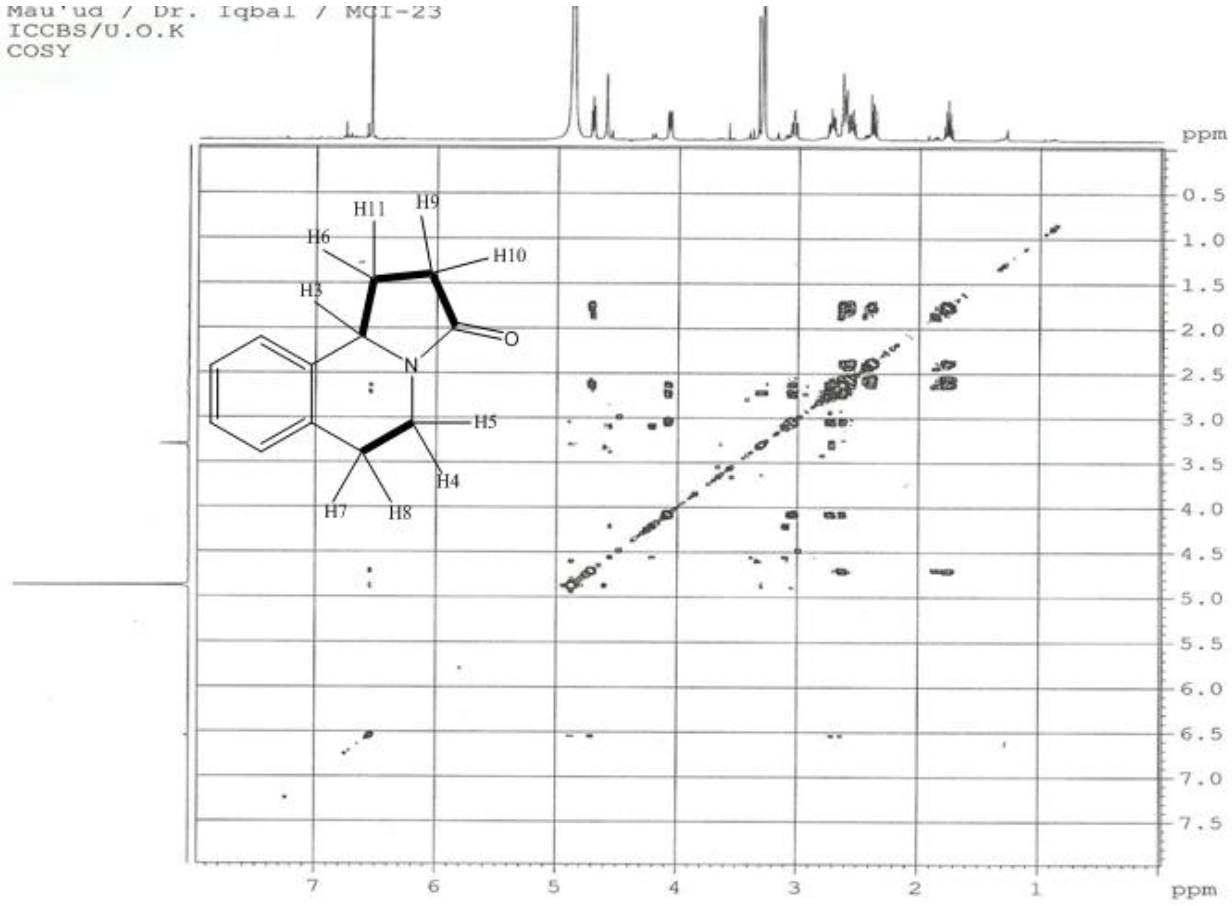

Figure 4.9: ^{1}H-^{1}H COSY Spectrum for Compound 1

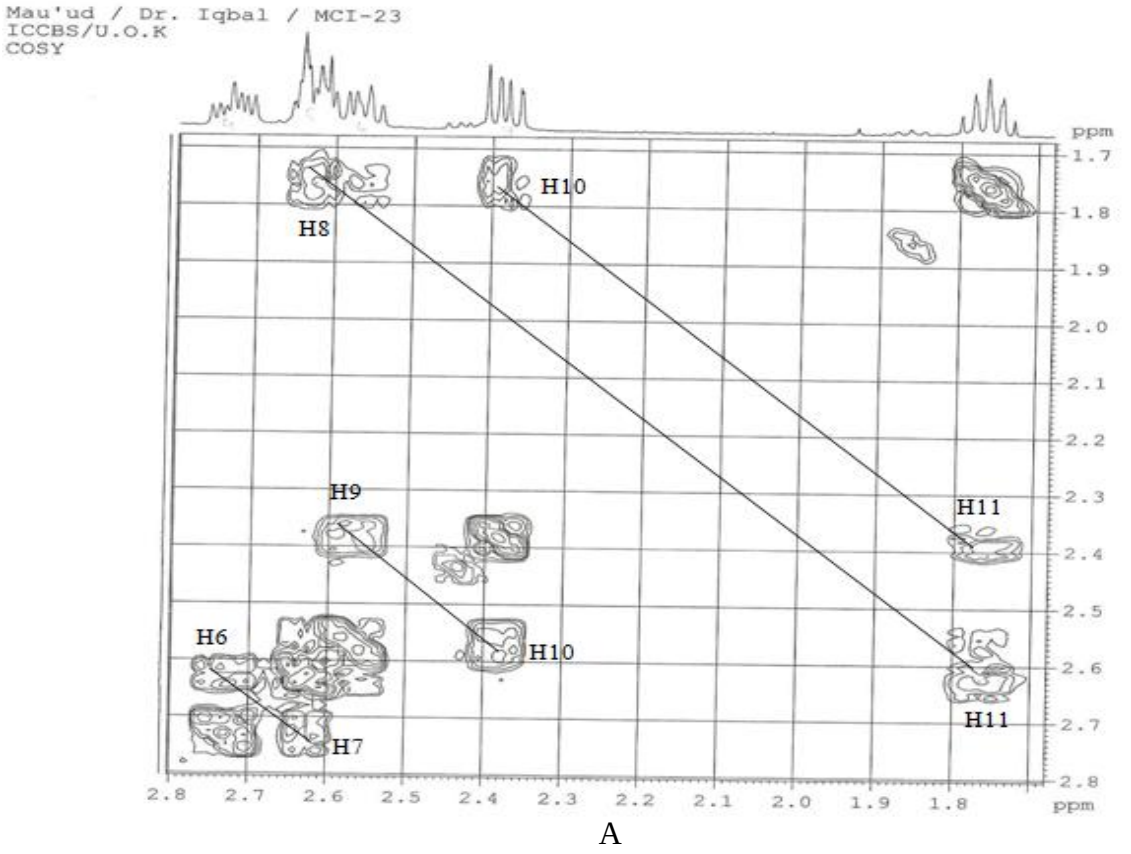

A

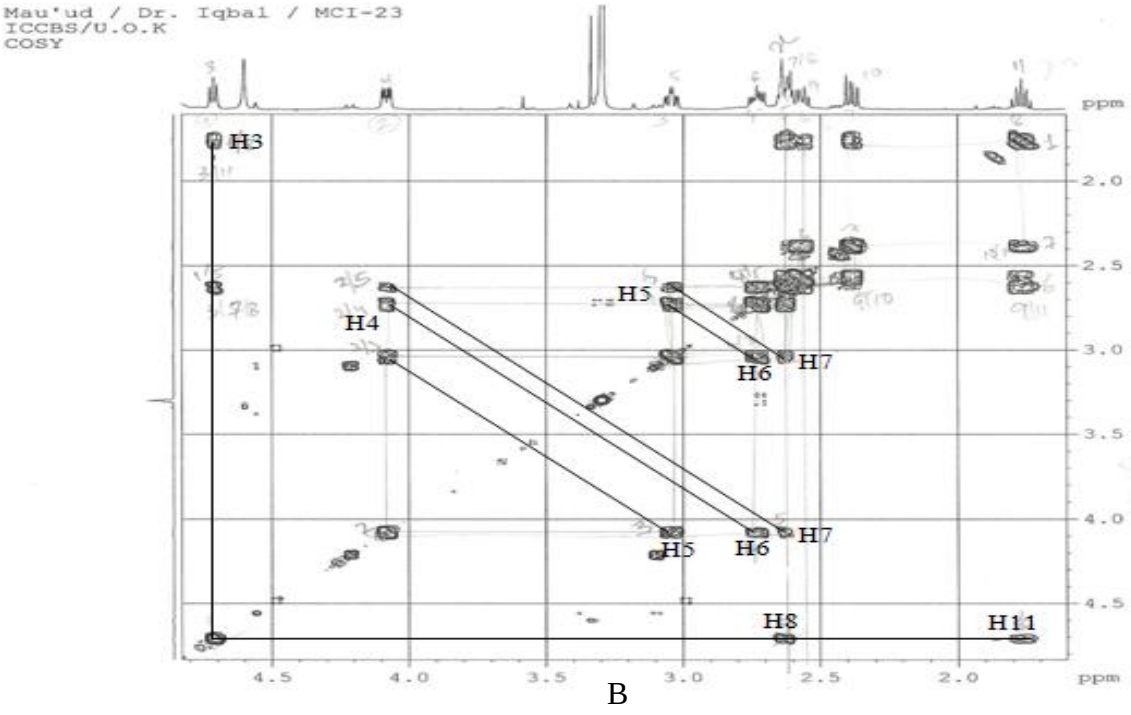

B

Figure 4.10: Expanded Regions 1.8-2.8 ppm (A) and 2.0-4.5 ppm (B) Showing ^{1}H-^{1}H COSY for Compound 1

4.6.2 HSQC Spectral Analysis for Compound 1

The HSQC analysis identified carbons and the respective attached protons. Two protons appeared in the aromatic region (aromatic protons) while 4 methylene and one methine carbon were observed as follows: C(112) - $^{H}\delta$ 6.55; C(116) - $^{H}\delta$ 6.55; C(58.3) - $^{H}\delta$ 4.72; C(38.64) - $^{H}\delta$ 4.08 and 3.04; C(32.69) - $^{H}\delta$ 2.41 and 2.56; C(28.75) - $^{H}\delta$ 1.73 and 2.66; C(28.82) - $^{H}\delta$ 2.66 and 2.76 (Figures 4.11 and 4.12).

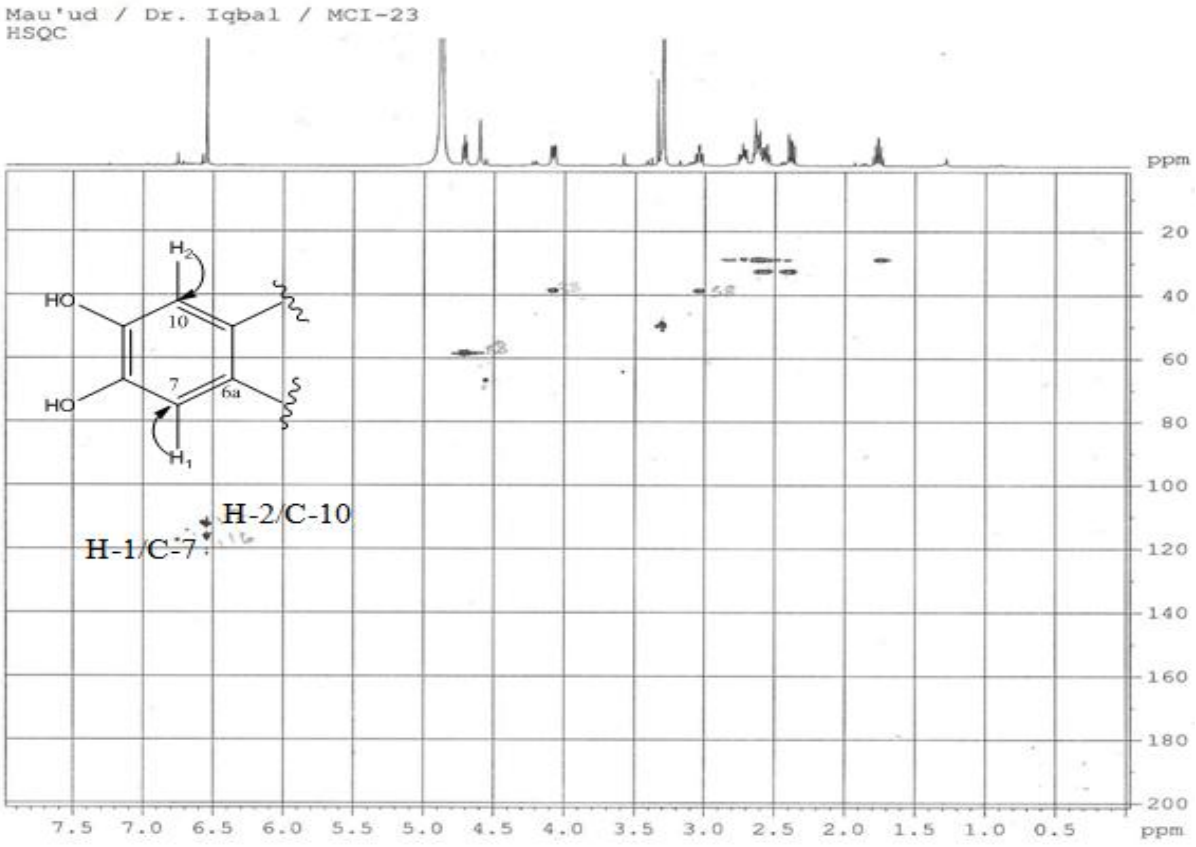

Figure 4.11: HSQC Spectrum for Compound 1

The arrow (⟶) shows proton-carbon correlations.

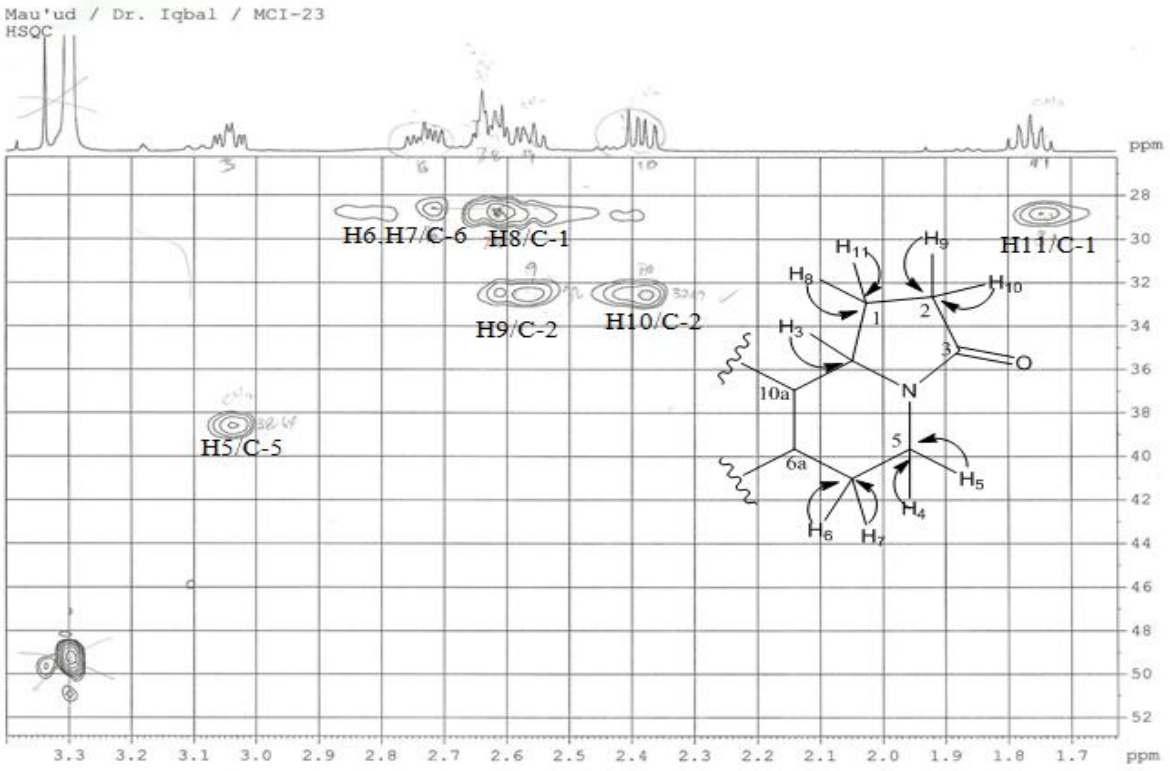

A

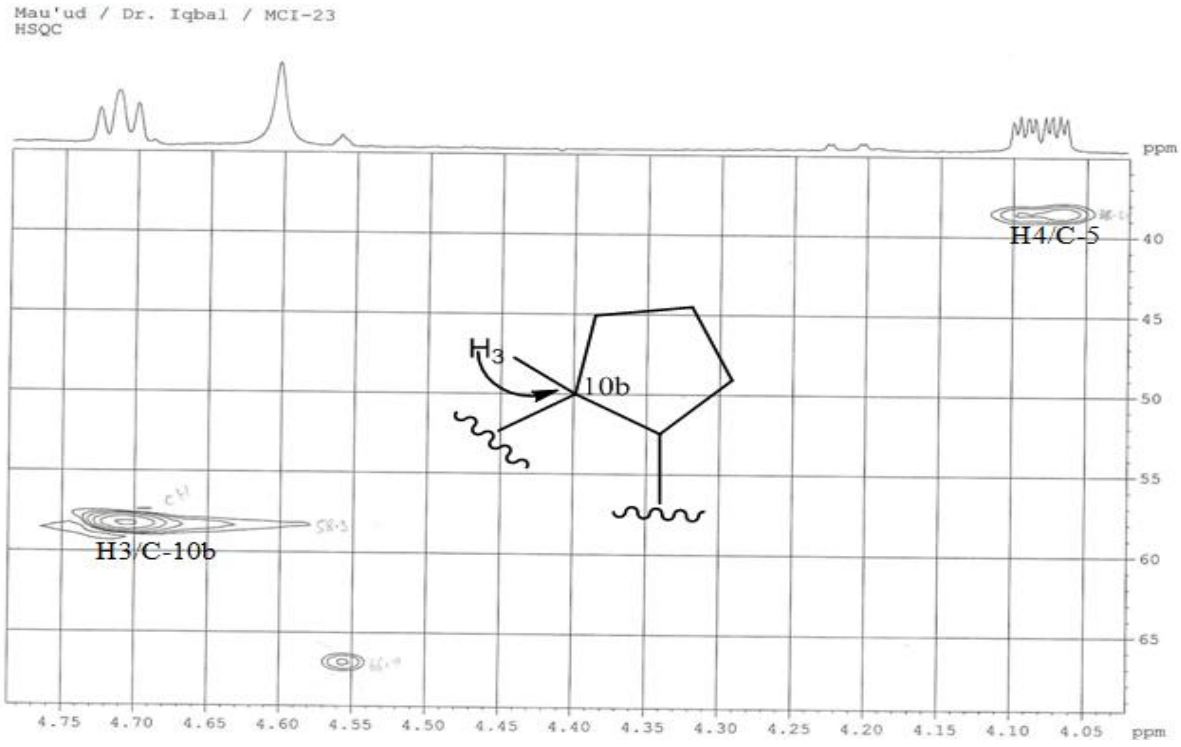

B

Figure 4.12: Expanded Regions (proton chemical shift) 1.7-1.3 ppm (A) and 4.05-4.75 ppm (B) Showing Proton-Carbon HSQC Correlations for Compound 1

The arrow (⟶) shows proton-carbon correlations.

4.6.3 HMBC Spectral Analysis of Compound 1

HMBC spectral analysis in Figures 4.13 and 4.14 showed 2-3 bond long range proton-carbon correlations described as follows: $^{H}\delta$ 6.55 correlated with C-28.82, C-58.30, C-125.53, C-129.79 and C-145; $^{H}\delta$ 4.72 correlated with C-28.75, C-125.53, C-129.79; $^{H}\delta$ 4.08 correlated with C-28.82, C-58.30, C-125.53, C-175.86; $^{H}\delta$3.04 correlated with C-28.82, C-125.53, C-175.86; $^{H}\delta$2.76 correlated with C-38.64, C-116.24, C-125.53, C-129.79, C-145.46; $^{H7}\delta$2.66 correlated with, C-116, C-125.53, C-129.79; $^{H8}\delta$2.66 C-32.69, C-58.30 C-175.86; $^{H}\delta$ 2.56 correlated with C-28.75, C-175.86; $^{H}\delta$ 2.41 showed correlation with C-28.75, C-58.30, C-175.86; $^{H}\delta$ 1.73 correlated with C-32.69, C-58.30 and C-129.79.

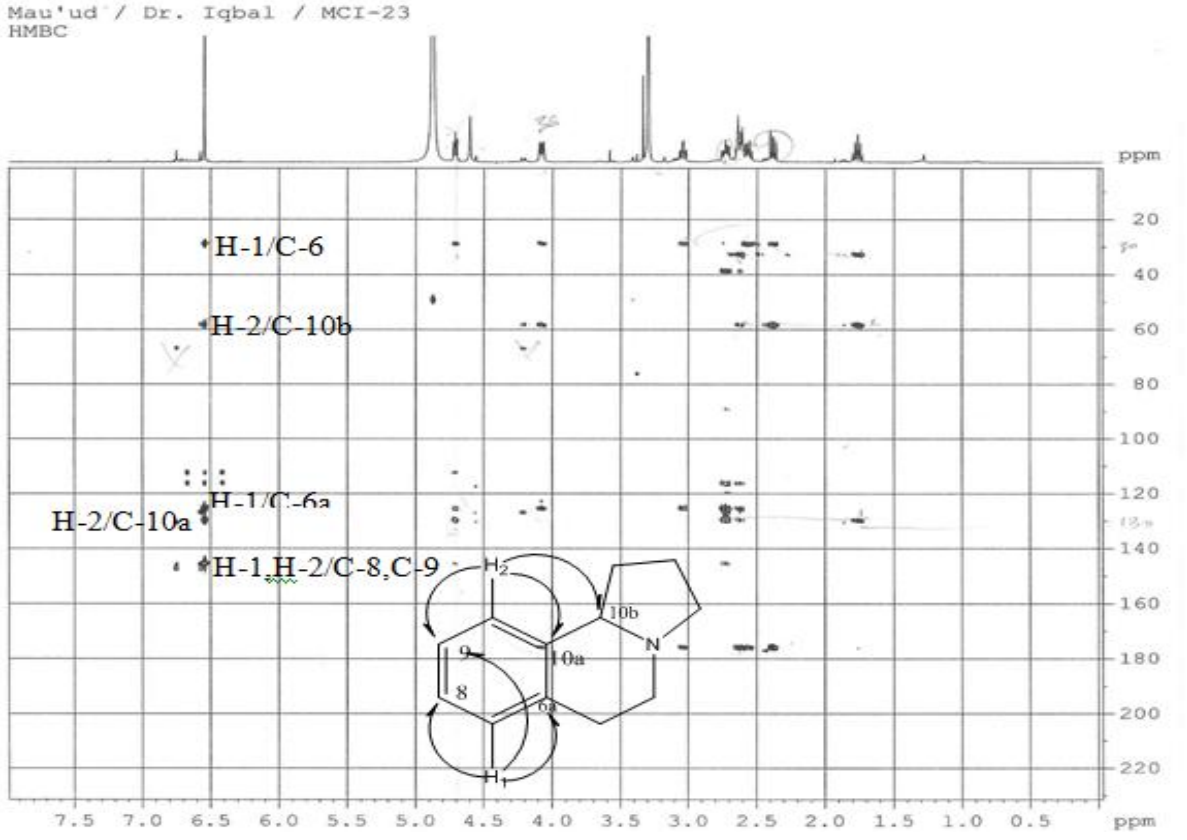

Figure 4.13: HMBC of Compound 1

The arrow (⟶) shows the 2-3 (long range) bond proton-carbon coherence.

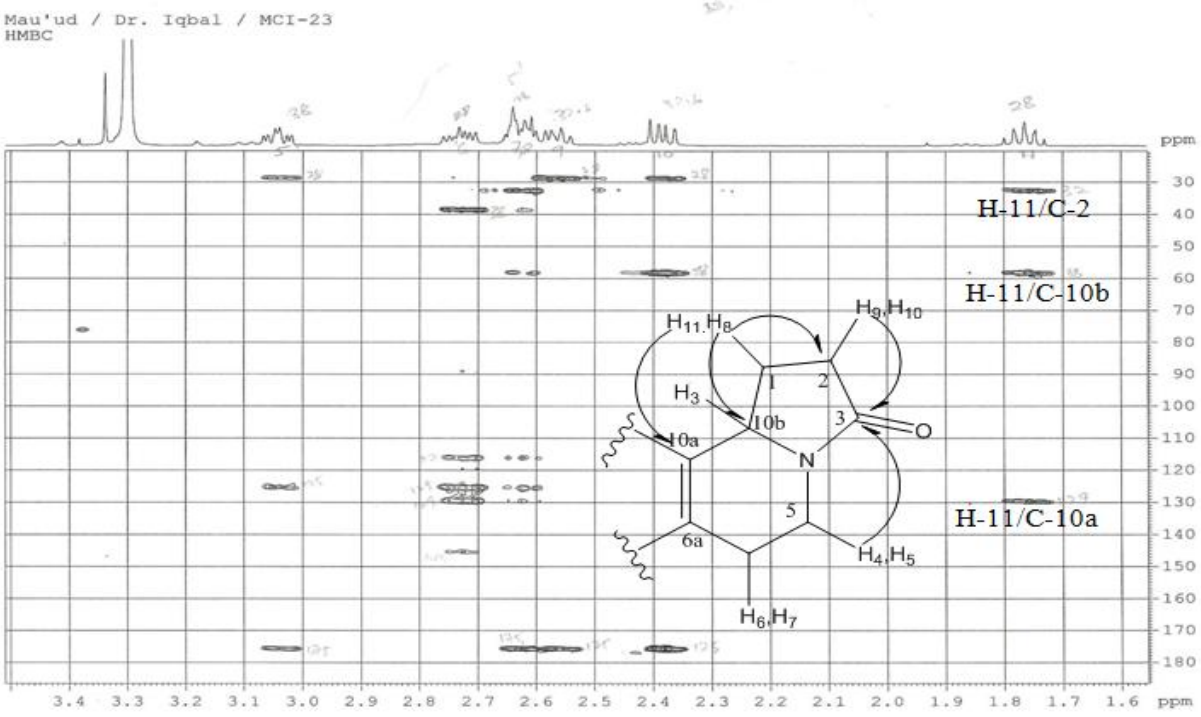

A

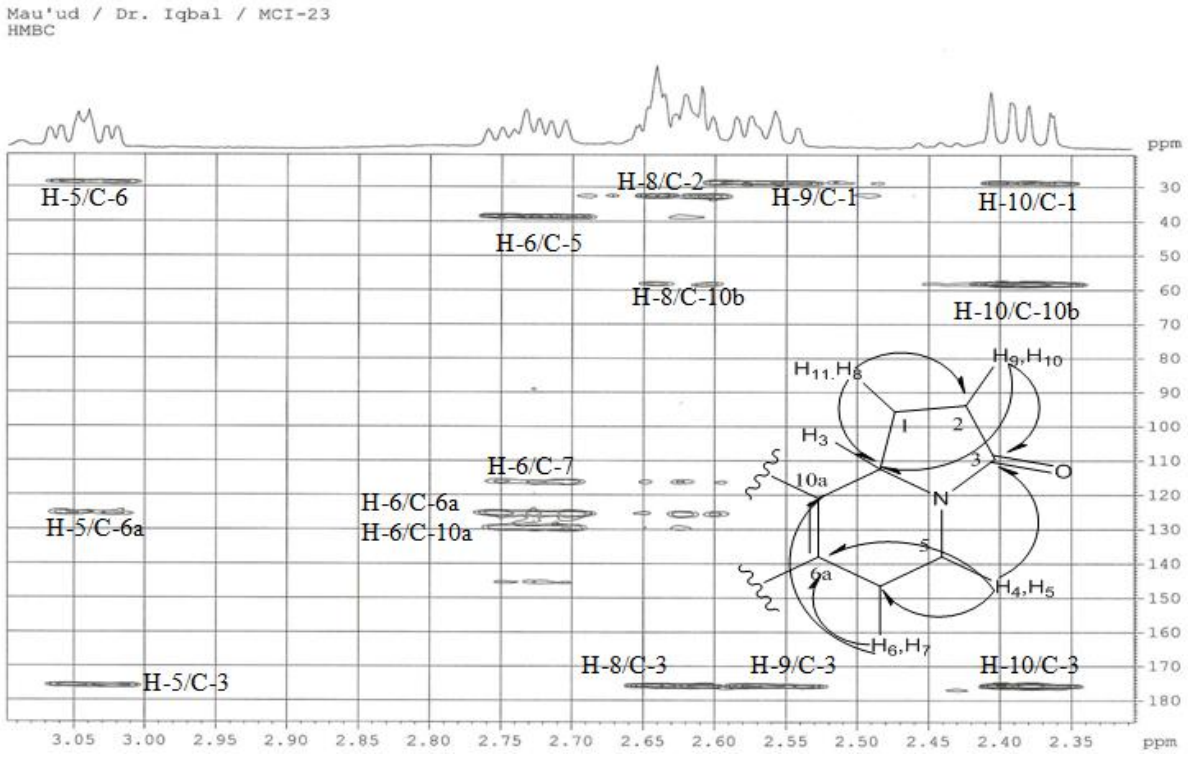

B

Figure 4.14: Expanded Regions (proton chemical shift) 1.6-3.4 ppm (A) and 2.35-3.05 ppm (B) Showing 2-3 Bond Correlations of Compound 1

The arrow (⟶) shows the 2-3 (long range) bond proton-carbon coherence

4.7 Mass Spectral Analysis of Compound 1

The molecular ion peak (positive mode ESI) was observed as an intense peak appearing at m/z 220 (Figure 4.15). The high resolution EI-MS of the compound (Figure 4.16) also showed a molecular ion peak at m/z 219 with a base peak at m/z 218 probably due to loss of a single proton and relative stability of the compound within the time frame of fragmentation. The elemental composition from the high resolution EI-MS elemental analysis suggested the molecular formula $C_{12}H_{13}O_3N$ with calculated degree of unsaturation (ring plus double bond, RDB) of 7.

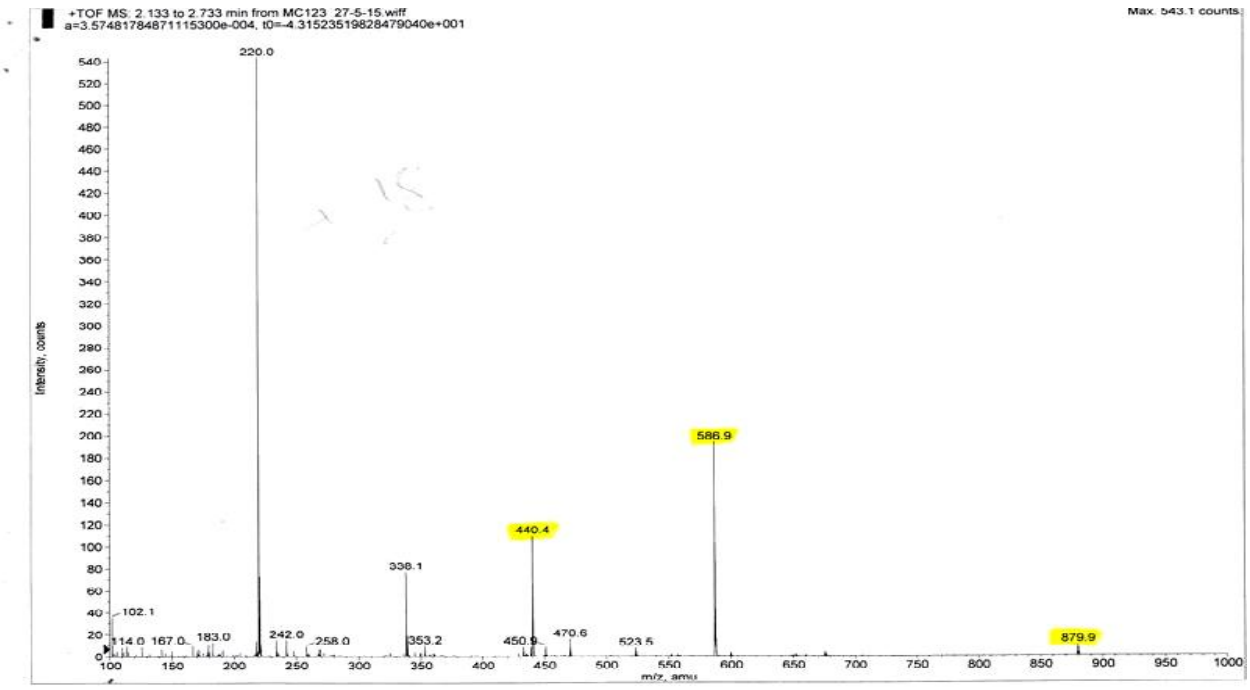

Figure 4.15: ESI-MS Spectrum of Compound 1

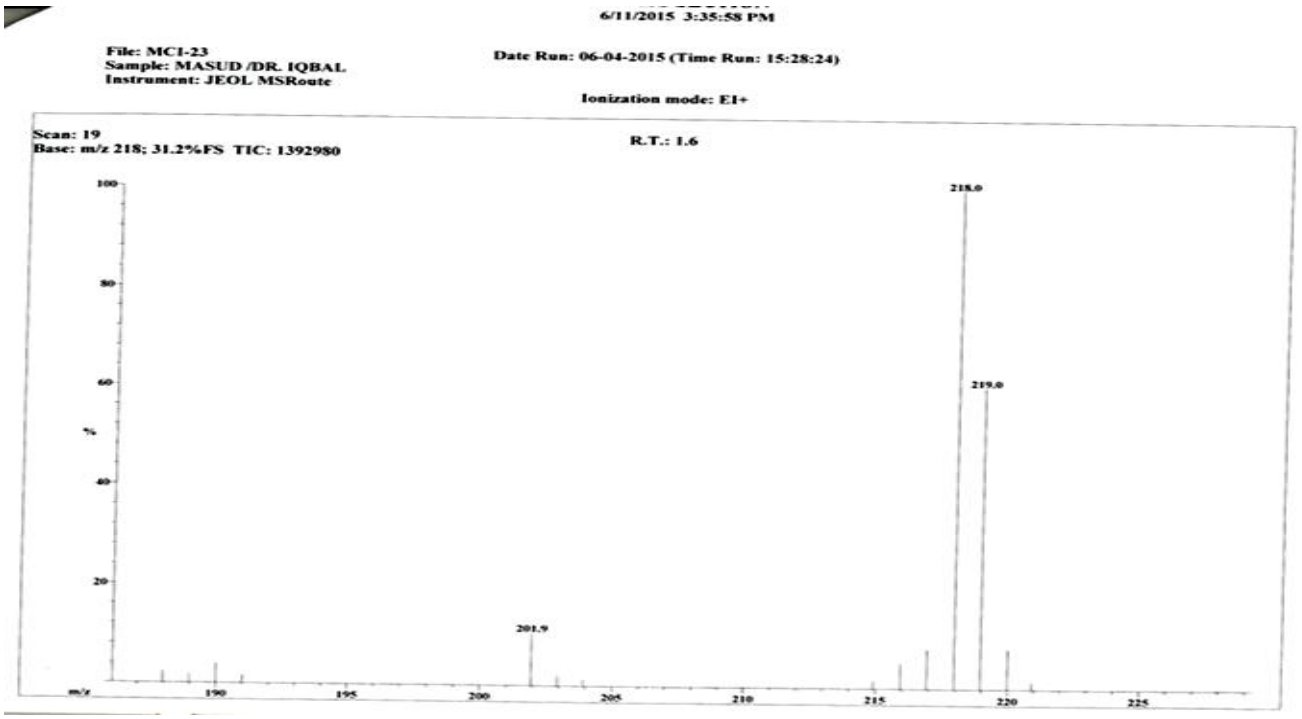

A

Mass	Relative Intensity	Theoretical Mass	Delta [ppm]	Delta [mmu]	RDB	Composition
		186.0555	-13.6	-2.5	8.5	$C_{12}H_8O_2N_1$
188.0712	4.3	188.0712	0.1	0.0	7.5	$C_{11}H_{10}O_2N_1$
		188.0685	14.4	2.7	3.0	$C_9H_{12}O_5$
189.0759	2.2	189.0763	-2.2	-0.4	2.5	$C_8H_{13}O_5$
		189.0790	-16.4	-3.1	7.0	$C_{11}H_{11}O_2N_1$
190.0852	5.1	190.0841	5.6	1.1	2.0	$C_9H_{14}O_5$
		190.0868	-8.5	-1.6	6.5	$C_{11}H_{12}O_2N_1$
202.0870	9.5	202.0868	0.7	0.1	7.5	$C_{12}H_{12}O_2N_1$
		202.0841	14.0	2.8	3.0	$C_9H_{14}O_5$
203.0910	1.5	203.0919	-4.8	-1.0	2.5	$C_8H_{15}O_5$
		203.0946	-18.0	-3.7	7.0	$C_{12}H_{13}O_2N_1$
215.0577	2.8	215.0582	-2.5	-0.5	9.0	$C_{12}H_9O_3N_1$
216.0666	3.4	216.0661	2.4	0.5	8.5	$C_{12}H_{10}O_3N_1$
217.0740	6.0	217.0739	0.4	0.1	8.0	$C_{12}H_{11}O_3N_1$
218.0820	87.1	218.0817	1.1	0.2	7.5	$C_{12}H_{12}O_3N_1$
219.0882	45.7	219.0895	-6.4	-1.4	7.0	$C_{12}H_{13}O_3N_1$
220.0909	6.5	220.0888	9.7	2.1	11.0	$C_{16}H_{12}O_1$
263.0677	1.4	263.0708	-12.0	-3.2	12.5	$C_{17}H_{11}O_3$

B

Figure 4.16: High Resolution EI-MS Spectrum (A) and Resulting Elemental Analysis (B) of Compound 1

4.8 Summary of Characteristics and Spectroscopy Data of Compound 1

Physical appearance: brownish powder, test positive to dragendorff reagent

UV-Vis: 229 nm, 287 nm

FTIR spectrum: 3425 cm^{-1}(s), 1649 (s), 2925(m) 1527 (w), 1452(m)

ESI-MS: positive mode (M+H*) m/z 220.1 appearing also as base peak

HREI-MS: (M-H) pseudo M* ion peak at 218 (base peak). Elemental analysis suggests a molecular mass of 219.0882

Molecular formular: $C_{12}H_{13}O_3N$

Degree of unsaturation (RDB): 7

Table 4.3: Summary of 1D and 2D NMR Spectral Analyses of compound 1

Carbon position	**δ_C type**	**Type**	**δ_H (*J* in Hz)**	**HMBC**
1	28.75	CH_2	2.66, 1.73 (9.6, 20) m	2, 10a, 10b
2	32.69	CH_2	2.41, 2.56 (6, 16)	1, 3, 10b
3	175.9	C		
5	38.64	CH	4.08, (2.4, 4.2,6) ddd; 3.04 (4.2, 12) td	3, 6, 6a, 10b
6	28.82	CH_2	2.76 (10.8); 2.66 m	5, 6a, 7, 8, 10a,
6a	125.53	C		
7	116.24	CH	6.55 s	6, 6a, 8, 10a
8	145.46	C		
9	145.61	C		
10	112.39	CH	6.55 s	6a, 9, 10a, 10b,
10a	129.79	C		
10b	58.30	CH	4.72 (7.8, 16.2)	1, 3, 6a

$^{\delta}$C= carbon chemical shift in ppm; $^{\delta}$H = proton chemical shift in ppmm.= multiplets; *J* = coupling constant;; s= singlet; d= doublets; dd=doublet of doublets; m=multiplets; td= triplet of doublets

Proposed structure of compound 1

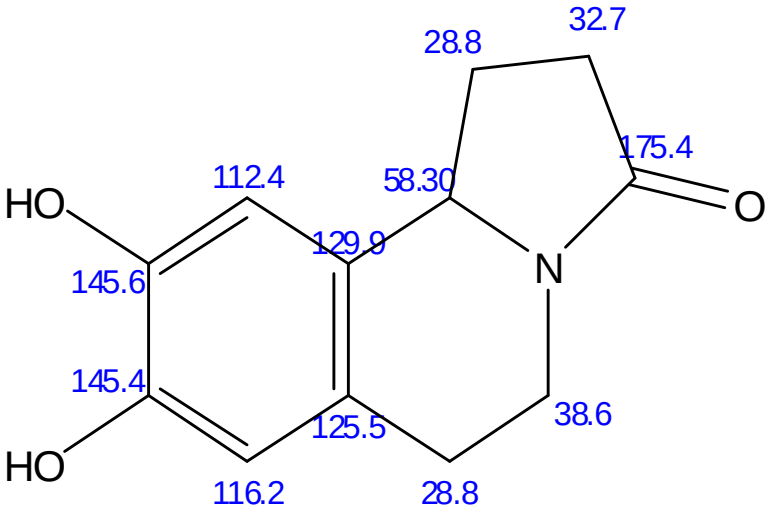

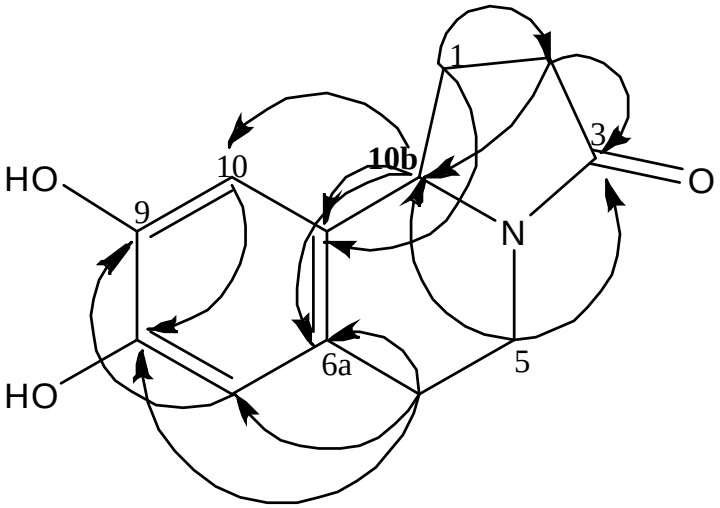

The arrows show HMBC

4.9 Nuclear Magnetic Resonance (NMR) Spectral Analyses of Compound 2

4.9.1 Proton (^{1}H) Nuclear Magnetic Resonance for Compound 2

The proton (^{1}H) NMR spectrum revealed signals as follows: 3.42, 3.44, 3.55, 3.72, 3.94, 5.38, 6.18, 6.37, 6.91, 7.57-7.59 and 7.92 (Figures 4.17 and 4.18).

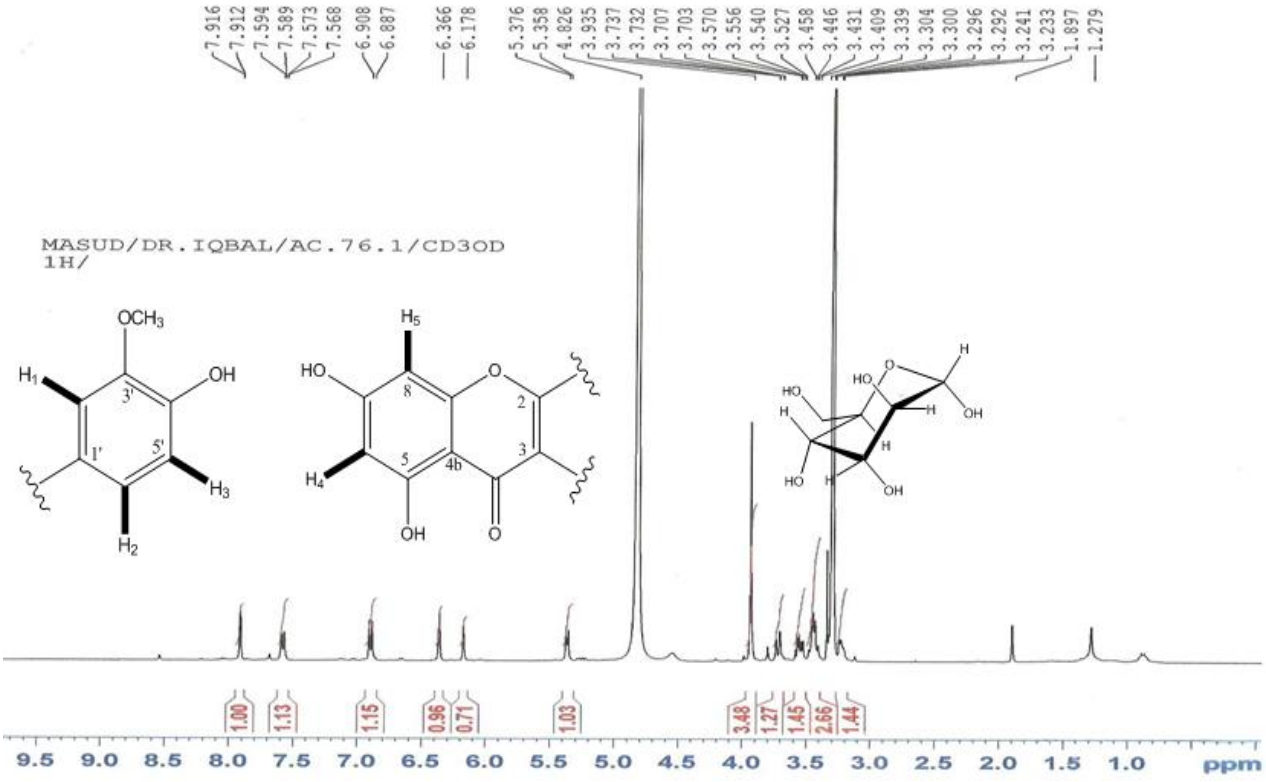

Figure 4.17: ^{1}H NMR (600MHz, MeOD) of Compound 2

The thick line (▬) indicates the referenced protons

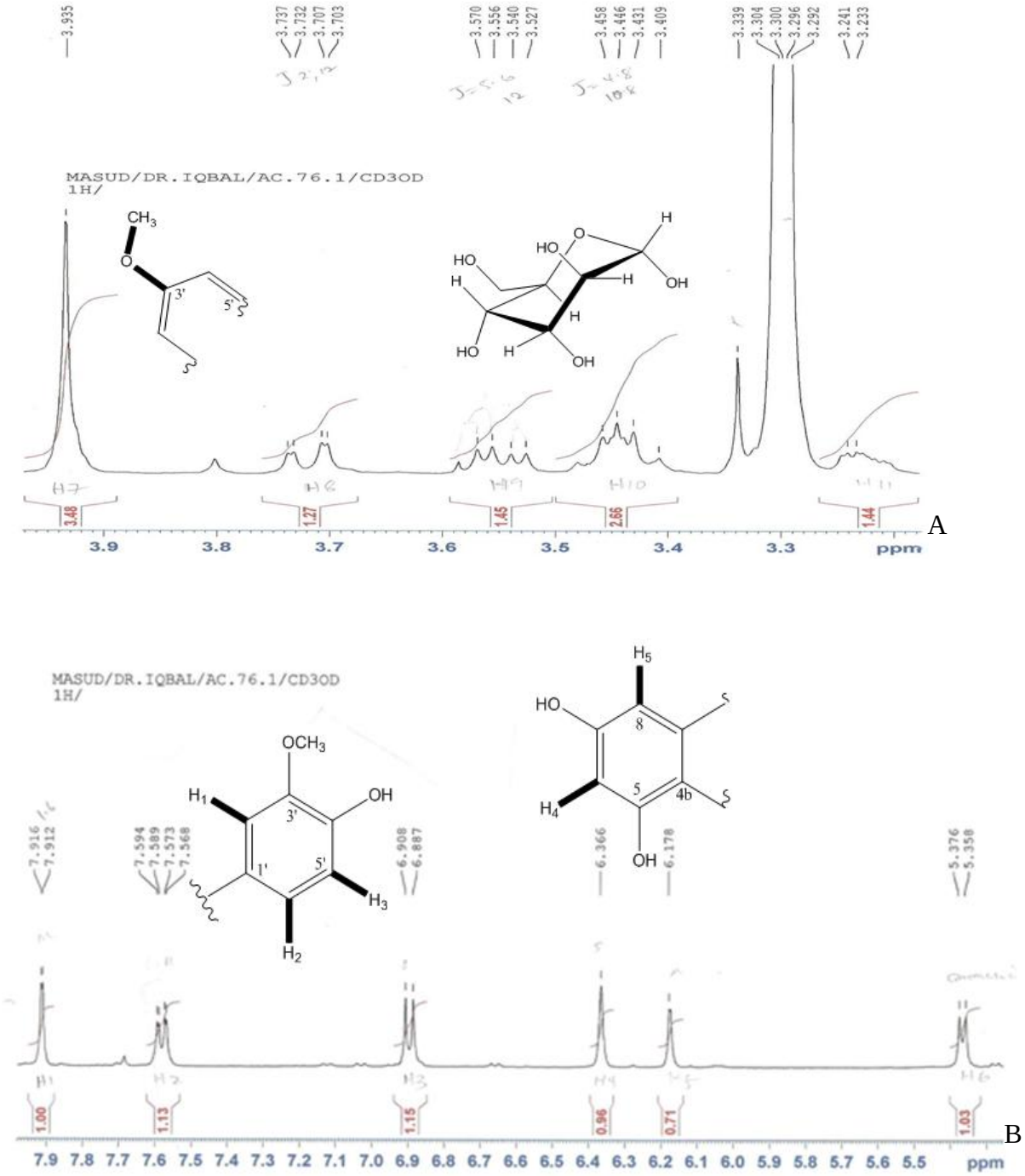

Figure 4.18: Expanded Regions 3.3-3.9 ppm (A) and 5.5-7.9 ppm (B) Proton NMR Spectra for Compound 2

The thick line (▬) indicates the referenced protons

4.9.2 Carbon-13 and DEPT Spectral Analyses of Compound 2

Figures 4.19 and 4.20 present signals observed on the C-13 spectrum of compound 2: 56.76 (C-9), 62.51 (C-6”), 71.46 (C-4”), 75.91 (C-2”), 78.08 (C-5”), 78.55 (C-3”), 94.97 (C-8), 100.30 (C-6), 103.66 (C-1”), 114.31 (C-2’), 116.08 (C-5’), 123.79 (C-6’), 105.47 (C-4a), 123.10 (C-1’), 135.36 (C-3), 148.42 (C-4’), 150.86 (C-3’), 158.51 (C-2), 158.57 (C-8a), 163.05 (C-5), 167.16 (C-7) and 179.29 (C-4).

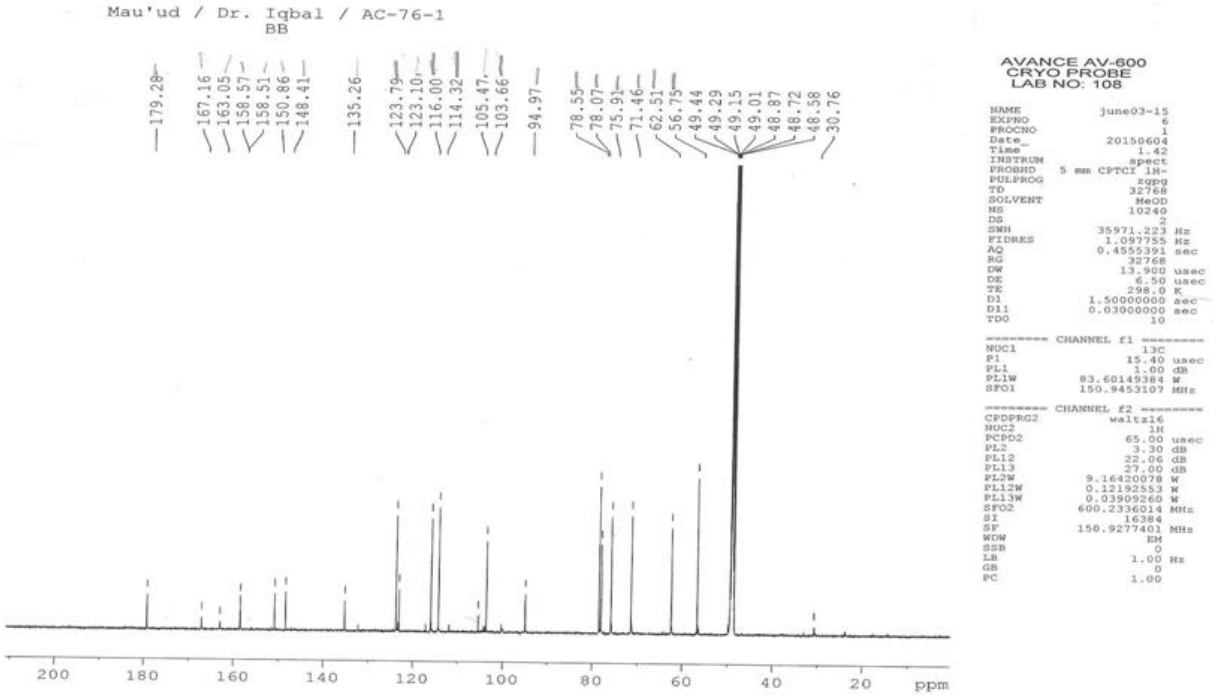

Figure 4.19: C-13 NMR Spectrum for Compound 2

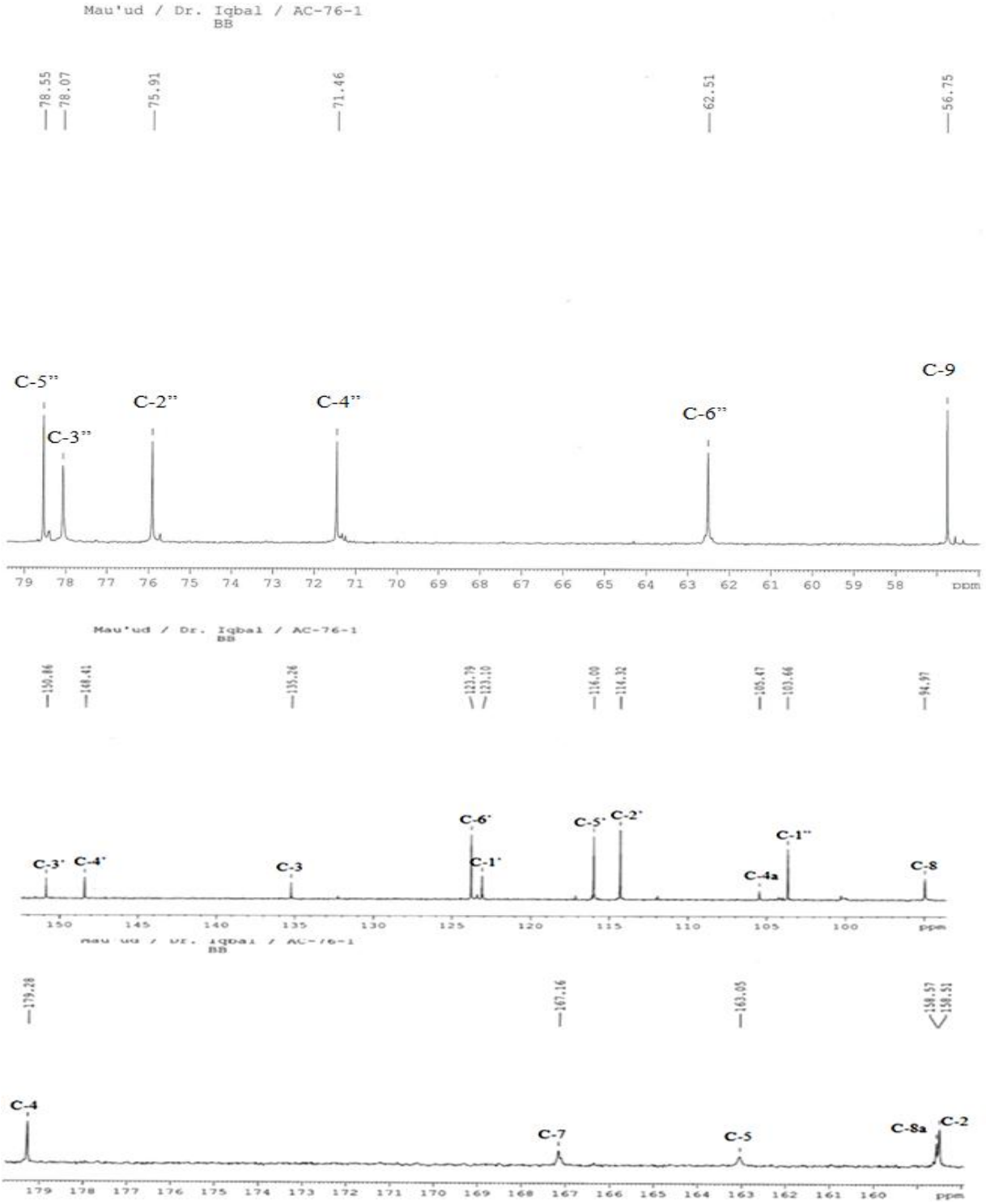

Figure 4.20: Expanded C-13 Spectrum of Compound 2

The DEPT 90 spectrum (Figure 4.21) revealed 10 methine carbon signals as follows: 71.46 (C-4”), 75.91 (C-2”), 78.08 (C-5”), 78.55 (C-3”), 94.97 (C-8), 100.30 (C-6), 103.66 (C-1”), 114.31 (C-2’), 116.08 (C-5’) and 123.79 (C-6’).

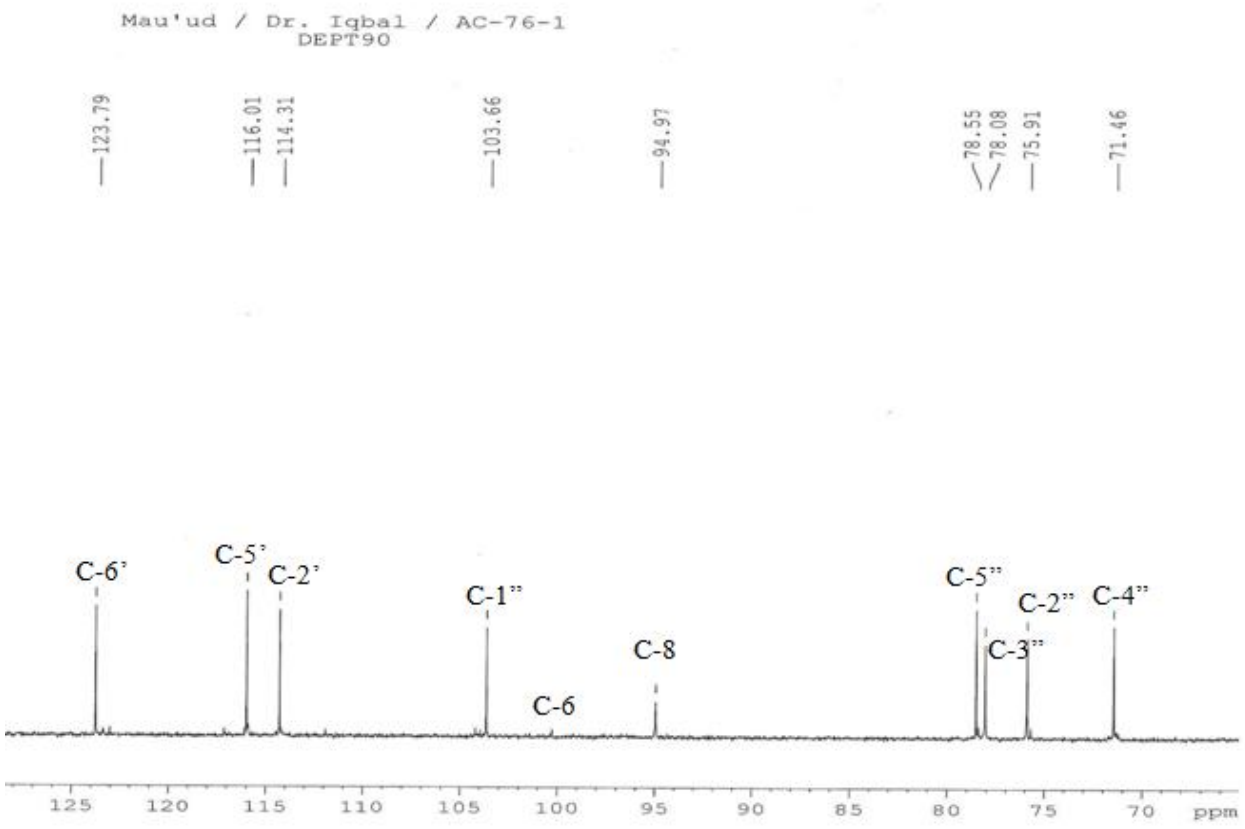

Figure 4.21: DEPT 90 Spectrum of Compound 2

The DEPT 135 spectrum (Figure 4.22) revealed one methylene carbons (appearing as negative peak) and methyl (methoxy) carbon as follows: 62.51 (C-6”) and 56.76 (C-9) respectively. Eight quaternary carbons identified included 105.47 (C-4a), 135.36 (C-3), 148.42 (C-4’), 150.86 (C-3’), 158.51 (C-2), 158.57 (C-8a), 163.05 (C-5), 167.16 (C-7) while the carbonyl chemical shift appeared at 179.29 (C-4).

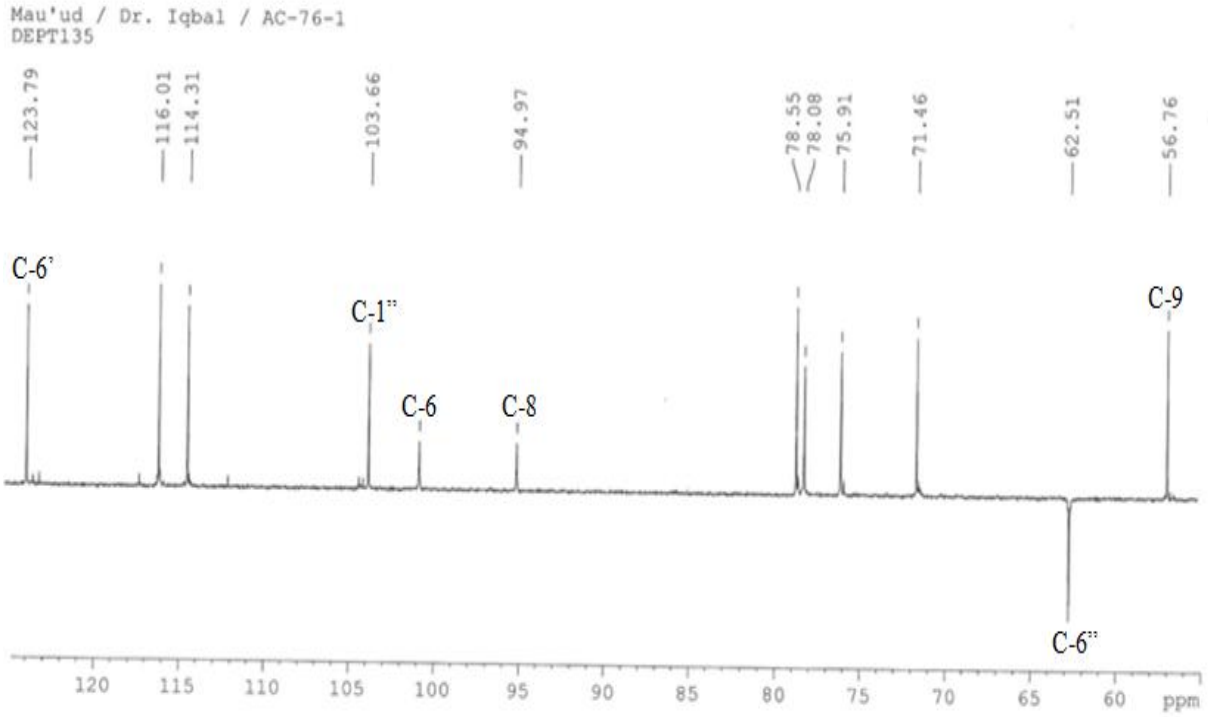

Figure 4.22: DEPT 135 Spectrum of Compound 2

4.10 Two Dimensional (2D) Spectral Analyses of Compound 2

4.10.1 ^{1}H-^{1}H Correlation Spectroscopy (COSY) of Compound 2

The ^{1}H-^{1}H COSY of compound **2** revealed correlation (Figure 4.23-Figure 4.25) between the following protons: H1 (7.92) #H2 (7.57); (3.94); H2 (7.57) #H3 (6.91), H4 (6.37) #H5 (6.18) and #H6" (3.53); H1" (5.38) #H2" (3.55).

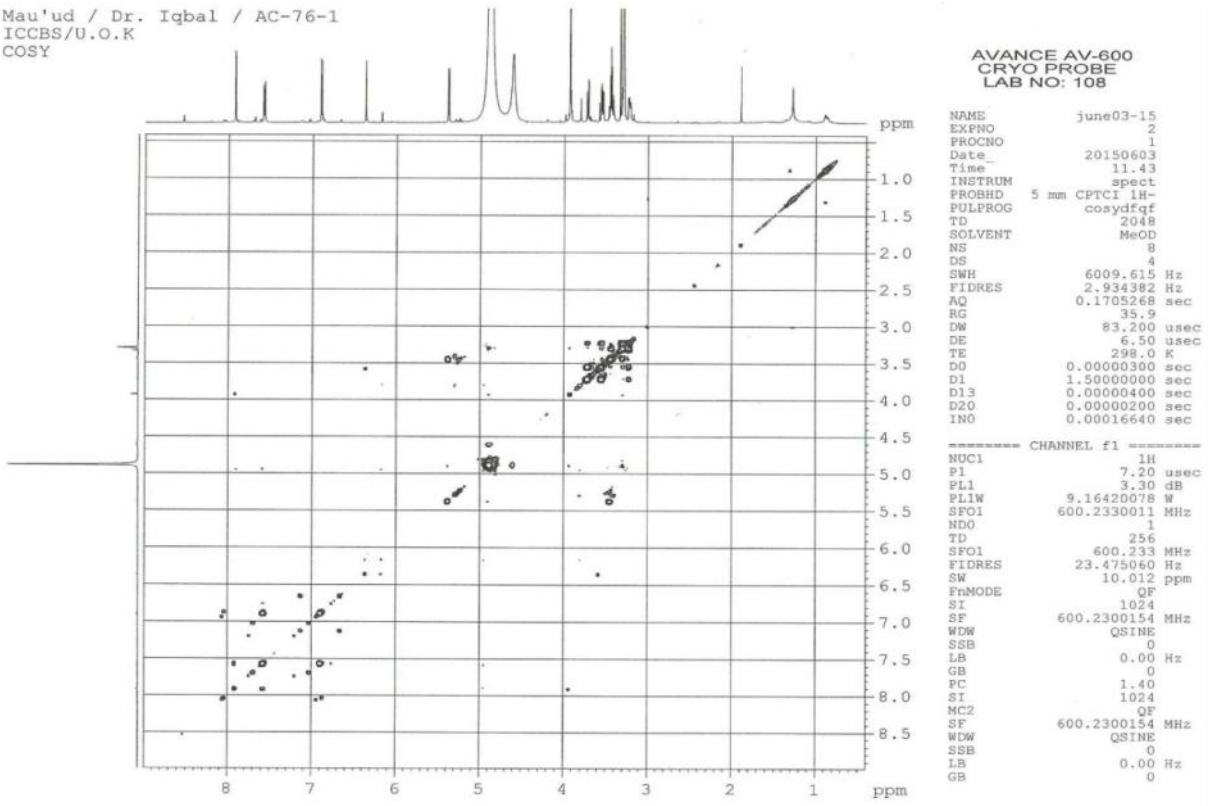

Figure 4.23: ^{1}H-^{1}H COSY Spectrum for Compound 2

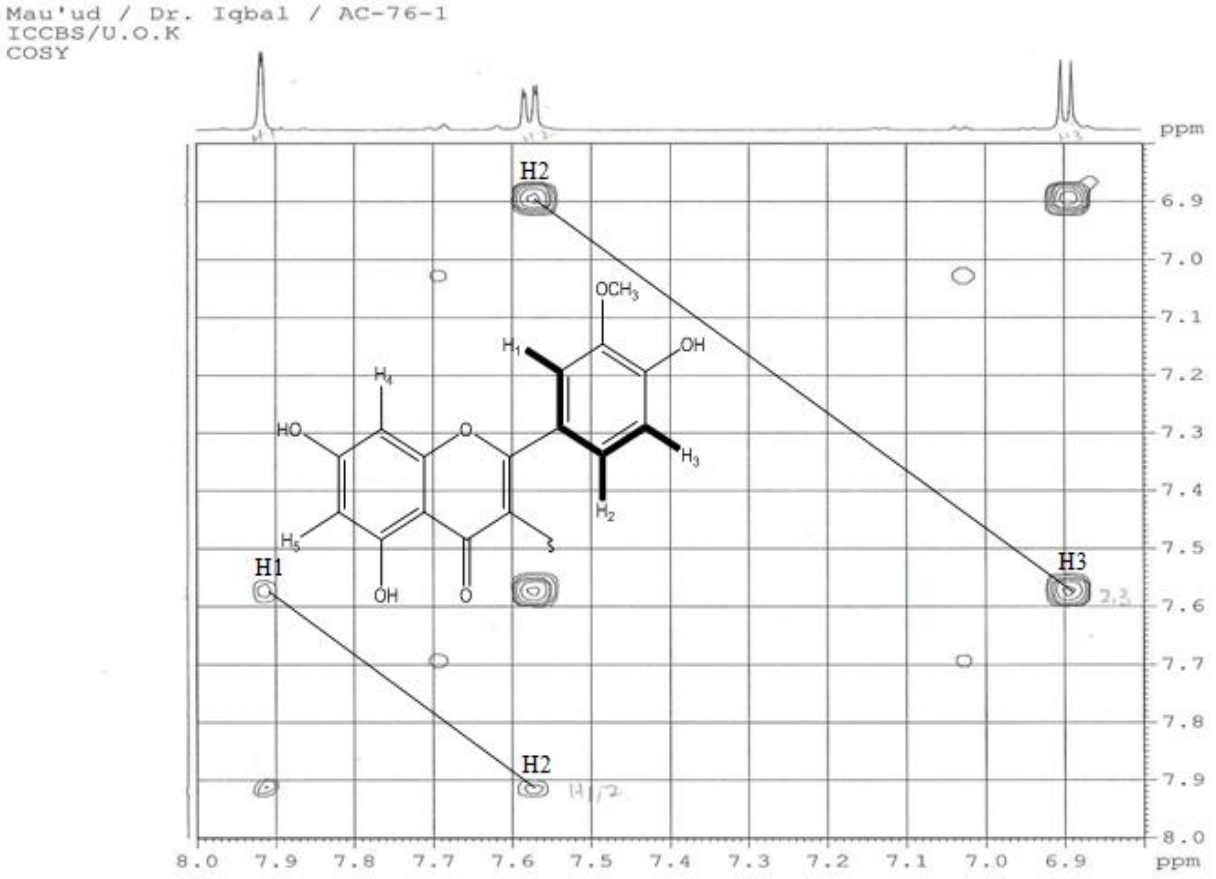

Figure 4.24: ^{1}H-^{1}H COSY Expanded Regions (6.9-8.0 ppm) of Compound 2

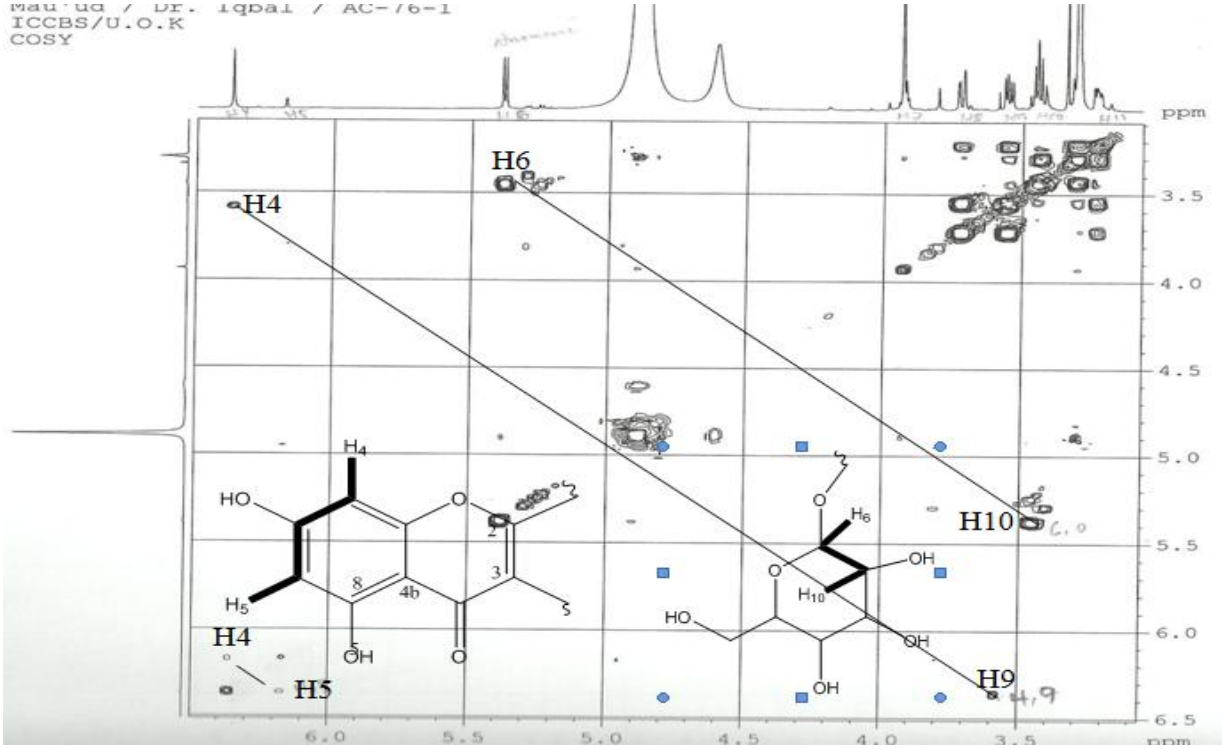

A

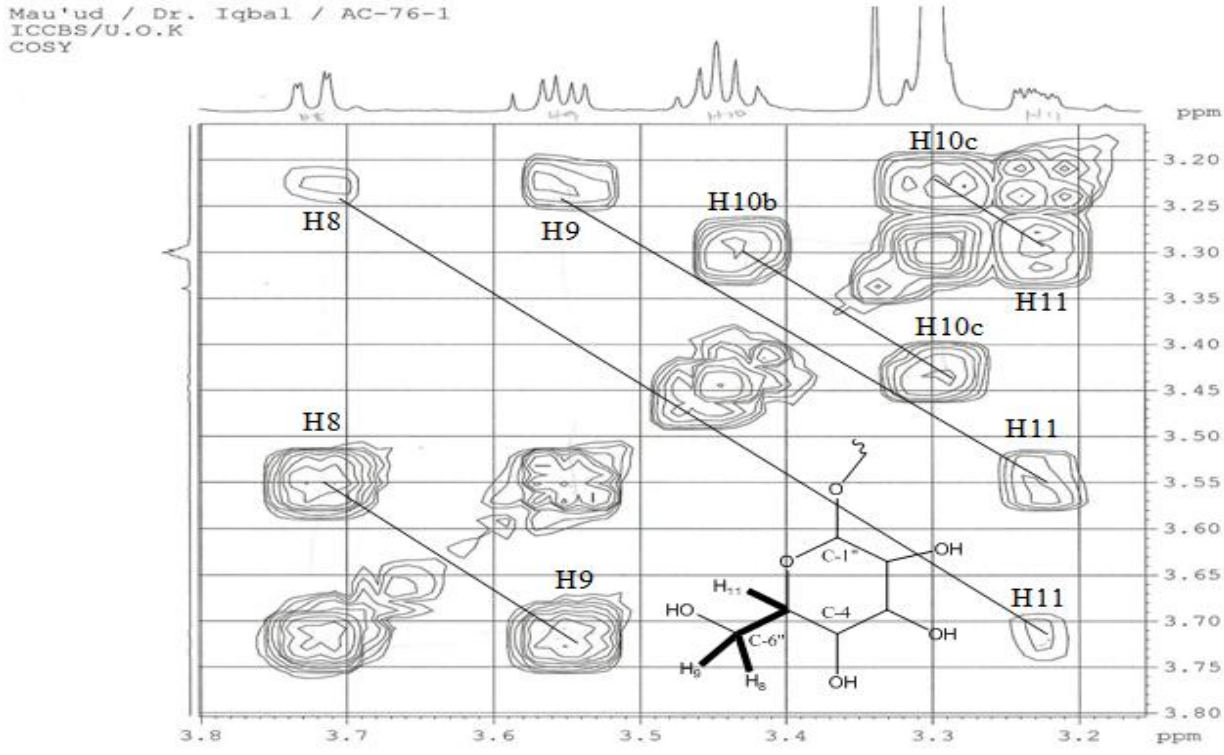

B

Figure 4.25: **^{1}H-^{1}H COSY Expanded Regions 3.5-6.0 ppm (A) and 3.2-3.8 ppm (B) of Compound 2**

4.10.2 HSQC Spectral Analysis of Compound 2

Protons attached to carbons are shown on the HSQC as follows: C (123.79)#7.57, C(114.31)#7.92, C(116)#6.91, C(100)#6.18, C(94)#6.37, C(103)#5.38, C(56.76)#3.94, C(62.51)#3.70-3.74 (Figures 4.26 and 4.27).

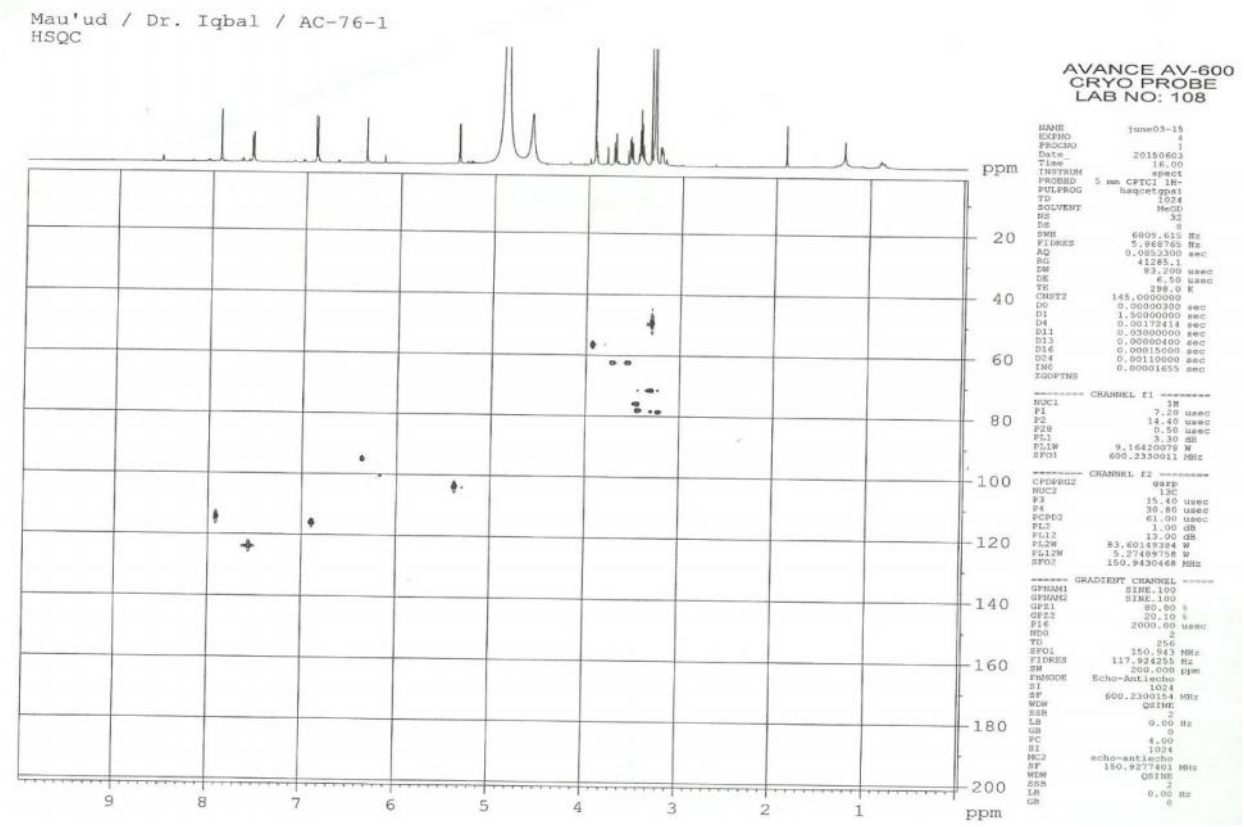

Figure 4.26: HSQC Spectrum of Compound 2

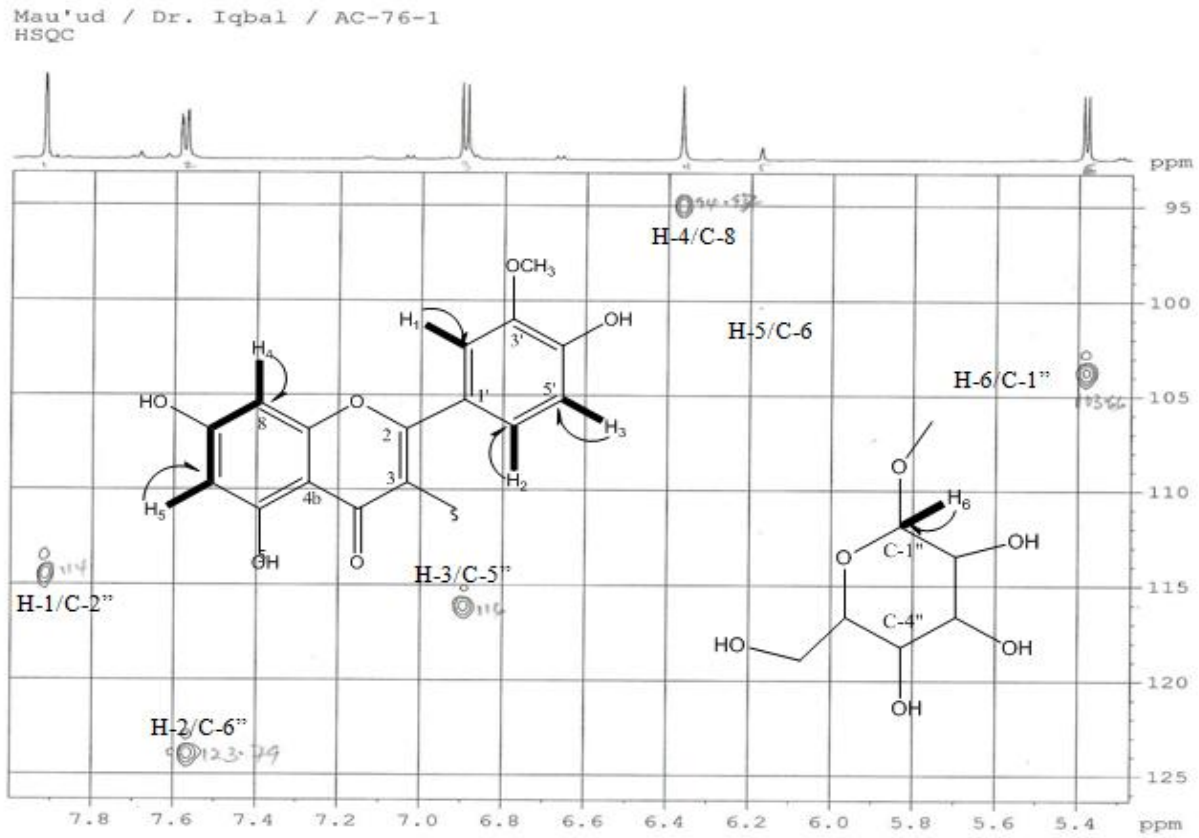

A

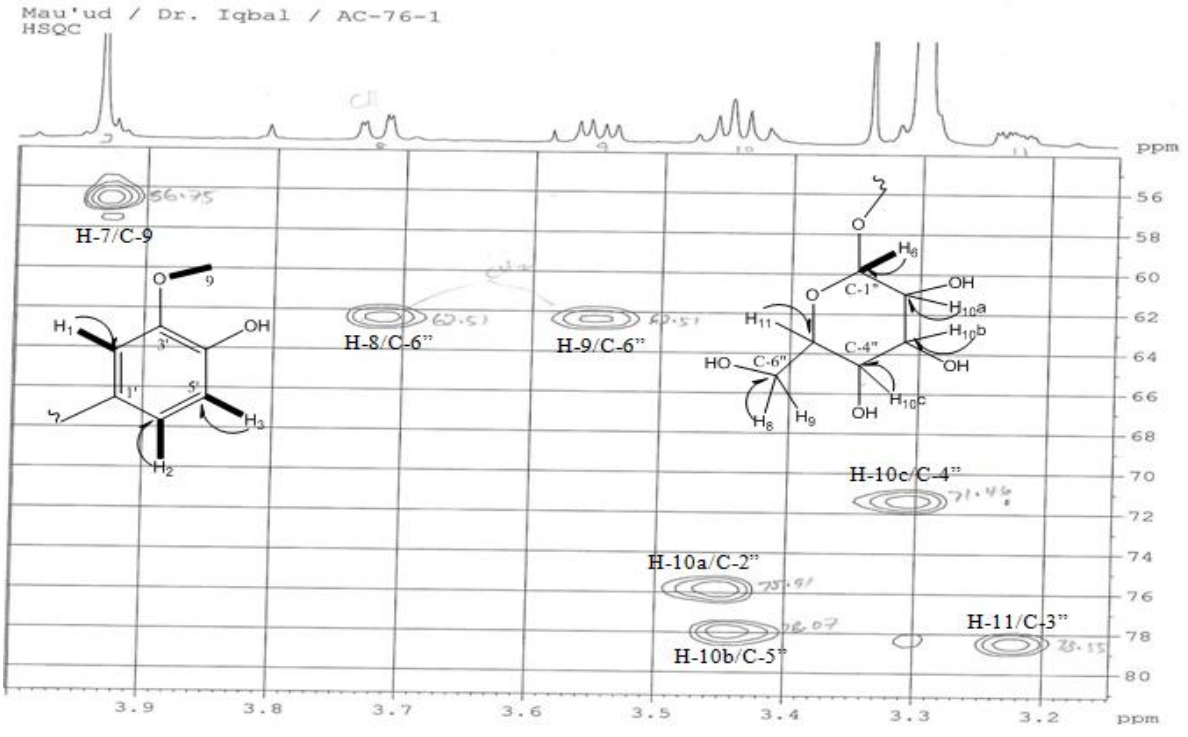

B

Figure 4.27: HSQC Expanded Spectrum of Compound 2 Showing Regions 5.4-7.8 ppm (A) and 3.2-3.9 ppm (B)

The arrow (⟶) shows the proton-carbon correlations

4.10.3 HMBC Spectral Analysis of Compound 2

The following HMBC proton-carbon 2-3 bond correlations as presented in Figures 4.28 and 4.29 were observed in the spectrum for compound 2 as follows: $^{H}\delta$ 7.92 correlated with C-158.51, C-148.42, C-123.79; $^{H}\delta$ 7.57 correlated with C-158.51, C-150.86, C-114.31, $^{H}\delta$ 6.91 correlated with C-150.86, C-148.42, C-123.79; $^{H}\delta$ 6.37 correlated with C-179.29, C-167.16, C-158.51, C-105.47, C-100.30; $^{H}\delta$ 6.1 showed correlation with C-135 while $^{H}\delta$ 3.94 correlated with 150.86.

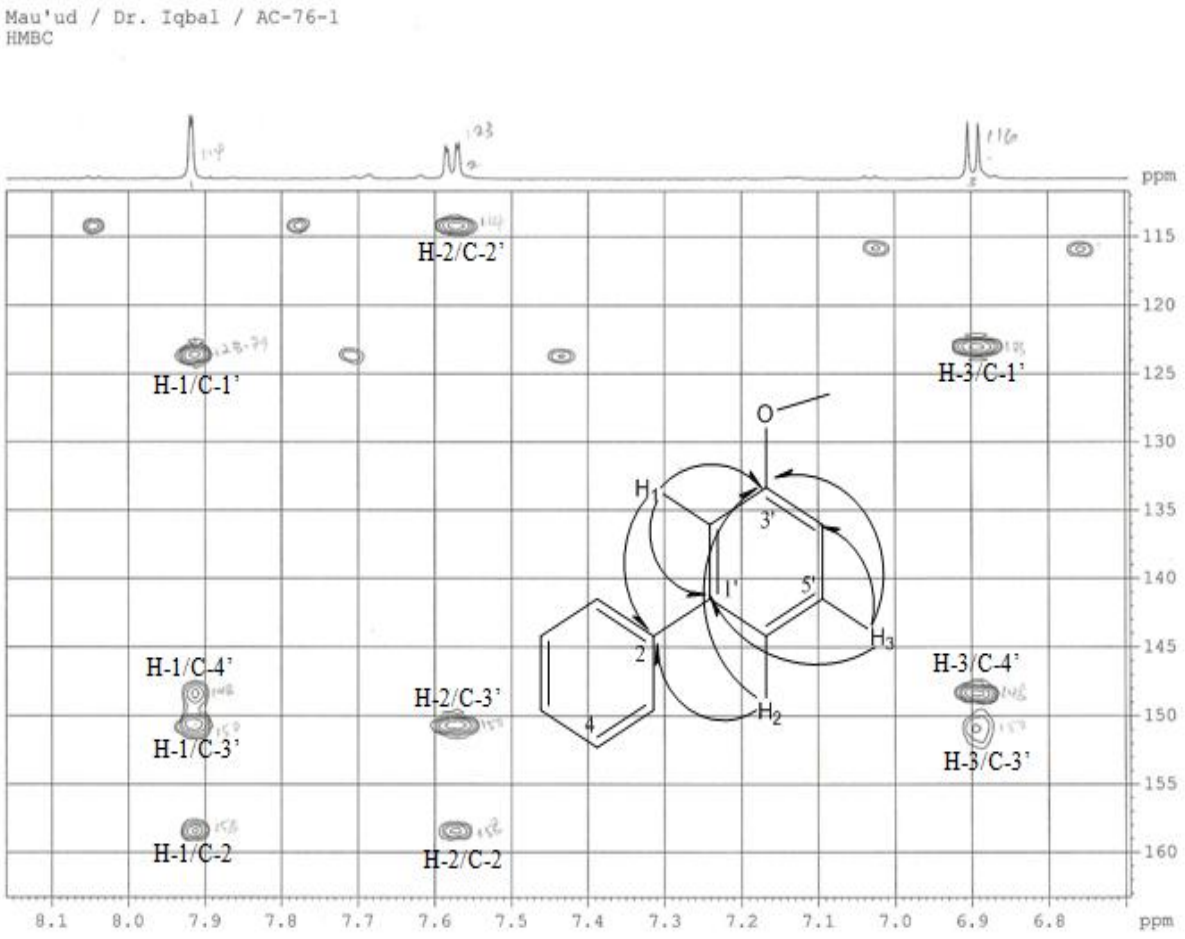

Figure 4.28: HMBC Spectrum Expanded Regions 6.8-8.1 ppm of Compound 2

The arrow (⟶) shows the proton-carbon 2-3 bond (long range) coherence

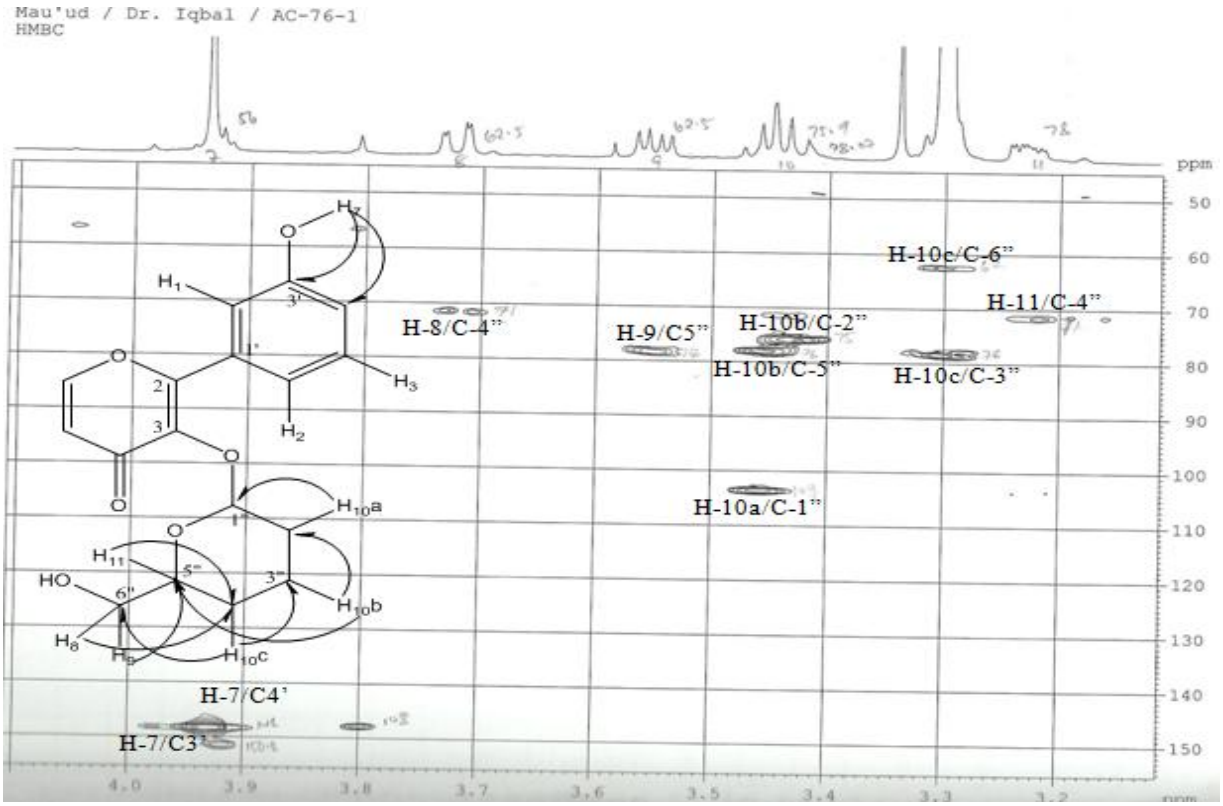

A

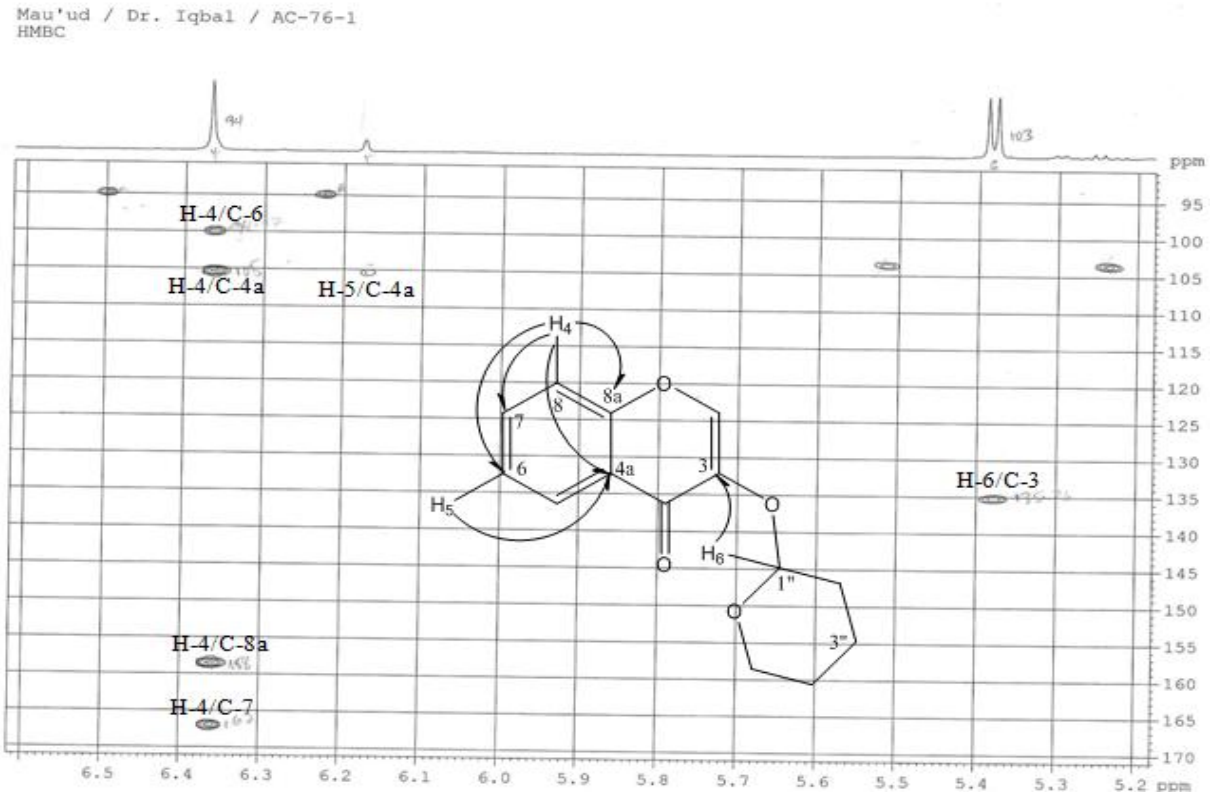

B

Figure 4.29: HMBC Spectrum of Compound 2 showing Expanded Regions 3.2-4.0 ppm (A) ppm and 5.2-6.5 ppm (B)

The arrow (⟶) shows the proton-carbon 2-3 bond (long range) coherence

4.11 Mass Spectral Analysis of Compound 2

The ESI-MS (positive mode) molecular ion for the compound appeared at m/z 479 with isotopic peaks appearing at m/z 480.1 and m/z 481.1 (Figure 4.30). The molecular mass of compound 2 is 478 (nominal mass) as indicated.

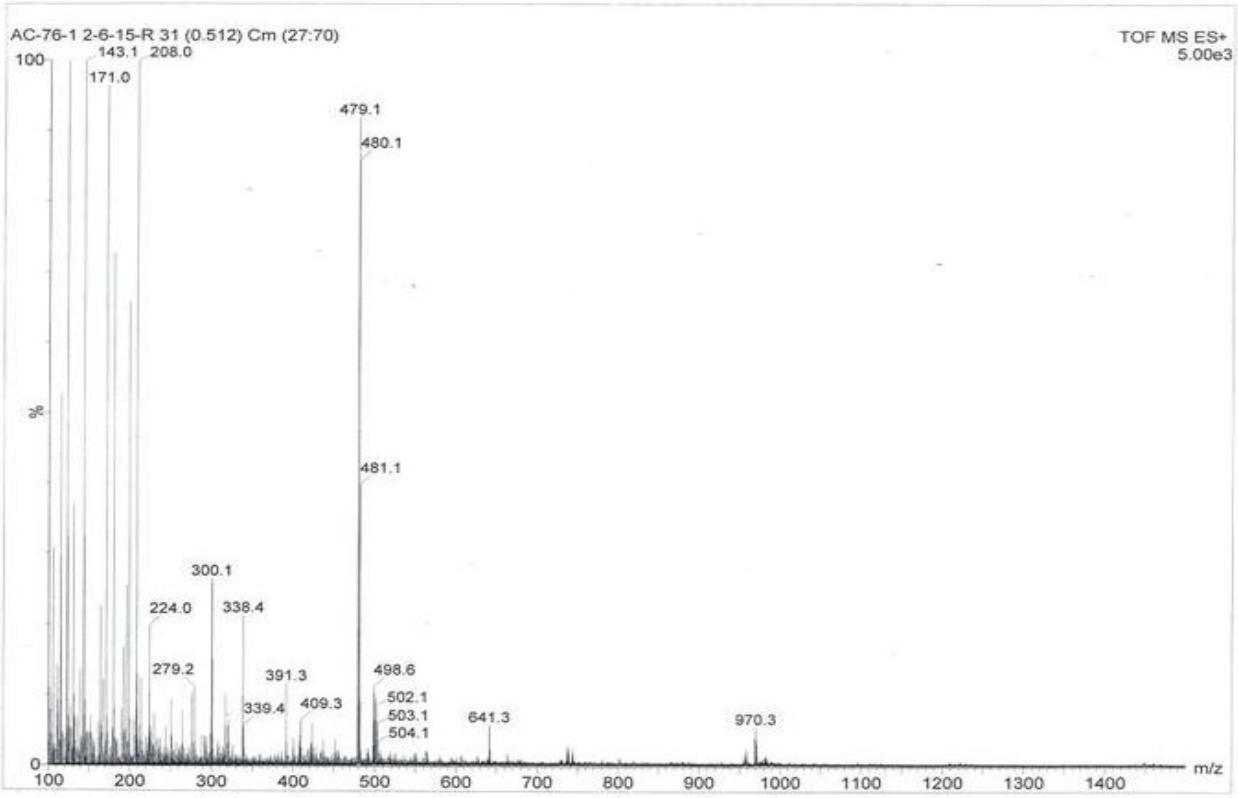

Figure 4.30: ESI-MS Spectrum of Compound 2

4.12 Summary of Characteristics and Spectroscopy Data of Compound 2

Physical appearance: yellow amorphous solid

ToF ESI-MS (positive mode): Moleuclar ion peak (M+H) m/z 479.1 with intense isotopic peaks appearing at m/z 480 and m/z 481.

Exact mass 478.1111; Molecular formula: $C_{22}H_{22}O_{12}$

Degree of unsaturation (RDB): 12

Table 4.4: Summary of 1D and 2D NMR Spectral Analyses of Compound 2

Position	$^{\delta}C$	Type	δ_H (*J* in Hz)	HMBC
2	158.51	C		
3	135.36	C		
4	179.29	C=O		
4a	105.47	C		
5	163.05	C		
6	100.30	CH	6.18 (1.6) d	4a
7	167.16	C		
8	94.97	CH	6.37 (1.6) d	4a, 6, 7, 8a
8a	158.57	C		
9	56.76	CH_3	3.94 (s)	3′
1′	123.10	C		
2′	114.31	CH	7.92 (1.6) d	2, 4′, 6′
3′	150.86	C		
4′	148.42	C		
5′	116.08	CH	6.91 (12.6)	3′, 4′, 6′
6′	123.79	CH	7.58 (2, 12.6) dd	2, 2′, 3′
1′′	103.66	CH	5.38 (10.8) d	3
2′′	75.91	CH	m	1′′
3′′	78.55	CH	m	2′′, 5′′
4′′	71.46	CH	m	3′′, 6′′
5′′	78.08	CH	3.26 (4.8) d	4′
6′′	62.51	CH_2	3.70-3.74 (2, 12) dd	4′′, 5′′

$^{\delta}C$= carbon chemical shift in ppm; $^{\delta}H$ = proton chemical shift in ppm; *J* = coupling constant; s= singlet; d= doublets; dd=doublet of doublets; m=multiplets

Proposed structure of compound 2

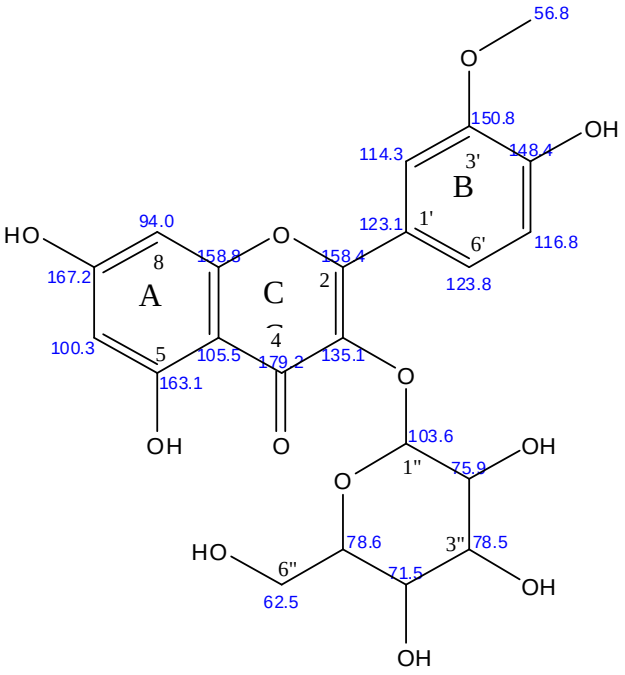

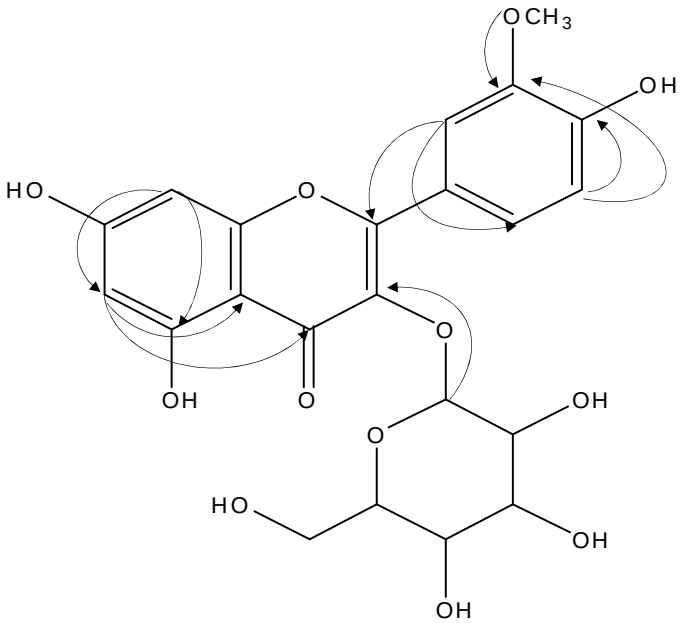

4.13 UV-Visible and FTIR Spectral Analyses of Compound 3

The UV-visible spectrum of compound 3 showed intense absorbance at 229 nm and a medium absorbance at 282 nm characteristic of conjugated aromatic pi electron system (Figure 4.31).

The characteristic functional group probably present in this compound was analysed by FTIR (Figure 4.32). The spectrum revealed absorbance in the region1664-1591 cm^{-1} typical of carbonyl group absorbance. The strong absorbance observed at 3404.1 cm^{-1} indicates presence of an amine group. The FTIR spectrum generally suggests presence of an amide linkage in the proposed structure of the compound.

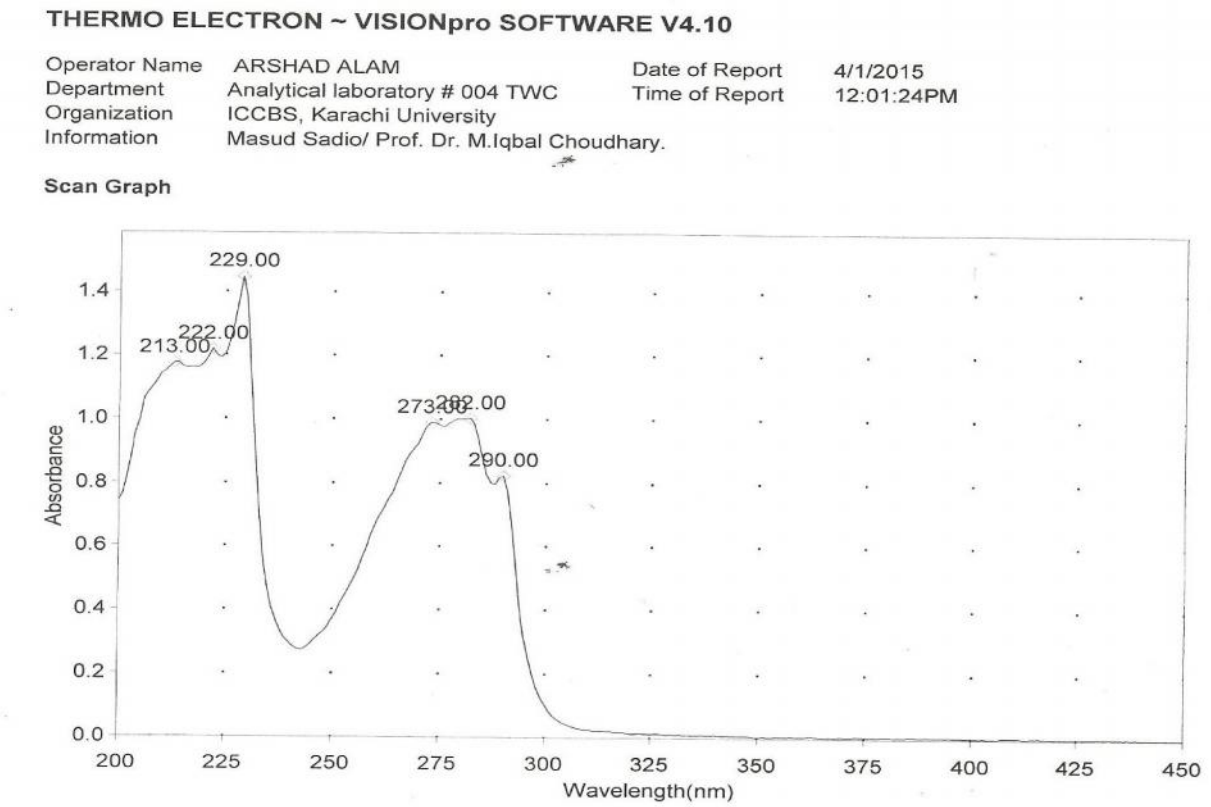

Figure 4.31: UV-visible Spectrum of Compound 3

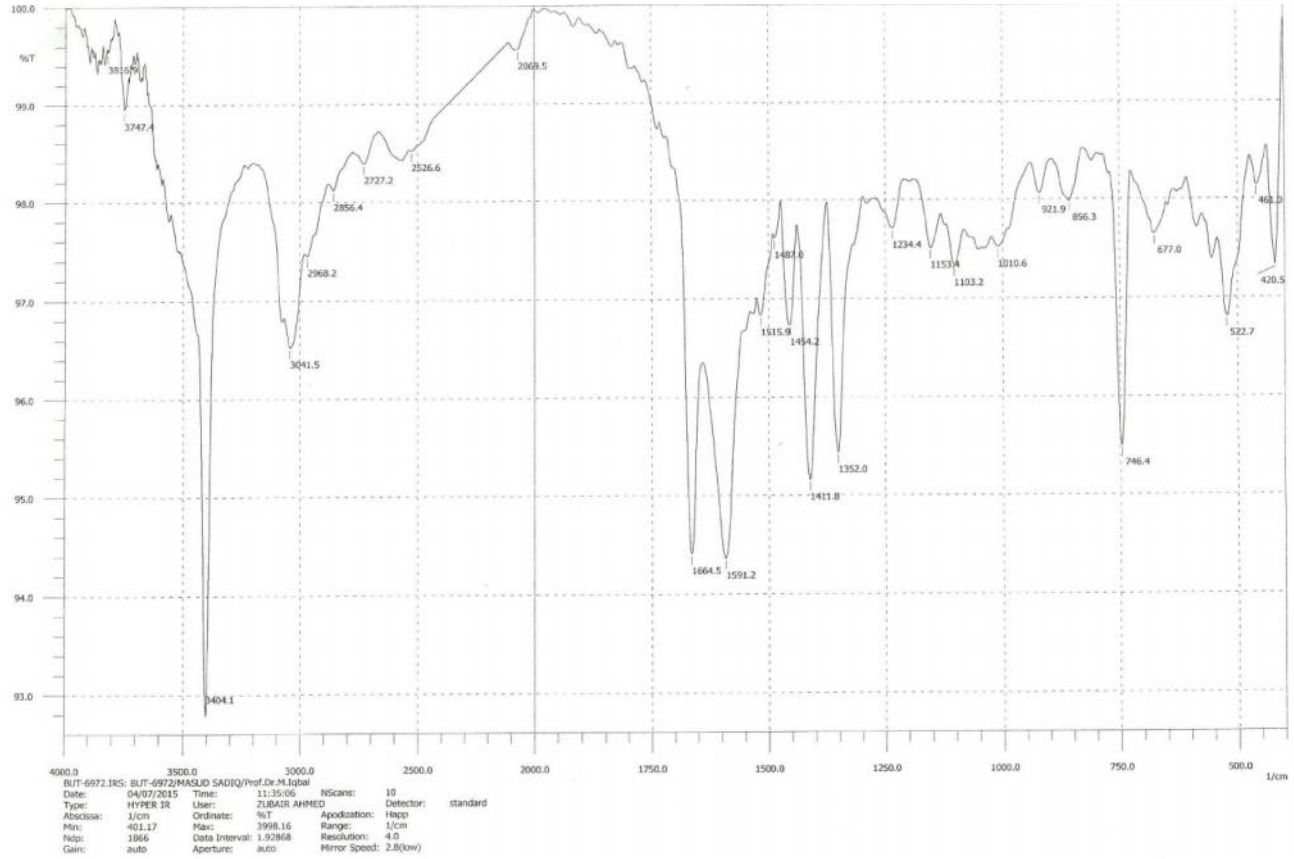

Figure 4.32: FTIR Spectrum of Compound 3

4.14 Nuclear Magnetic Resonance (NMR) Spectral Analyses of Compound 3

4.14.1 Proton (^{1}H) Nuclear Magnetic Resonance for Compound 3

The proton (^{1}H) NMR spectrum for compound **3** revealed signals in following regions: 3.14, 3.52, 3.84, 7.04, 7.11, 7.18, 7.36 and 7.70 (Figures 4.33 and 4.34).

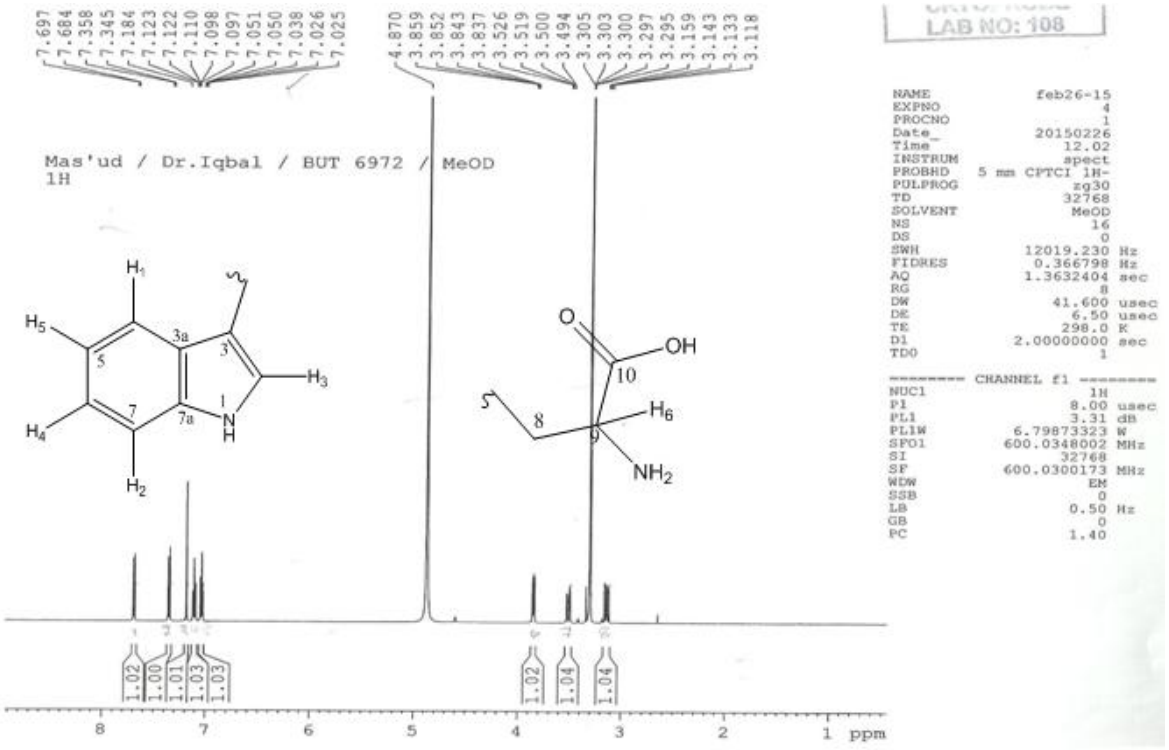

Figure 4.33: ^{1}H NMR (600MHz, MeOD) of Compound 3

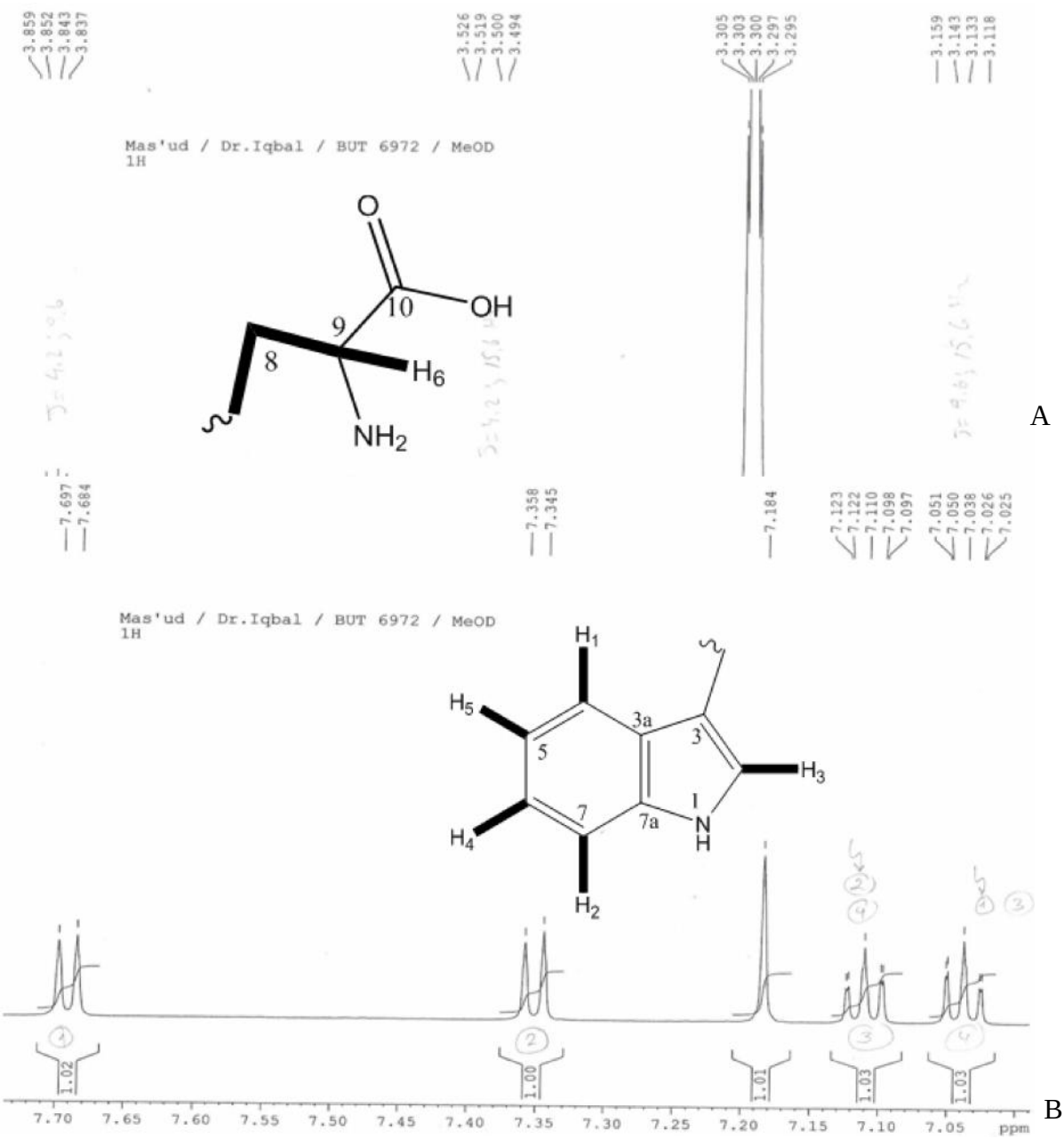

Figure 4.34: Expanded Regions 3.15-3.85ppm (A) and 7.05-7.70 ppm (B) Proton NMR Spectra for Compound 3

The thick line (▬) indicates the referenced protons

4.14.2 Carbon-13 and DEPT Spectral Analyses of Compound 3

The C-13 chemical shifts for the compound 3 (Figure 4.35) observed included: 28.50 (C-8), 56.69 (C-9), 112.43 (C-7), 119.36 (C-4), 120.11 (C-5), 122.75 (C-6), 125.16 (C-2), 109.53 (C-3), 128.45 (C-3a), 138.38 (C-7a) and 174.55 (C-10).

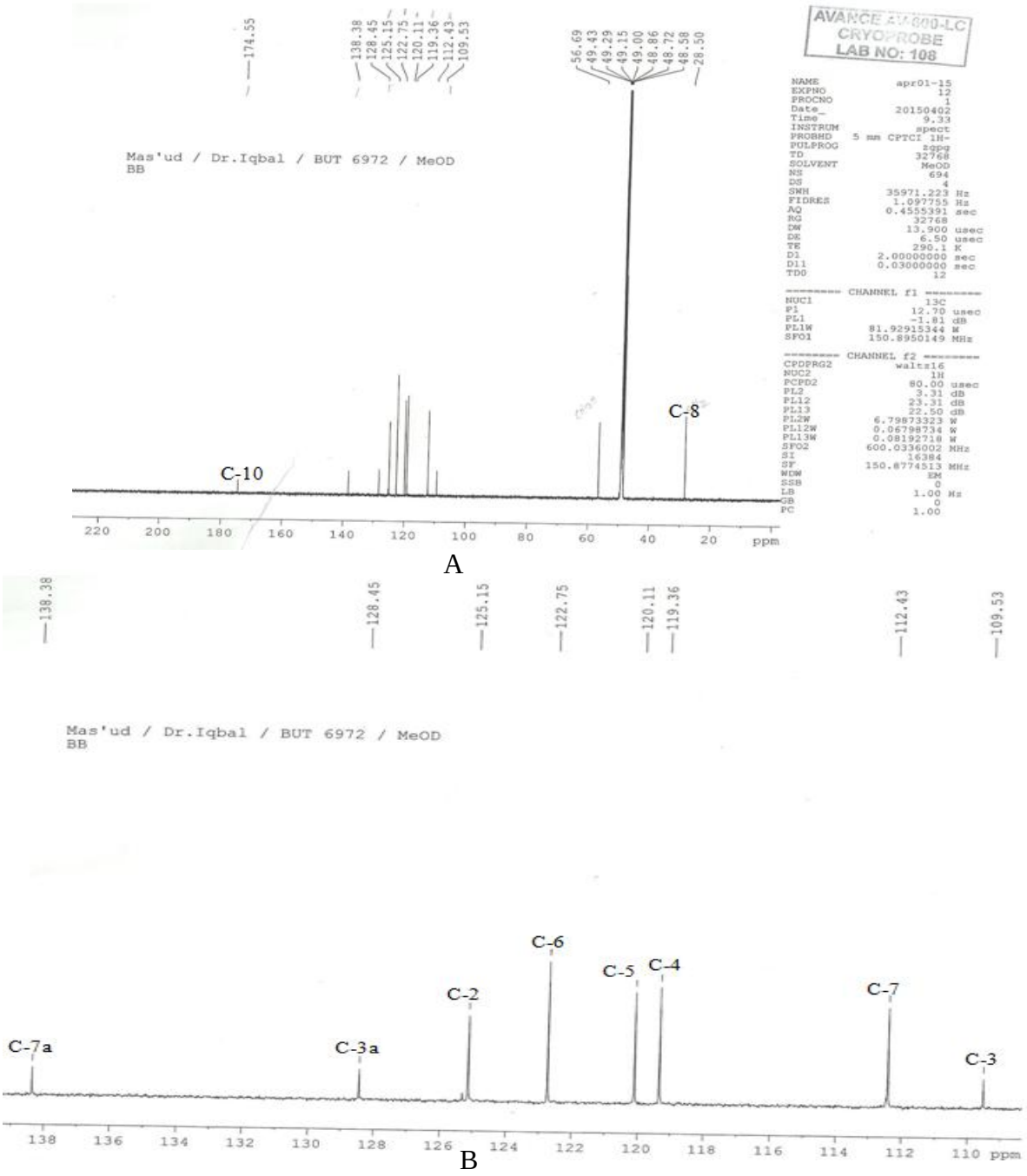

Figure 4.35: C-13 Spectrum of Compound 3 (A) and Expanded Regions 110-138 ppm (B)

Presented in Figure 4.36 is the DEPT 90 spectral analysis which revealed the following methine carbons: 56.69 (C-9), 112.43 (C-7), 119.36 (C-4), 120.11 (C-5), 122.75 (C-6) and 125.16 (C-2).

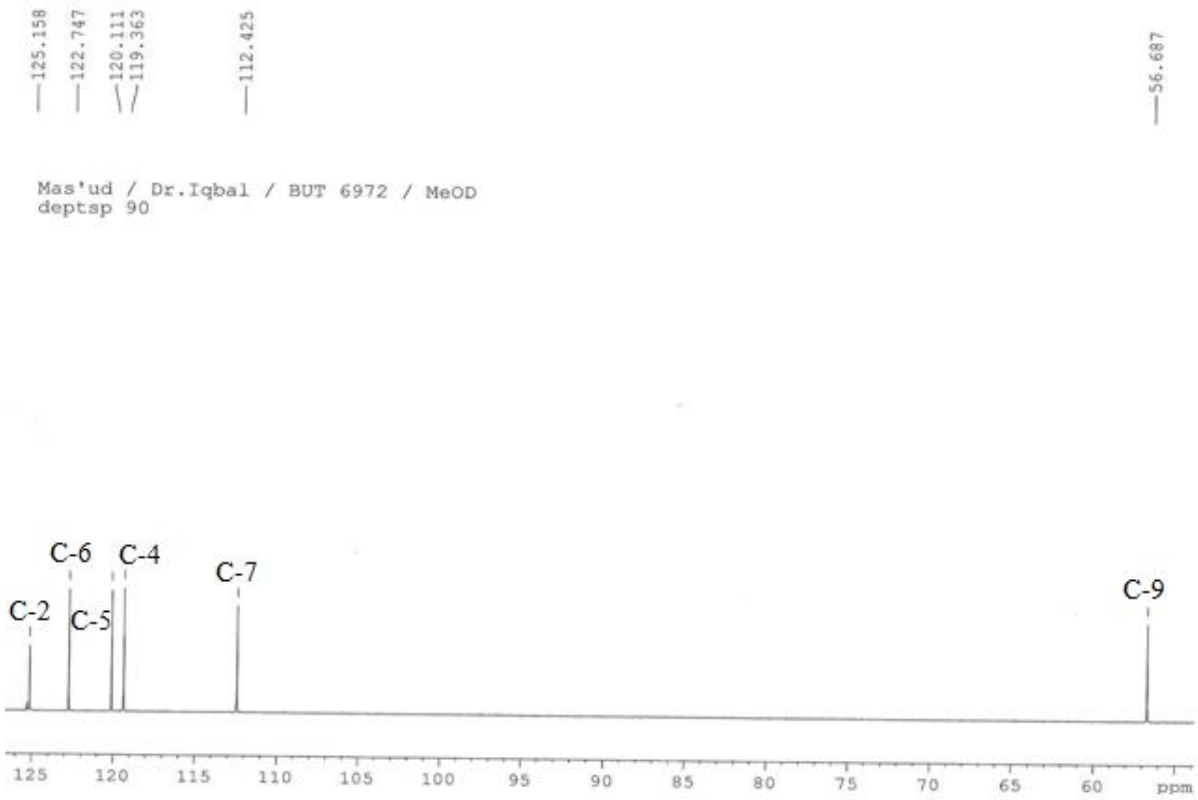

Figure 4.36: DEPT 90 Spectrum of Compound 3

DEPT 135 spectral analysis as shown in Figure 4.37 included the only methylene carbon appearing at 28.50 (C-8). Other proton bearing carbons included 56.69 (C-9), 112.43 (C-7), 119.36 (C-4), 120.11 (C-5), 122.75 (C-6) and 125.16 (C-2). Quartenary carbons identified are the following: 109.53 (C-3), 128.45 (C-3a), 138.38 (C-7a) and 174.55 (C-10).

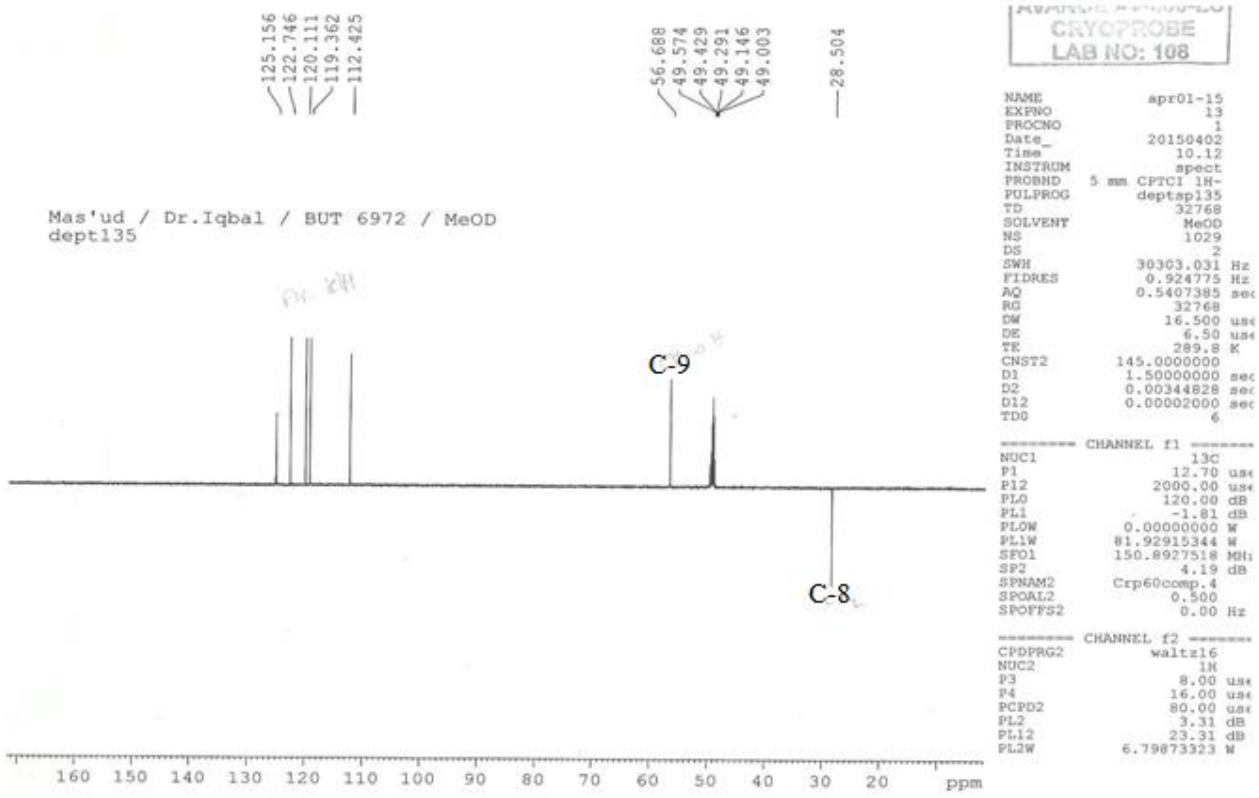

Figure 4.37: DEPT 135 Spectrum of Compound 3

4.15 Two Dimensional (2D) Spectral Analyses of Compound 3

4.15.1 ^{1}H-^{1}H Correlation Spectroscopy (COSY) of Compound 3

Figure 4.38 presents the ^{1}H-^{1}H COSY correlations for compound 3. The spectrum revealed the following correlations: H1 (7.19) correlated with #H5 (7.03); H2 (7.36) correlated with #H4 (7.11); H4 (7.11) correlated with #H5 (7.04); H6 correlated with #H7 (3.52) and H8 (3.14); H7 (3.52) correlated with #H8 (3.14).

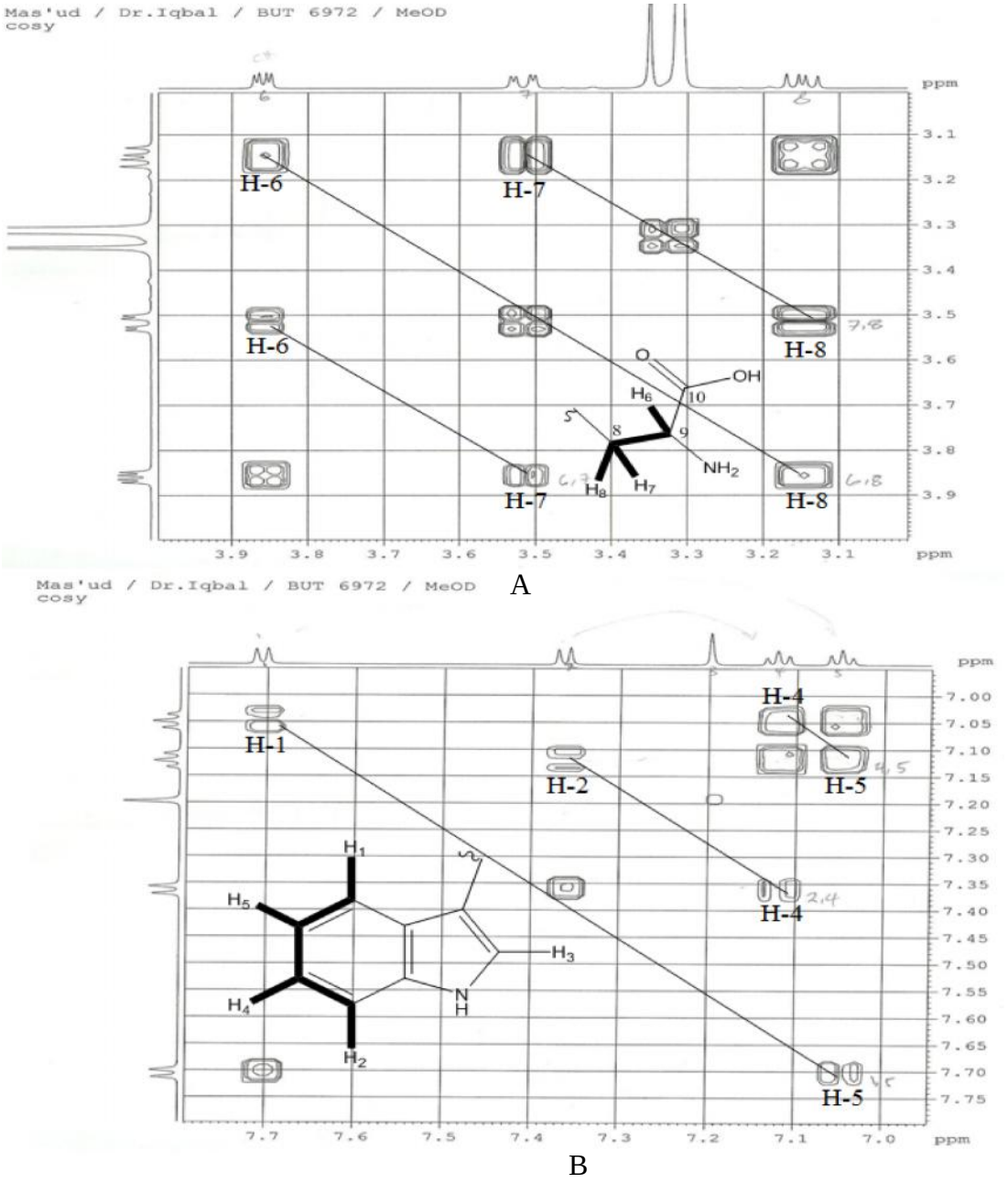

A

B

Figure 4.38: ^{1}H-^{1}H COSY Spectrum for Compound 3 Showing Expanded Regions 3.1-3.9 ppm (A) and 7.0-7.7 ppm (B)

The thick line (━) indicates the referenced protons

4.15.2 HSQC Spectral Analysis of Compound 3

The HSQC spectra (Figures 4.39 and 4.40) identified proton bearing carbons as follows: C(119.36)# 7.69, C(112.43)#7.36, C(125.15)#7.18, C(122.75)#7.11, C(120.11)#7.04, C(55.69)#3.84, C(28.50)#3.52 and 3.14.

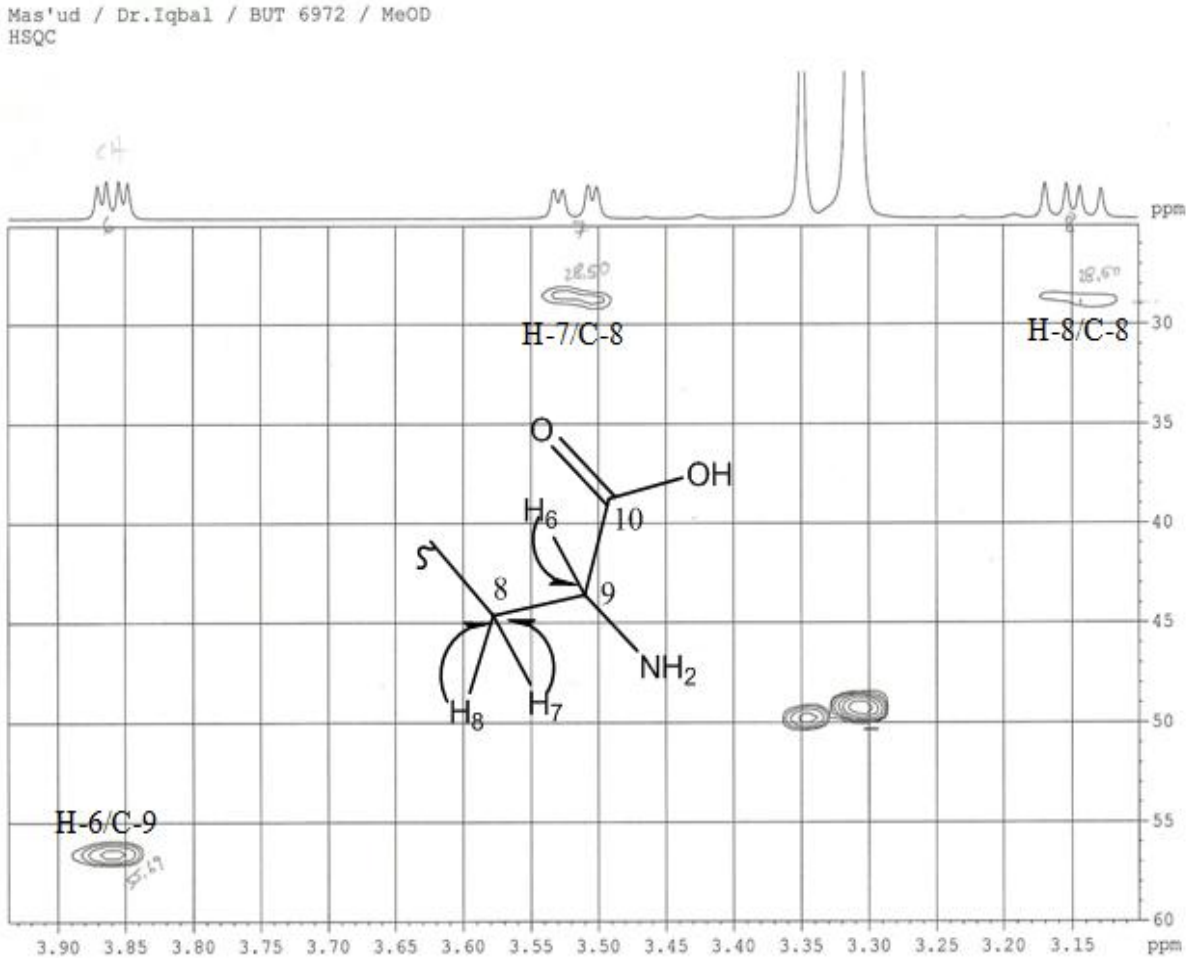

Figure 4.39: HSQC of Compound 3 Showing Expanded Regions 3.15-3.90 ppm

The arrow (⟶) shows the proton-carbon correlations

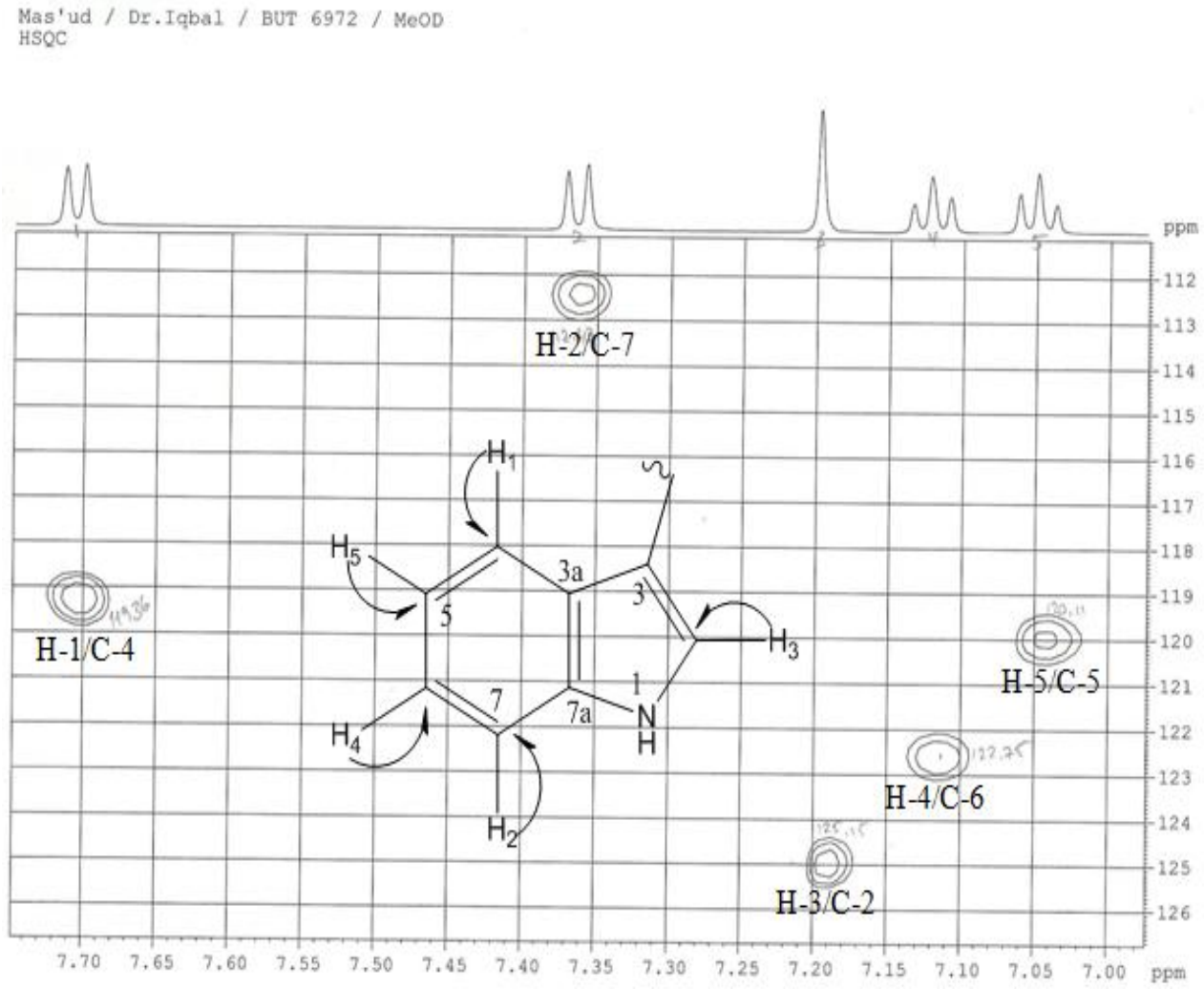

Figure 4.40: HSQC of Compound 3 Showing Expanded Regions 7.00-7.70 ppm

The arrow (⟶) shows the proton-carbon correlations

4.15.3 HMBC Spectral Analysis of Compound 3

The HMBC spectrum of compound **3** revealed long range proton - carbon correlations as shown Figures 4.41 and 4.42: $^{\delta}$H 7.69 correlated with C-109.53, C-112.43, C-122.75, C-128.45 and C-138.38; $^{\delta}$H 7.34 correlated with C-120.11, C-125.15 and 128.45; $^{\delta}$H 7.18 correlated with C-28.50, C-109.53, C-128.45 and C-138.38; $^{\delta}$H 7.11 correlated with C-120.11, C-119.36 and C-138.38 $^{\delta}$H 7.04 correlated with C-112.43 and C-128.45; $^{\delta}$H 3.84 correlated with C-109.53 and C-174.55; $^{\delta}$H 3.52 showed correlation with C-109.53, C-121.15, C-128.45 and C-174.55; $^{\delta}$H 3.14 correlated with C-109.53, C-125.15, C-128.45 and C-174.55.

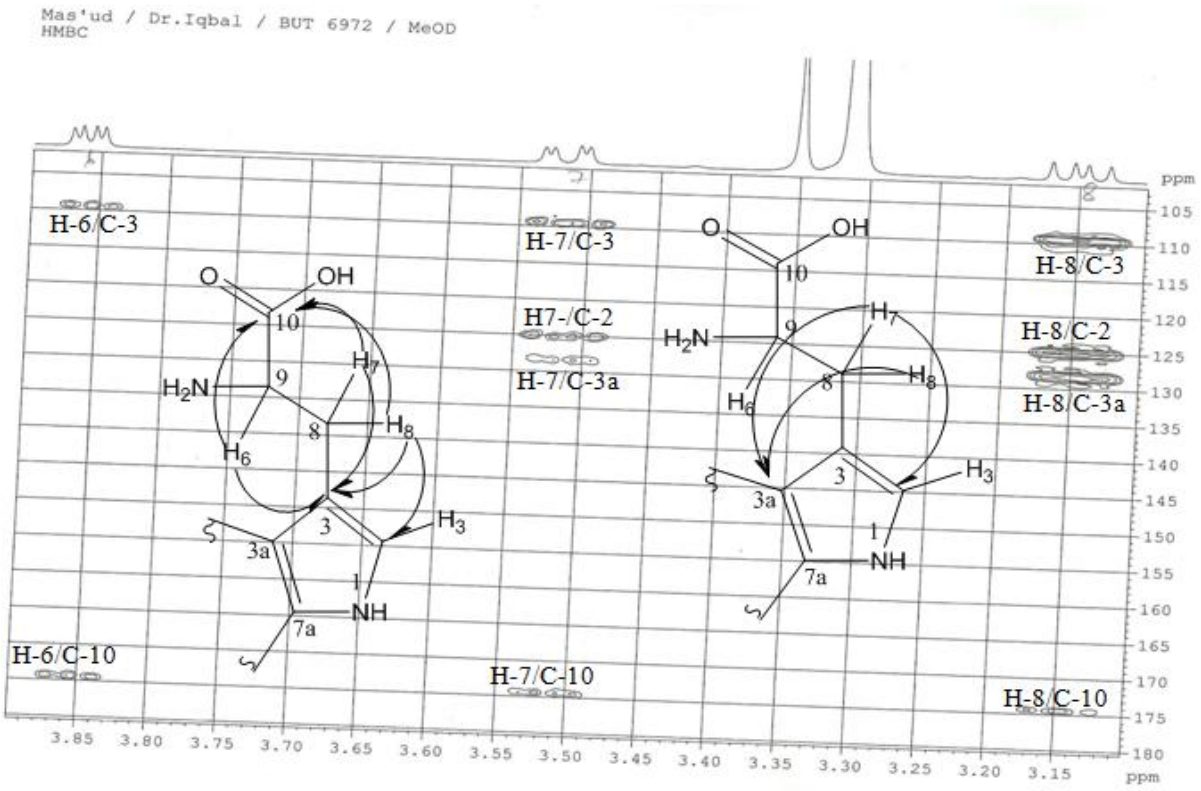

Figure 4.41: HMBC Spectrum of Compound 3 Showing Expanded Region 3.15-3.85 ppm

The arrow (⟶) shows the 2-3 bond long range proton-carbon correlations

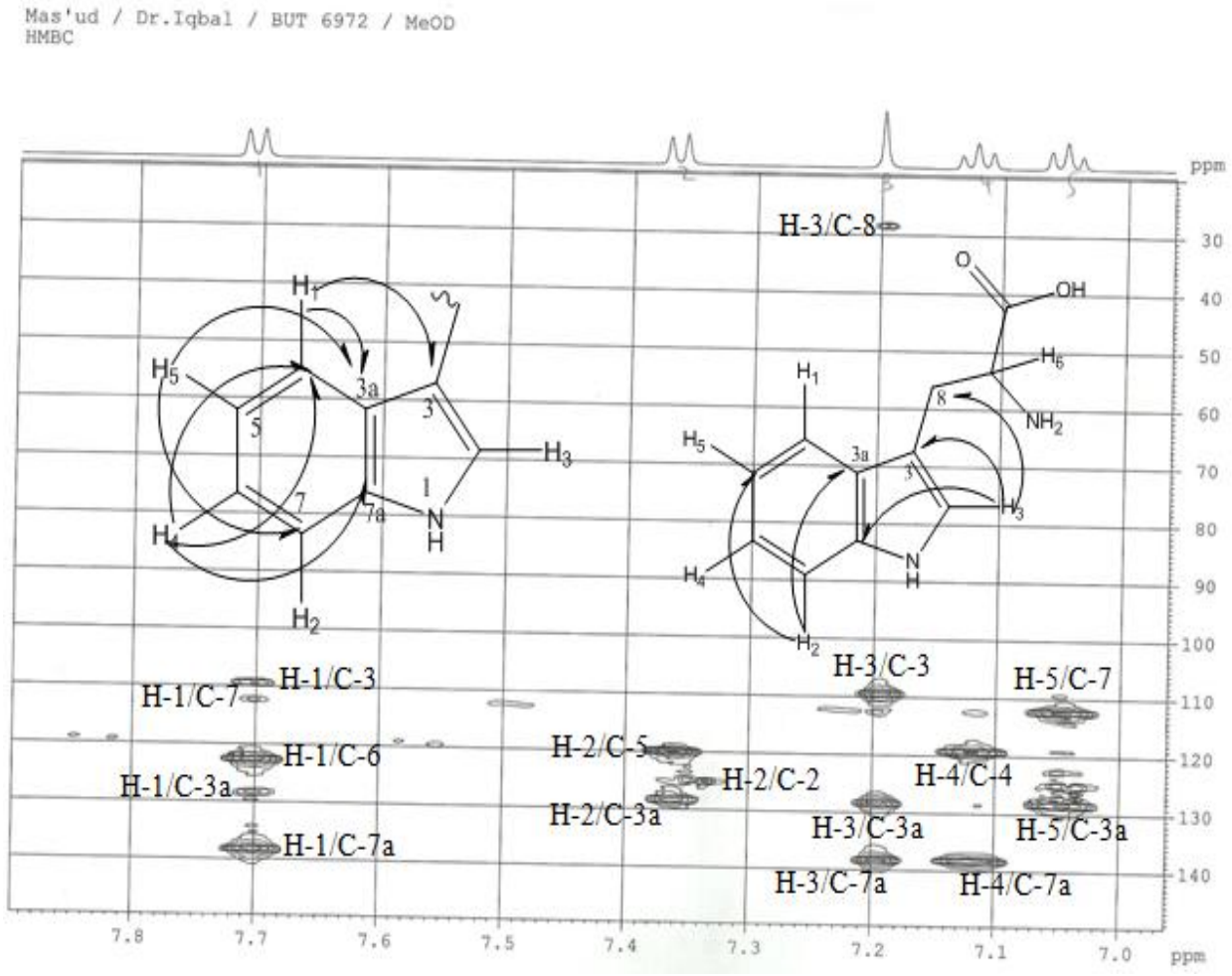

Figure 4.42: HMBC Spectrum of Compound 3 Showing Expanded Region 7.0-7.8 ppm

The arrow (⟶) shows the 2-3 bond long range proton-carbon correlations

4.16 Mass Spectral Analysis of Compound 3

The EI-MS spectrum of compound 3 revealed a molecular ion peak with m/z 204.1 and a base peak with m/z 130 (Figure 4.43 A). the molecular mass for the compound was also determined using ESI-MS ToF (positive mode) technique and a molecular ion at m/z 205 with an intense peak also appearing at m/z 188 (Figure 4.43 B)

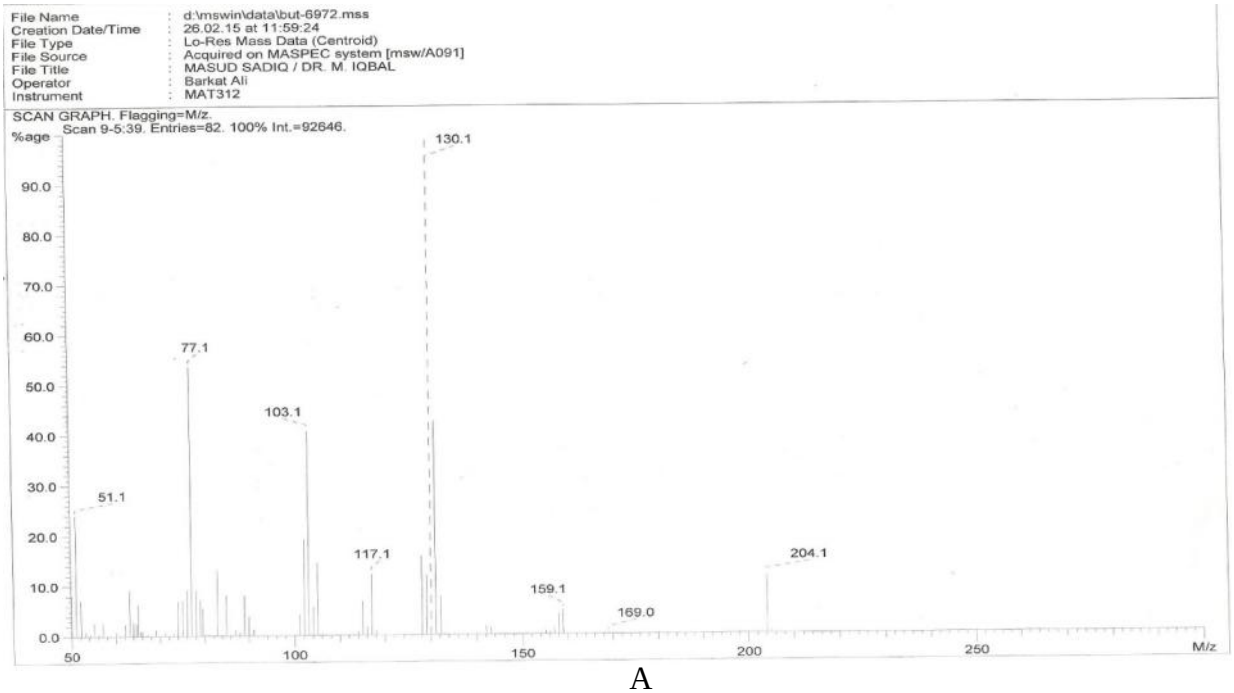

A

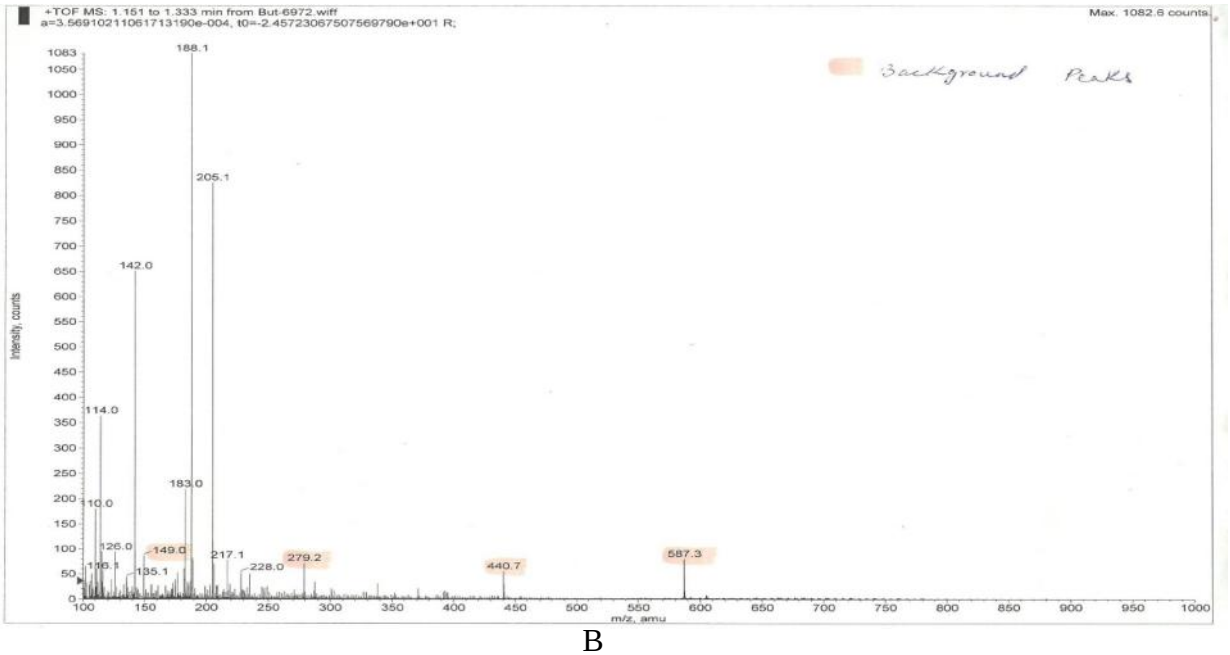

B

Figure 4.43: EI-MS (A) and ESI-MS (B) Spectra of Compound 3

4.17 Summary of Characteristics and Spectroscopy Data of Compound 3

Physical appearance: pale whitish-yellow, amorphous.

UV-Vis: 229 nm, 273 nm, 290 nm

FTIR: 3404.1 cm^{-1} (s), 3041.5 cm^{-1} (m), 1664.5-1591 cm^{-1} (m, doublet), 1411 cm^{-1} (m) 1352 cm^{-1} (m).

EI-MS: M^* m/z 204.1;

ESI-MS (ToF positive mode): $M\text{-}H^*$ m/z 205.1

Exact mass: 204.0899

Molecular formula: $C_{11}H_{12}N_2O_2$

Degree of unsaturation (RDB): 7

Table 4.5: ^{1}H and ^{13}C NMR Chemical Shifts and Proton Integration for 3

Position	$^{\delta}C$	Type	δ_H (*J* in Hz)	HMBC
2	125.16	CH	7.18 (s)	3, 3a, 7a, 8
3	109.53	C		
3a	128.45	C		
4	119.36	CH	7.69 (7.8) d	3, 3a, 6, 7, 7a
5	120.11	CH	7.04 (0.6, 7.8) td	3a, 7,
6	122.75	CH	7.11 (0.6, 7.8) d	4, 5, 7a
7	112.43	CH	7.36 (7.8) d	2, 3a, 5
7a	138.38	C		
8	28.50	CH_2	3.52, 3.14 (4.2, 15.6; 9.6, 15.6) dd, dd	2, 3, 3a, 5, 10
9	55.69	CH	3.84 (4.2, 9.6) dd	3, 10
10	174.55	C=O		

$^{\delta}C$= carbon chemical shift in ppm; $^{\delta}H$ = proton chemical shift in ppm; *J* = coupling constant; s= singlet; d= doublets; dd=doublet of doublets; td = triplet of doublets

Proposed Structure of Compound 3

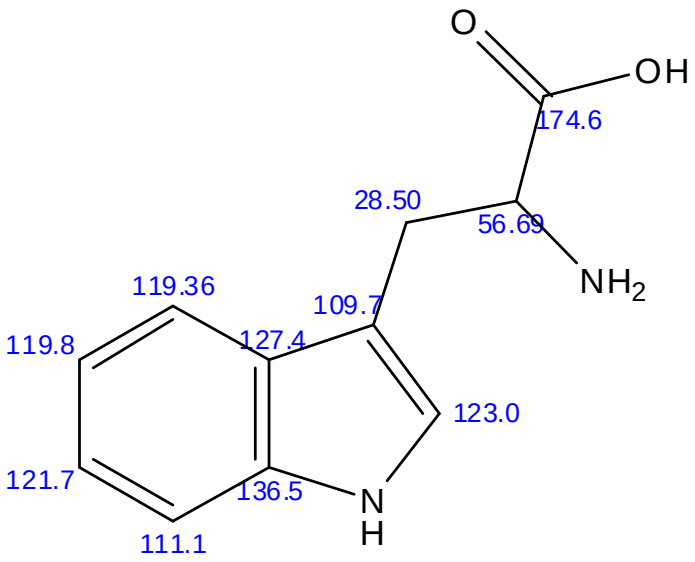

4.18 Nuclear Magnetic Resonance (NMR) Spectral Analyses of Compound 4

4.18.1 Proton (^{1}H) Nuclear Magnetic Resonance for compound 4

The proton (^{1}H) NMR spectrum of compound **4** revealed characteristic proton chemical shifts: 5.33, 3.49, 2.27, 2.21, 1.96, 0.98, 0.88 and 0.78 (Figure 4.44).

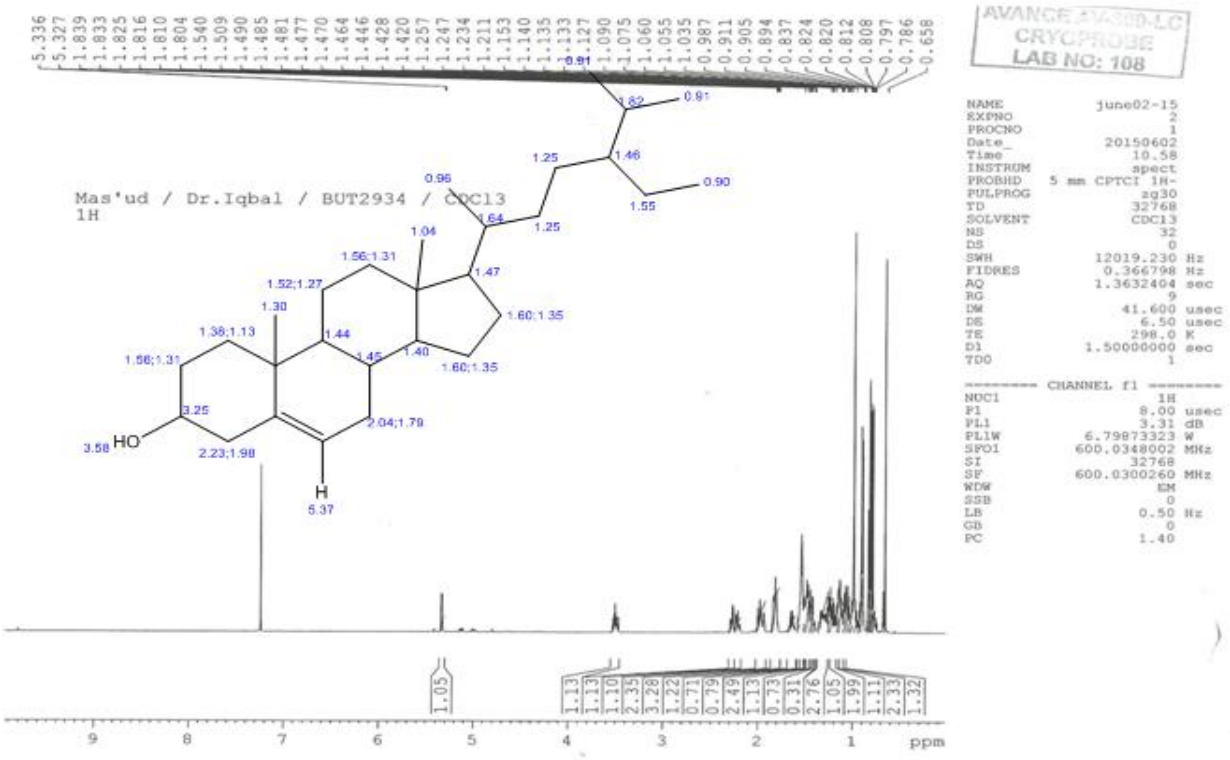

Figure 4.44: ^{1}H NMR (600 MHz, $CDCl_3$) of Compound 4

4.18.2 Carbon-13 and DEPT Spectral Analyses of Compound 4

The C-13 chemical shifts (Figures 4.45 and 4.46) observed for compound 4 are presented as follows: 11.83 (C-29), 11.95 (C-24), 18.74 (C-28), 18.97 (C-19), 19.38 (C-26), 19.82 (C-27), 21.04 (C-11), 22.99 (C-23), 24.27 (C-16), 25.92 (C-15), 28.23 (C-21), 29.08 (C-25), 31.62 (C-2), 31.85 (C-7), 31.88 (C-8), 33.87 (C-20), 36.11 (C-18), 37.19 (C-10), 37.21 (C-1), 39.70 (C-12), 42.23 (C-13), 42.26 (C-4), 45.74 (C-22), 50.04 (C-9), 55.96 (C-17), 56.71 (C-14), 71.78 (C-3), 121.72 (C-6) and 140.70 (C-5).

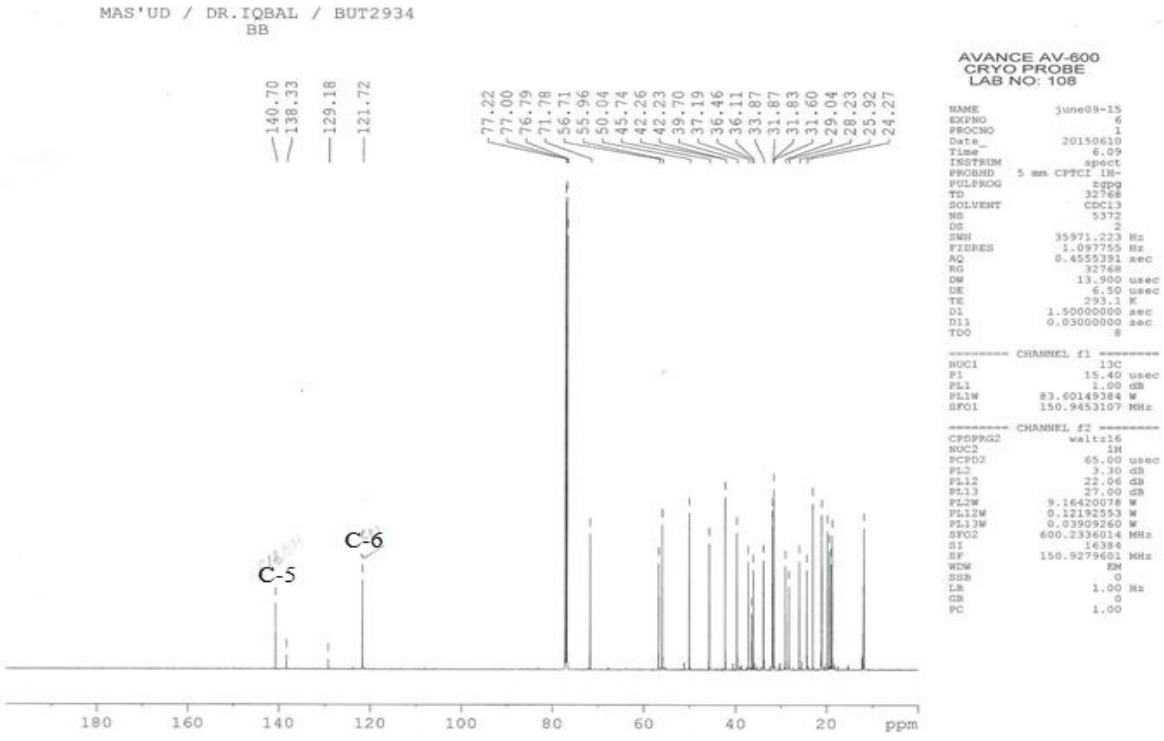

Figure 4.45: C-13 Spectrum of Compound 4

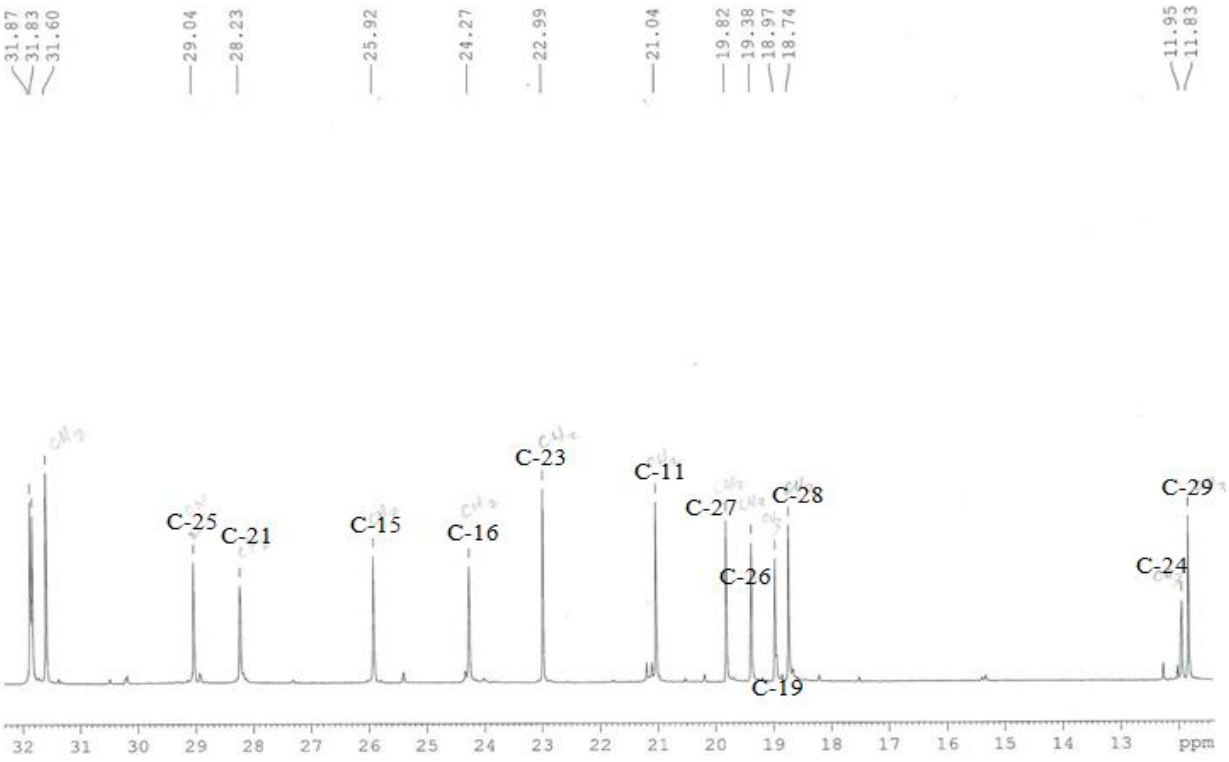

A

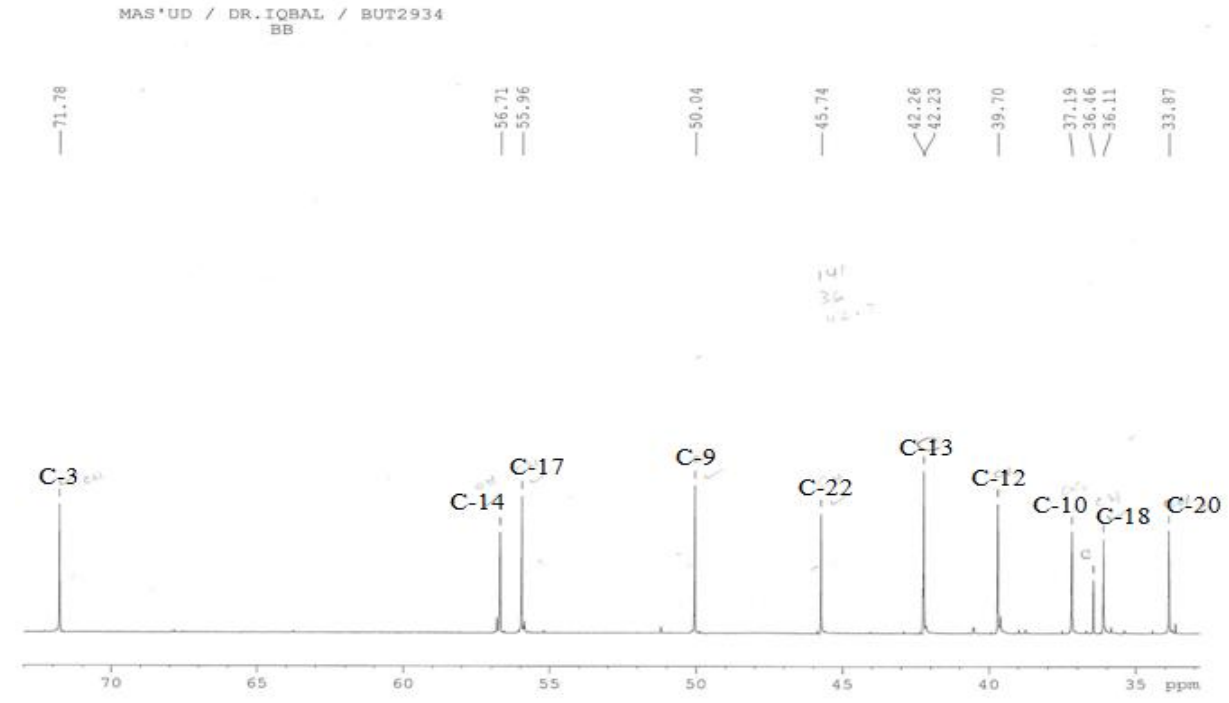

B

Figure 4.46: Expanded C-13 Spectrum of Compound 4 Showing Regions 13-32 ppm (A) and 35-70 ppm (B)

The DEPT 90 spectrum (Figure 4.47) identified methine carbons as follows: 29.08 (C-25), 31.88 (C-8), 36.11 (C-18), 45.74 (C-22), 50.04 (C-9), 55.96 (C-17), 56.71 (C-14), 71.78 (C-3), and 121.72 (C-6).

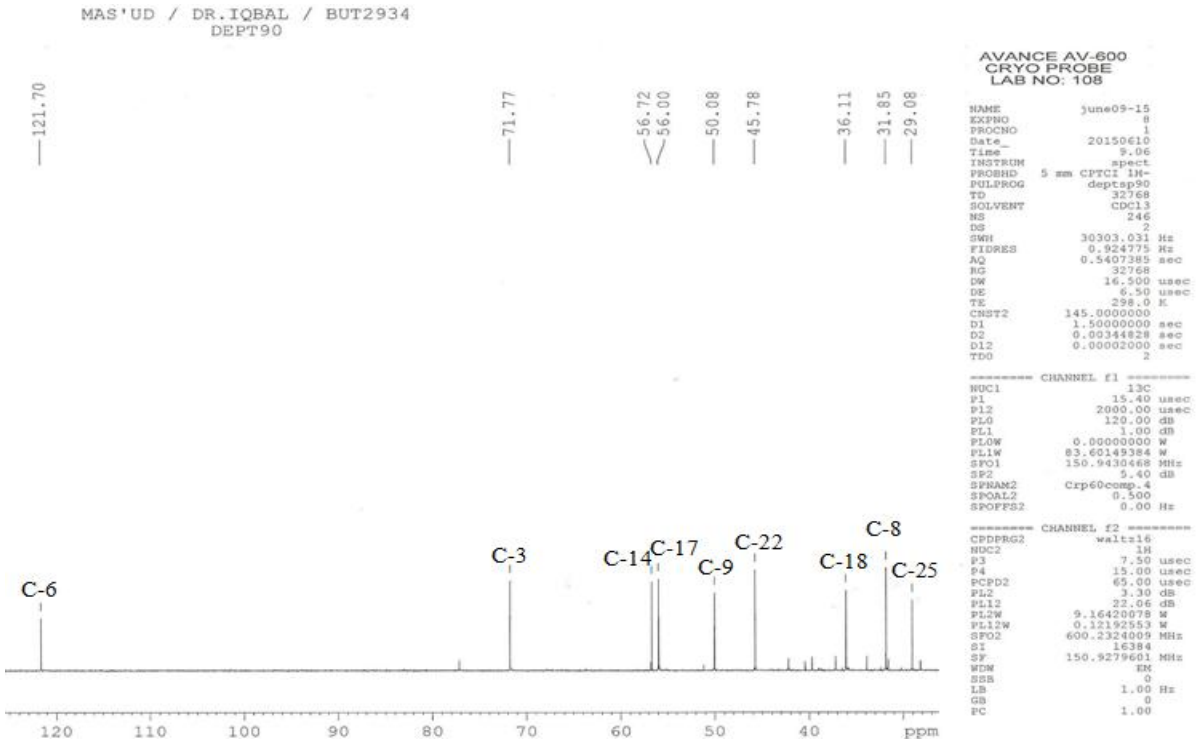

Figure 4.47: DEPT 90 Spectrum of Compound 4

The DEPT 135 spectrum presented in Figures 4.48 and 4.49 identified methyl carbons, methylene carbons which appeared as negative peaks and other proton bearing carbons. Methyl carbons: 11.83 (C-29), 11.95 (C-24), 18.74 (C-28), 18.97 (C-19), 19.38 (C-26), 19.82 (C-27); methylene carbons: 21.04 (C-11), 22.99 (C-23), 24.27 (C-16), 25.92 (C-15), 28.23 (C-21), 31.62 (C-2), 31.85 (C-7), 33.87 (C-20), 37.21 (C-1), 39.70 (C-12) and 42.26 (C-4).

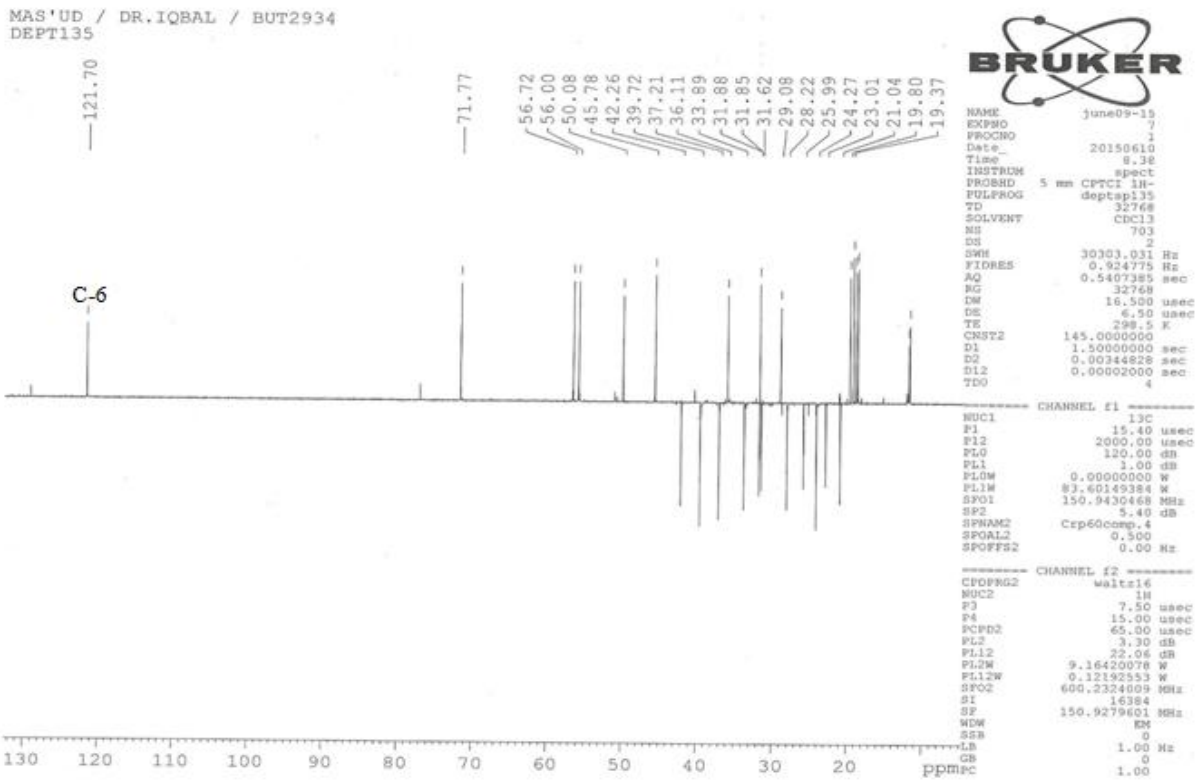

Figure 4.48: DEPT 135 Spectrum of Compound 4

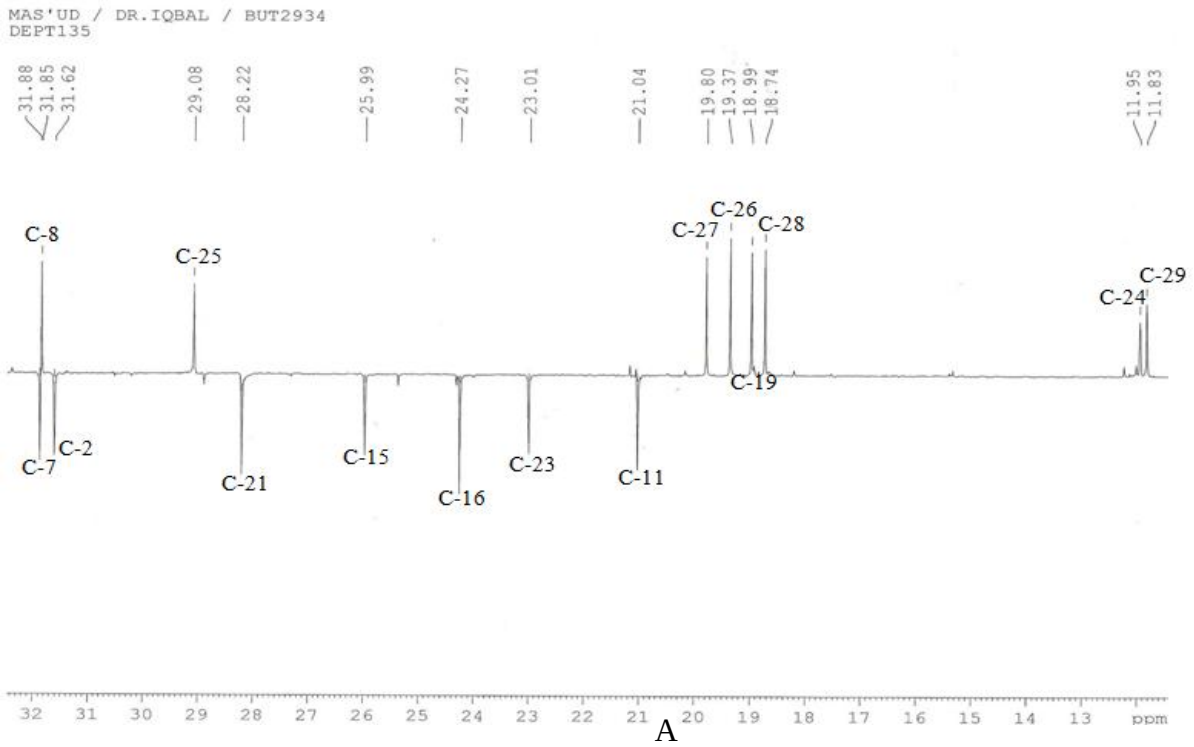

A

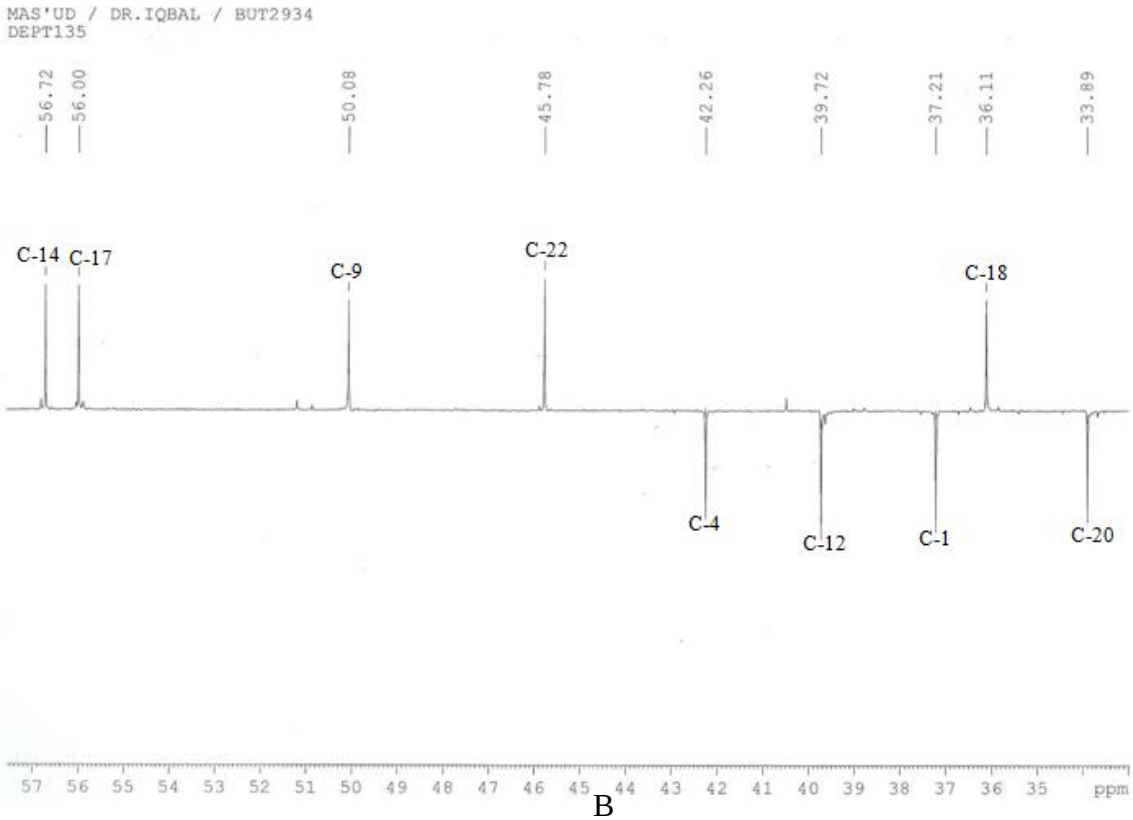

B

Figure 4.49: DEPT 135 Spectrum of Compound 4 Expanded Regions 13-32 ppm (A) and 35-57 ppm (B)

4.19 Two Dimensional (2D) NMR Spectral Analyses of Compound 4

4.19.1 ^{1}H-^{1}H Correlation Spectroscopy (COSY) of Compound 4

^{1}H-^{1}H COSY was observed for the following selected protons H1 (5.30) correlated with #H-4 (2.18); H-2 (3.46) correlated with #H-3 (2.25) and H-6 (1.76) correlated with #H-28 (0.80) (Figures 4.50 and 4.51).

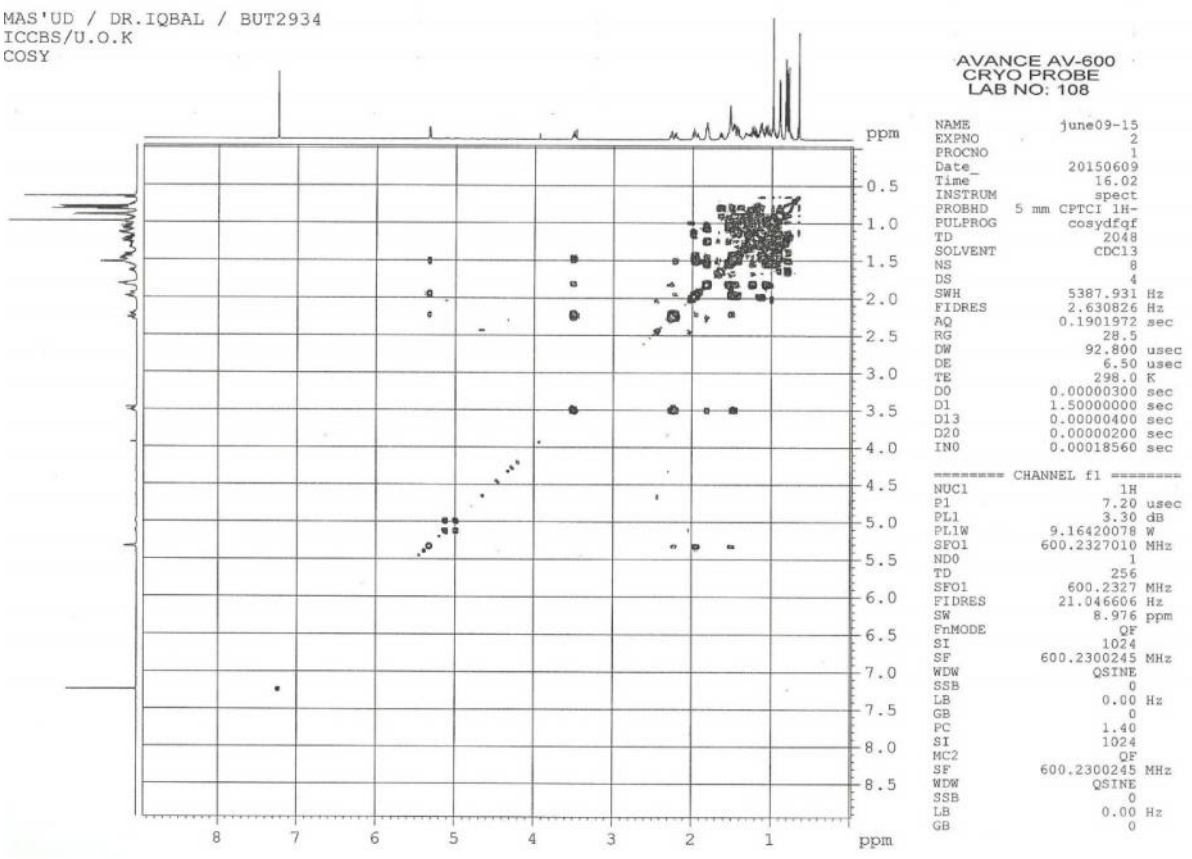

Figure 4.50: ^{1}H-^{1}H COSY Spectrum for Compound 4

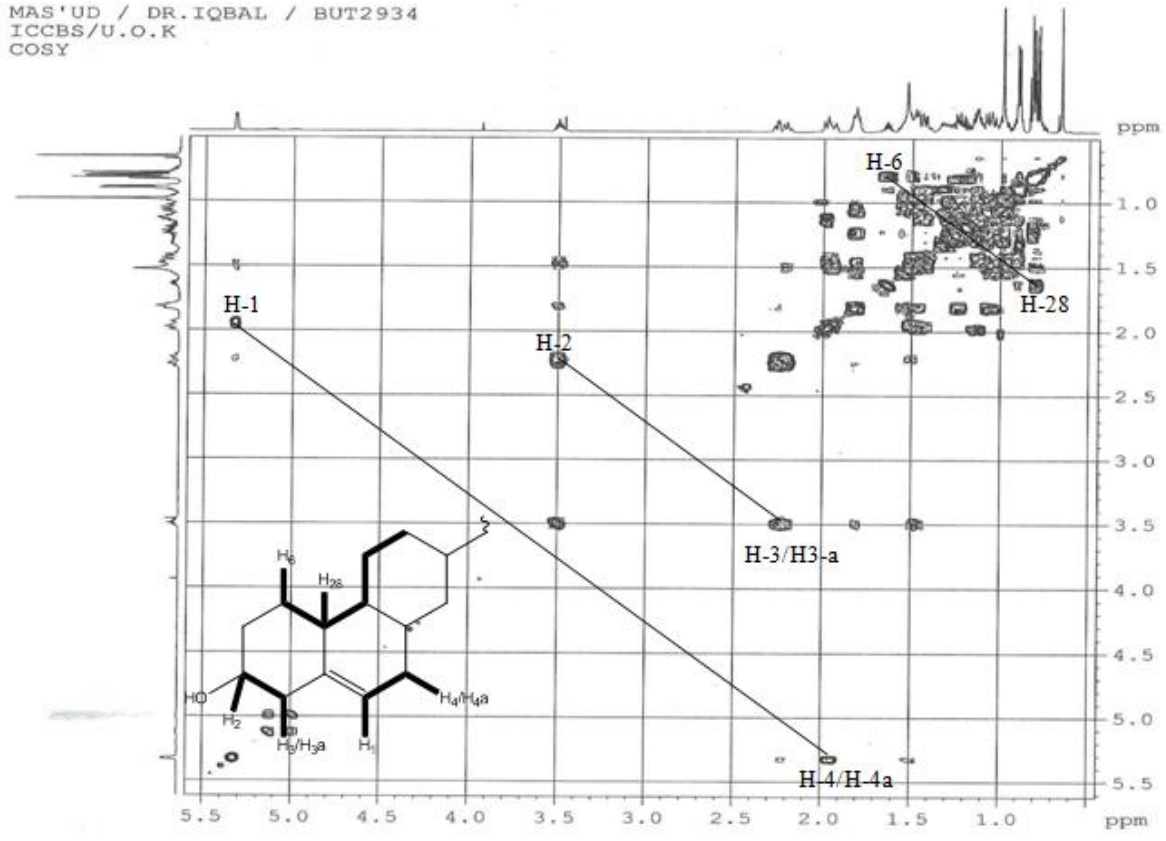

Figure 4.51: ^{1}H-^{1}H COSY Spectrum of Compound 4 Showing Expanded Regions 1.0-5.5 ppm

The thick line (▬) indicates the referenced protons

4.19.2 HSQC Spectral Analysis of Compound 4

In HSQC spectrum of compound **4**, the following correlations were observed : C(121.72)#5.30 C(71.78)#3.46, C(42.26)# 2.25 and 2.18; C(39.70)#1.92 and C(37.21)#1.76 (Figures 4.52 and 4.53).

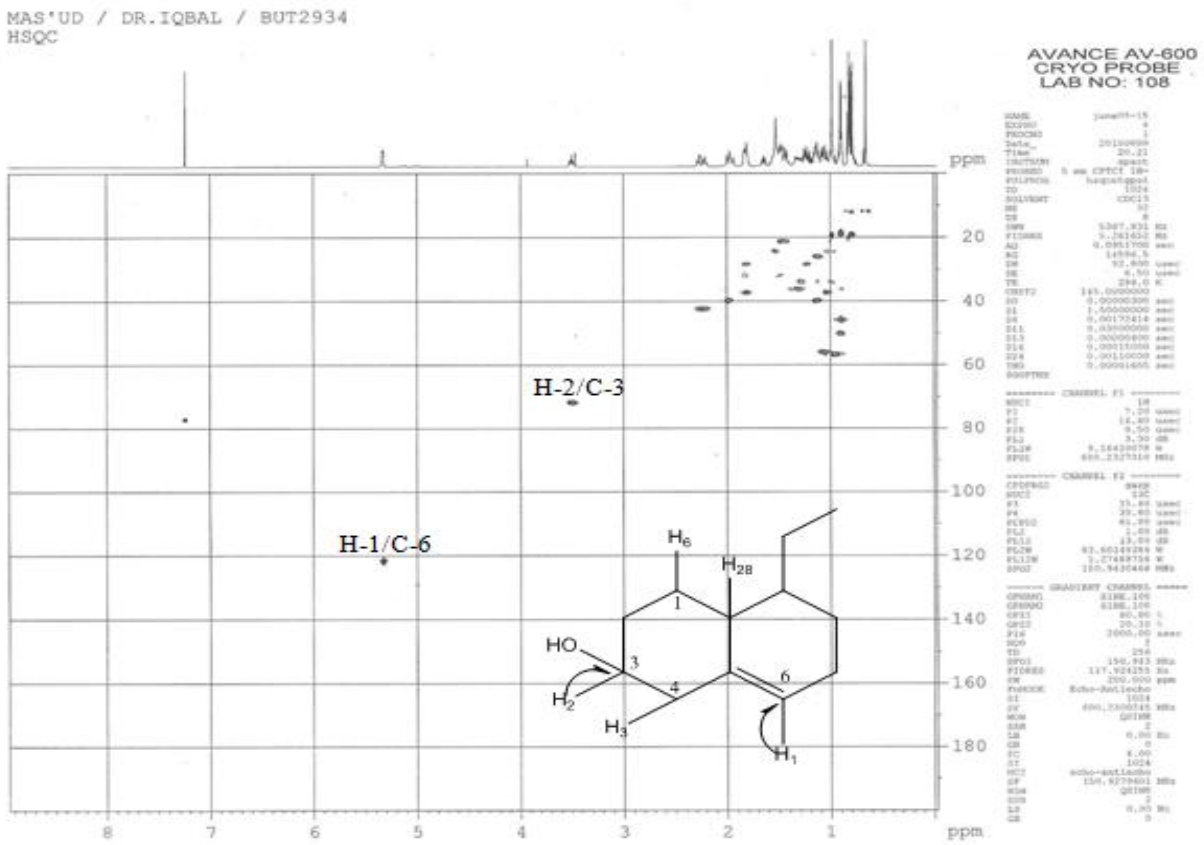

Figure 4.52: HSQC Spectrum of Compound 4

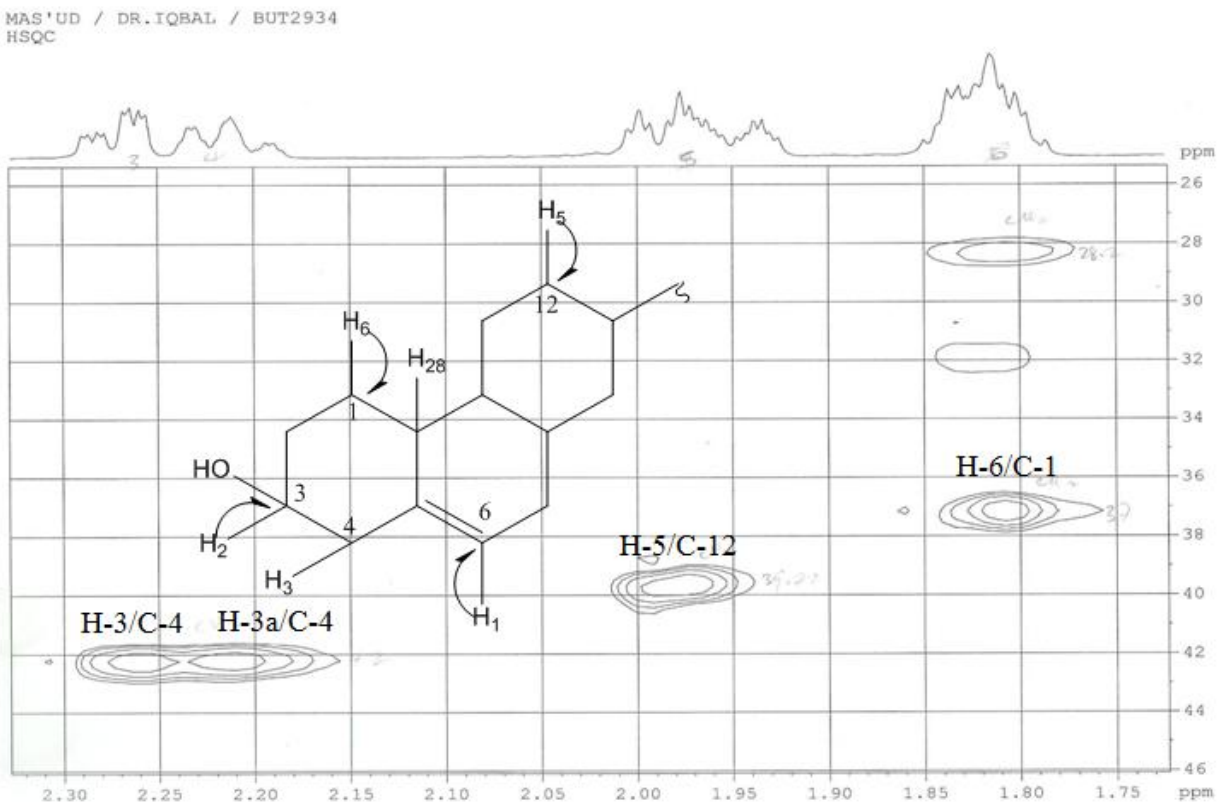

Figure 4.53: HSQC Spectrum of Compound 4 Showing Expanded Regions 1.75-2.30 ppm

The arrow (⟶) shows proton-carbon correlations

4.19.3 HMBC Spectral Analysis of Compound 4

The HMBC 2-3 bond long range correlations for compound 4 (Figures 4.54 and 4.55) were observed as follows: $^{\delta}$H 2.25 and 2.18 correlated with C-2, C-3, C-6 and C-5; $^{\delta}$H 1.92 correlated with C-9 and C-14; $^{\delta}$H 1.76 correlated with C-3 and C-5.

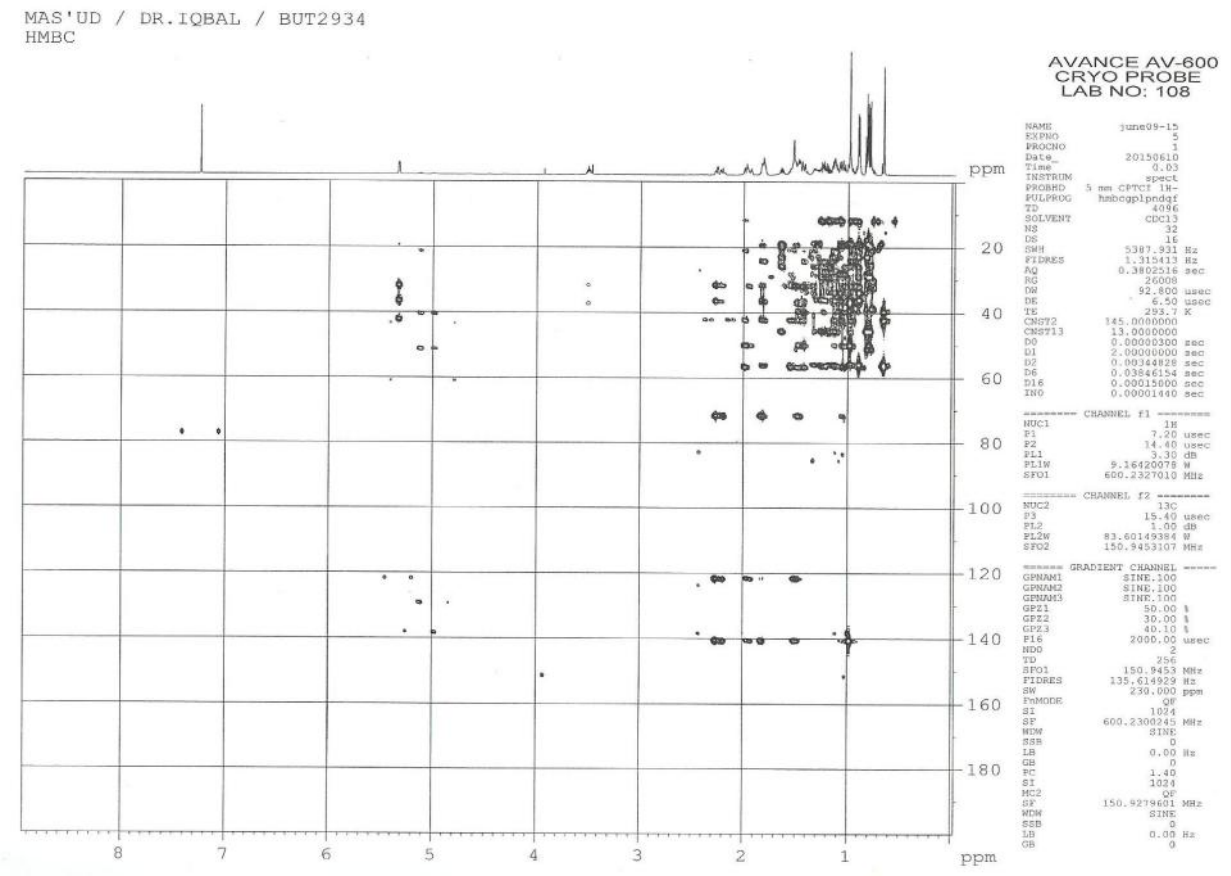

Figure 4.54: HMBC Spectrum for Compound 4

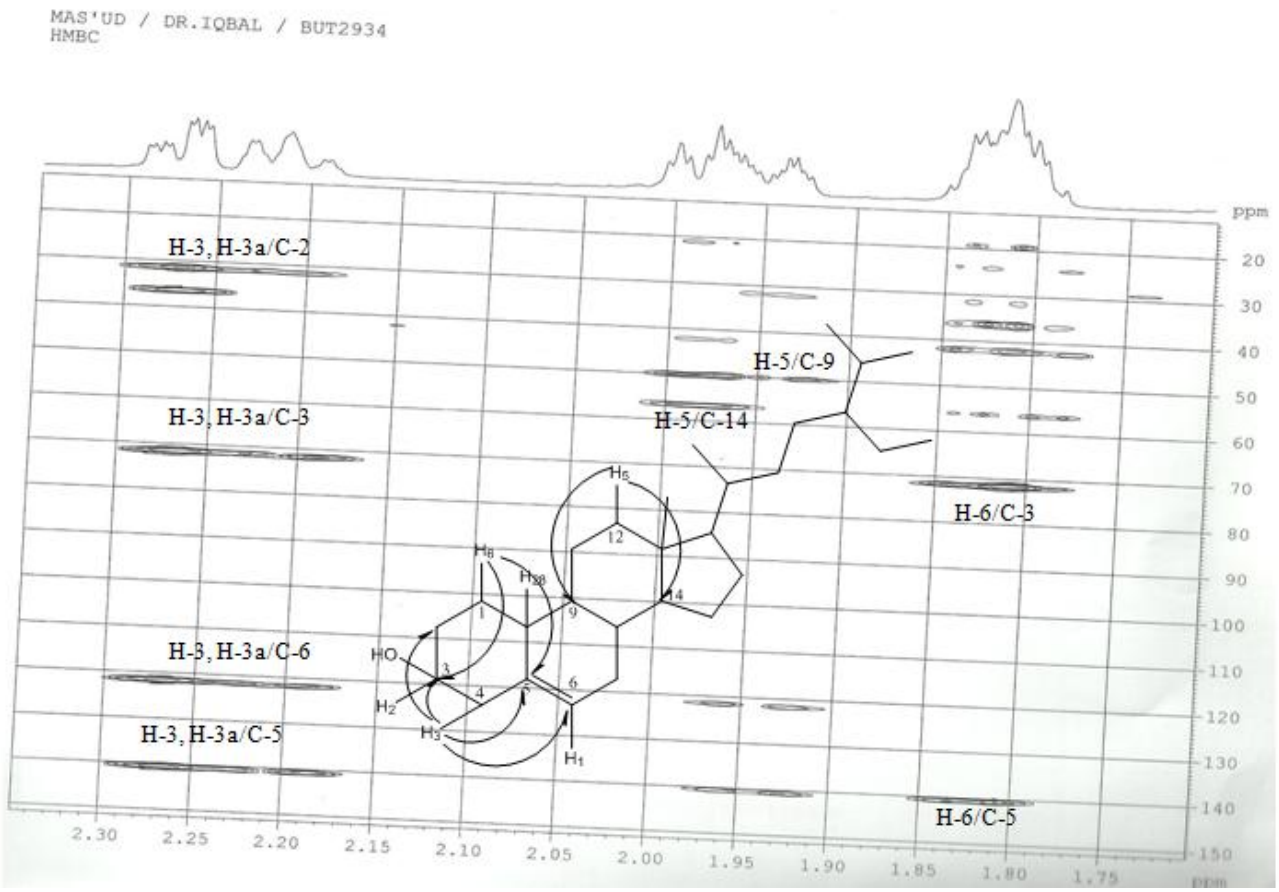

Figure 4.55: Expanded Spectra Showing HMBC in the Regions 1.75 - 2.30 ppm of Compound 4

The arrow (⟶) shows the 2-3 bond long range proton-carbon correlations

4.20 Mass Spectral Analysis of Compound 4

The EI-MS mass spectrum for compound 4 (Figure 4.56) showed a characteristic molecular ion peak at m/z of 414 and base peak of m/z 55. The peak appearing at m/z 381 is typical of loss of HO-CH_3 (M-32). The peak appearing at m/z 273 may also be due to loss of $C_{10}H_{21}$ (M-141).

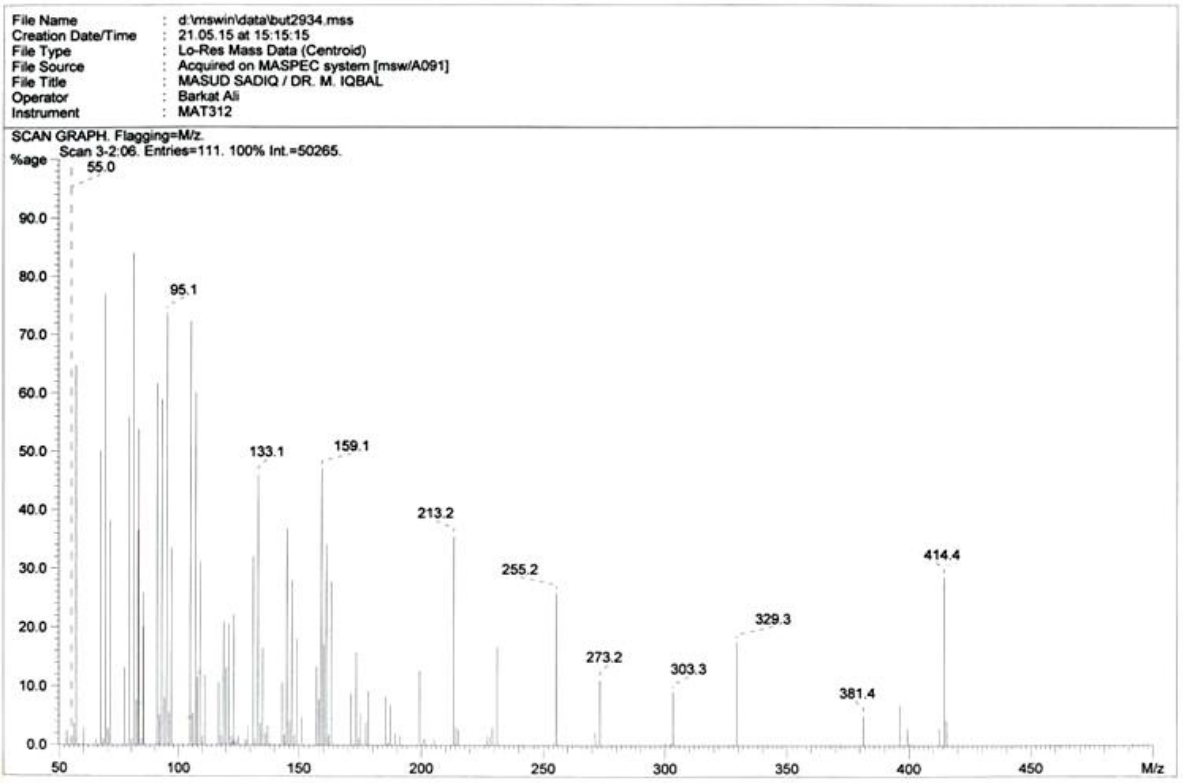

Figure 4.56: EI-MS of Compound 4

4.21 Summary of Characteristics and Spectroscopy Data of Compound 4

Physical appearance: white crystal-like solid

EI-MS: major fragments m/z 55 (base peak), 213.2, 255.2, 273.2, 303.3, 329.3, 381.4,

Molecular ion peak (M^+) m/z 414; Exact mass: 414.3862

Molecular formula: $C_{29}H_{50}O$; Degree of unsaturation (RDB): 5

Proposed structure of compound 4

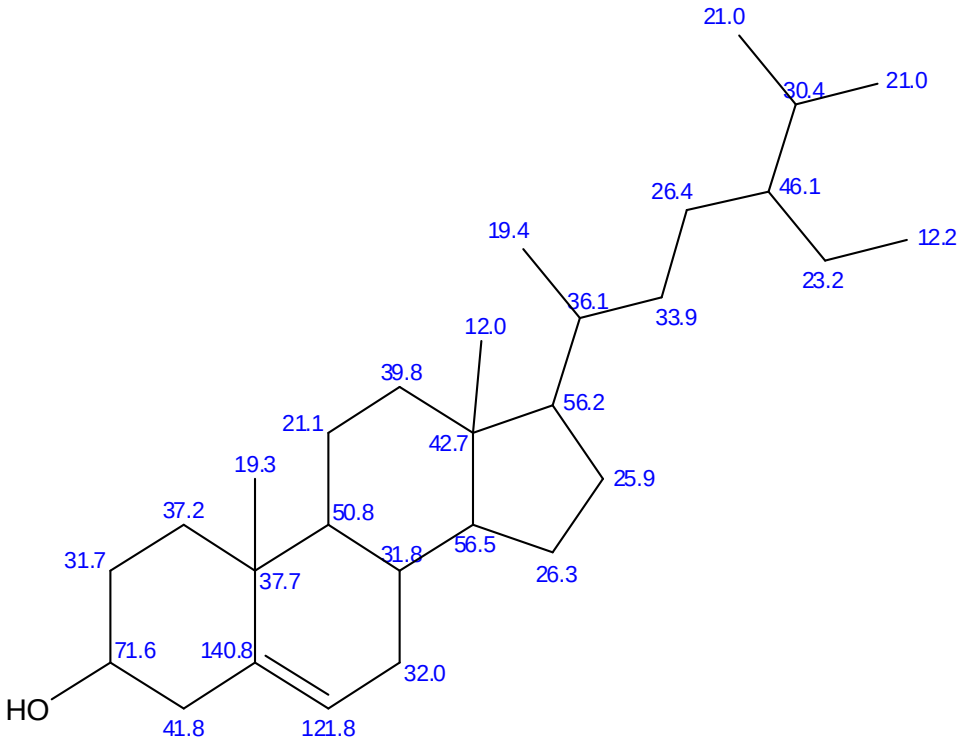

Table 4.6: Summary of 1D and 2D NMR Spectral Analyses of Compound 4

Position	$^{\delta}C$	Type	δ_H (*J* in Hz)	HMBC
1	37.21	CH_2	1.76	3, 5
2	31.62	CH_2		
3	71.78	CH	3.46	
4	42.26	CH_2	2.25, 2.18	2, 3, 5, 6
5	140.70	CH		
6	121.72	CH	5.30	
7	31.85	CH_2		
8	31.88	CH		
9	50.04	CH		
10	37.19	C		
11	21.04	CH_2		
12	39.70	CH_2	1.92	9, 14
13	42.23	C		
14	56.71	CH		
15	25.92	CH_2		
16	24.27	CH_2		
17	55.96	CH		
18	30.11	CH		
19	18.97	CH_3		
20	33.87	CH_2		
21	28.23	CH_2		
22	45.74	CH		
23	22.99	CH_2		
24	11.95	CH_3		
25	29.08	CH		
26	19.38	CH_3		
27	19.82	CH_3		
28	18.74	CH_3		
29	11.83	CH_3		

$^{\delta}C$= carbon chemical shift in ppm; $^{\delta}H$ = proton chemical shift in ppm.= multiplets; *J* = coupling constant; s= singlet; d= doublets; dd=doublet of doublets; m=multiplets

4.22 Prediction on Solubility of Isolated Compounds

Presented in Figure 4.57 are models used to predict solubility of the isolated compounds. Solubility of compound 1 was shown to be more in fasted state gastric fluid (FaSGF) i.e. 0.47 mg/ml followed by water (0.37 mg/ml). Compound 3 had highest solubility in FaSGF (0.92 mg/ml) of all solubilities predicted. The models showed compound 2 to be most soluble in fed state intestinal fluid (FeSIF) at 0.33 mg/ml then its solubility in water (0.23 mg/ml). The least soluble compound observed was compound 4 in all fluids simulated.

4.23 Prediction on Permeability Properties of Isolated Compounds

Prediction models on MDCK and jejunal permeability were used to predict the permeability properties of the isolated compounds as presented in Figure 4.58. Compound 1 was predicted to have high jejunal permeability (5.61 x 10^4 cm/sec) and MDCK permeabililty predicted to be 224 x10^7 cm/sec. Compound 4 was shown to have highest jejunal permeability (8.1 x 10^4 cm/sec) while compound 2 had least tendency to permeate the jejunum as predicted (0.28 x 10^4 cm/sec). The models generally indicate compounds with MDCK values < 25 x 10^{-7} cm/s and Peff < 0.1 cm/s x 10^{-4} have low permeability properties.

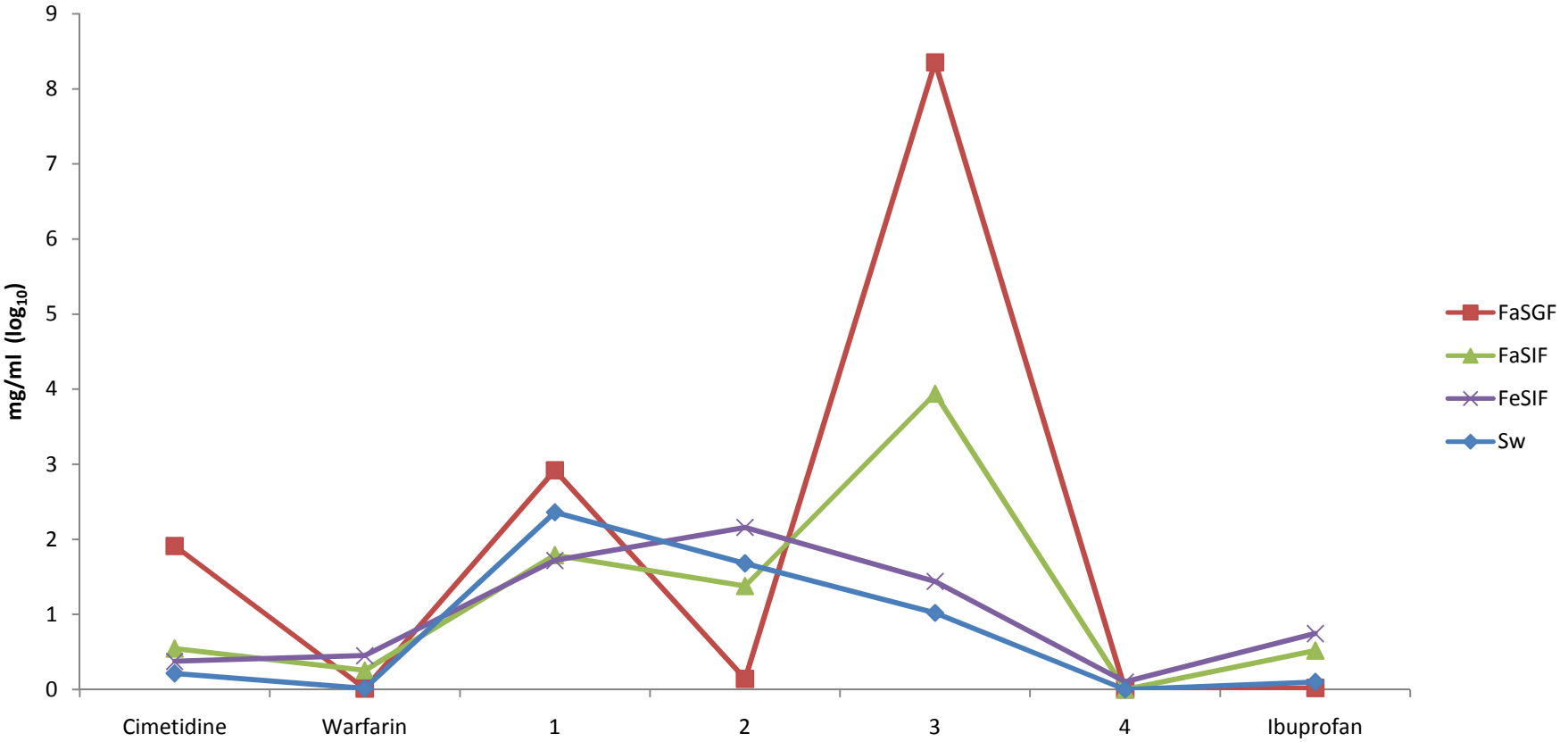

Figure 4.57: Prediction Models for Solubility of Compounds

FaSGF= solubility in simulated fasted state gastric fluid; FaSIF=solubility in simulated fasted state intestinal fluid; FeSIF=solubility in simulated fed state intestinal fluid; Simulations Plus; Sw=native solubility in water

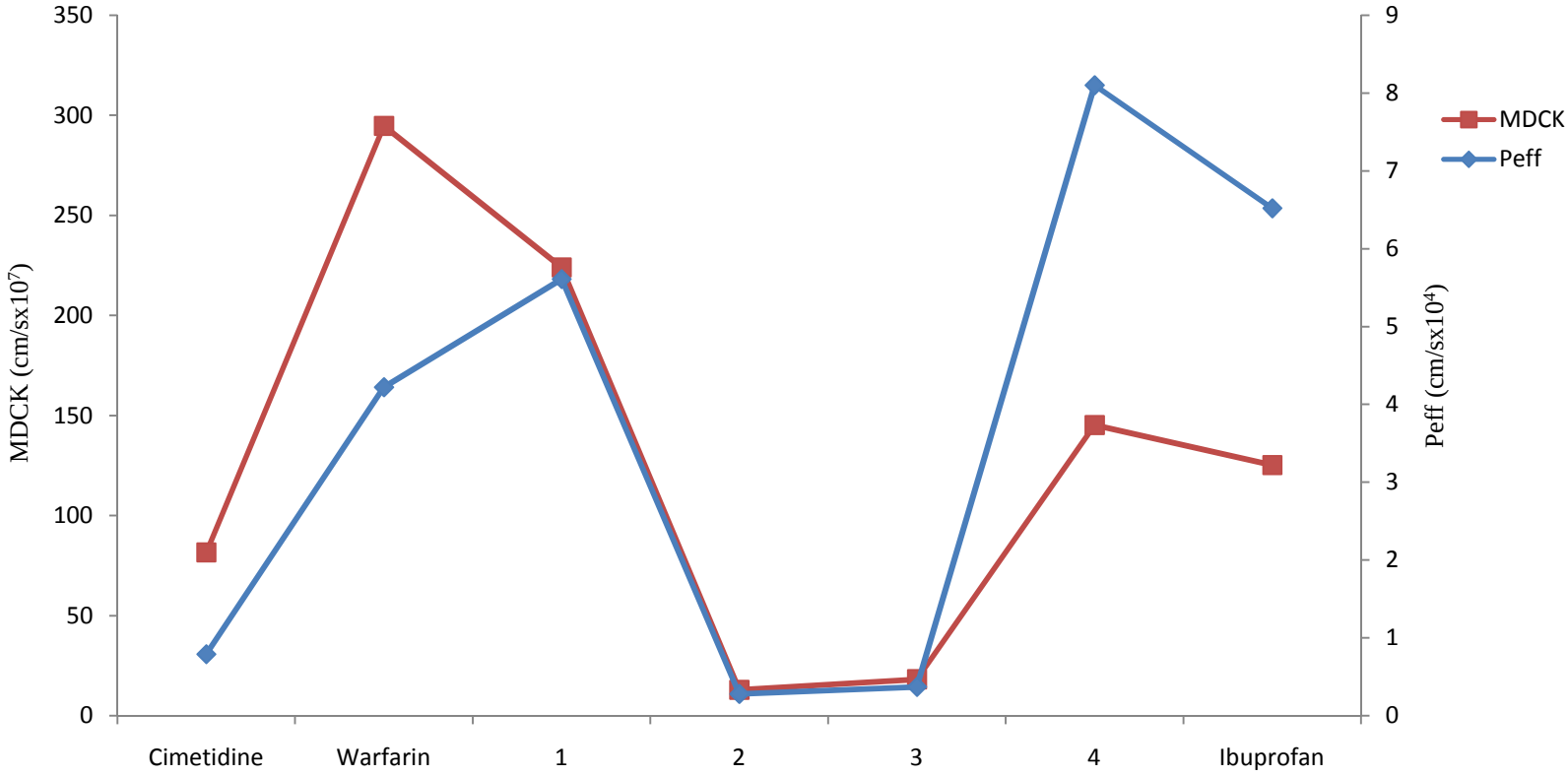

Figure 4.58: Permeability Prediction Models

Peff=human jejunal effective permeability; MDCK=apparent Mardin Darby Canine Kidney cells permeability

4.24 Predictions on Volume of Distribution and Plasma Protein Binding of Isolated Compounds

Predictions on volume of distribution of the compound as presented in Table 4.59 indicated compound 4 has the likelihood to be distributed within tissues (2.13 L/Kg). The compound was also predicted to be >95% bound to plasma proteins. Plasma protein binding predicted for compounds 1 and 3 were shown to be less likely as the values indicated 60.23% and 98% unbound to proteins in blood respectively. Tissue distribution for compounds 1 and 3 was in the range 0.92-0.95 L/Kg. Compound 2 was however predicted to most likely interact with plasma proteins (80.22% bound to plasma proteins) with tissue distribution of 0.62 L/Kg. The models predictions generally suggest compounds with Prunbound < 0.6-1.2 have high plasma protein interaction and V_d > 3.7-5.7 L/kg have high steady state volume of distribution.

4.25 Predictions on Qualitative Assessment of Liver Toxicity of Isolated Compounds

Presented in Table 4.7 are the predictions on enzyme biomarkers for assessing liver toxicity effects of the isolated compounds. Compound 1 was shown to have no related adverse effects that may result in elevated levels of the enzymes predicted. Compound 3 may cause an increase in levels of alkaline phosphatase (60% confidence on prediction) and aspartate amino transferase (AST) (at about 62% confidence levels of predictions). The propensity for compound 4 to cause elevated levels of lactate dehydrogenase enzyme (LDH) was predicted to high (93% prediction confidence).

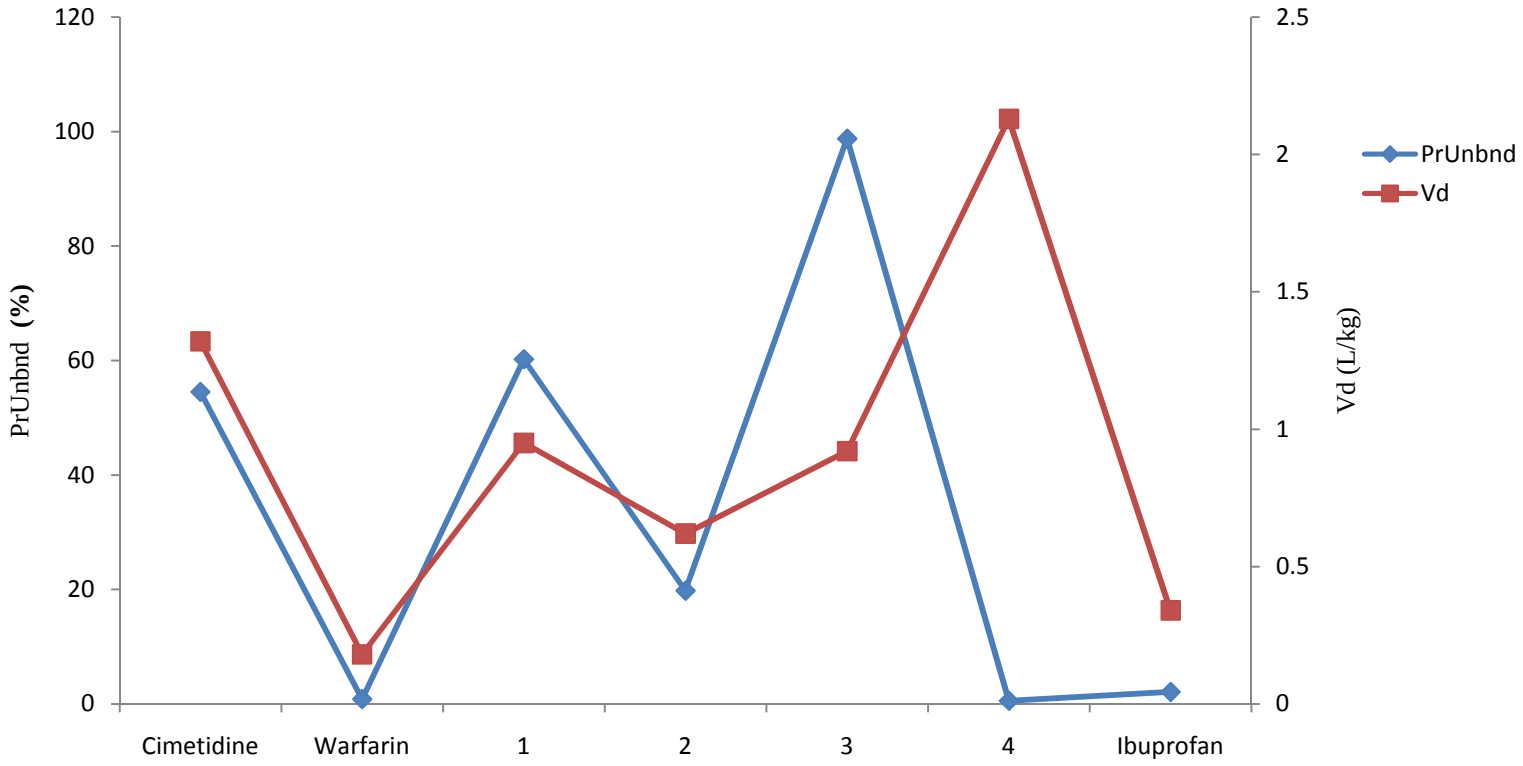

Figure 4.59: Prediction Models for Volume of Distribution and Plasma Protein Binding of Compounds

PrUnbnd=percent unbound to blood plasma proteins; Vd (L/Kg)=pharmacokinetic volume of distribution in human; RBP=blood-to-plasma concentration ratio in human; fumic=fraction unbound in human liver microsomes;

Table 4.7: Predictions for Likelihood for Liver Toxicity

Cpd	AlkPhos	GGT	LDH	AST	ALT
Cimetidine	Normal (70%)	Normal (99%)	Elevated (69%)	Normal (89%)	Elevated (51%)
Warfarin	Normal (57%)	Elevated (57%)	Normal (83%)	Normal (78%)	Elevated (63%)
1	Normal (84%)	Normal (88%)	Normal (69%)	Normal (65%)	Normal (70%)
2	Normal (95%)	Normal (81%)	Elevated (76%)	Normal	Elevated
3	Elevated (60%)	Normal (99%)	Normal (96%)	Elevated (62%)	Normal (99%)
4	Normal (95%)	Elevated (54%)	Elevated (93%)	Normal (89%)	Normal (99%)
Ibuprofan	Normal (95%)	Normal (99%)	Normal (96%)	Normal (89%)	Normal (70%)

Numbers in parenthesis indicate confidence in predictions

AlkPhos=human liver adverse effect as the likelihood of causing elevation in the levels of Alkaline Phosphatase enzyme; GGT= likelihood of causing elevation in the levels of GGT enzyme; LDH= likelihood of causing elevation in the levels of LDH enzyme; AST= likelihood of causing elevation in the levels of AST enzyme; ALT= likelihood of causing elevation in the levels of ALT enzyme

4.26 Prediction on Qualitative Assessment of Isoforms of CYP Metabolism of Isolated Compounds

Predictions on liver CYP 450 isoforms metabolism of the compounds are presented in Tables 4.8 to 4.12. Predictions on CYP2C9 (Table 4.9) indicated compound 1 to be a substrate of the enzyme with a Km value of 1.74 x 10^2 µM. ibuprofen, warfarin and cimetidine were also predicted to be substrates for the enzyme. However, compound 2 was predicted to likely be an inhibitor of the enzyme. The enzymes CYP2C19 and CYP2D6 were predicted not to metabolize any of the isolated compounds (Tables 4.10 and 4.11). Activity of the isoform CYP3A4 as shown in Table 4.12 may be inhibited by compounds 2 and 3 while compound 4 was shown to be a substrate with more than one catalytic site for the enzyme. The Km was predicted to be 23.1 µM for compound 4. Predictions by the software do not compare kinetic values but present them independent of compounds metabolized by same enzyme. Similarly, two or more enzyme metabolizing same substrate does not relate to substrate-enzyme affinity.

4.27 Qualitative Assessment on Glucuronidation of Isolated Compounds

Glucuronidation by isoforms of UDP glucuronosyltransferases is presented in Table 4.13. Except for compound 4 which was predicted not be a substrate for glucuronidation reaction by any of the enzyme isoforms, the other isolates were shown to be substrates to more than 2 isoforms. Compound 1 was predicted to be a substrate to all isoforms predicted except for UGT1A1 and UGT1A4. Compound 2 is most likely to be a substrate for UGT1A3 and UGT1A1 with prediction confidence levels given as 87% and 61% respectively.

Table 4.8: Predictions on Kinetics of CYP1A2 Mediated Catalysis

Compound	Inh	Substr	Sites	Km (µM)	Vmax (nmol/min/nmol enzyme)
Cimetidine	No (80%)	Yes (80%)	C1(956); S7(886); C14(646); C11(596)	$6.78x10^2$	9.97
Warfarin	Yes (66%)	No (57%)	NS	NS	NS
1	No (86%)	No (58%)	NS	NS	NS
2	Yes (73%)	No (96%)	NS	NS	NS
3	No (97%)	No (74%)	NS	NS	NS
4	No (91%)	No (96%)	NS	NS	NS
Ibuprofan	No (86%)	No (62%)	NS	NS	NS

NS =Non substrate. Percentages in parenthesis indicate confidence in prediction. Numbers in parenthesis under "sites" compares propensities for identified atoms as likely active sites in the 2D structures. A "yes" output suggests likelihood of being a substrate or inhibitor

Inh= qualitative estimation of general inhibitory action against CYP 1A2; Substr= qualitative assessment of a molecule being the substrate of CYP 1A2; Sites= specific sites of human CYP 1A2 mediated oxidation; Km= Michaelis-Menten Km constants for predicted sites of CYP 1A2; Vmax= Michaelis-Menten Vmax constants for predicted sites of CYP 1A2

Table 4.9: Predictions on Kinetics of CYP2C9 Mediated Catalysis

Compound	Inh	Substr	Sites	**Km** (μM)	**Vmax** (nmol/min/nmol enzyme)
Cimetidine	No (98%)	Yes (75%)	C1(972); S7(940); N15(904); C14(859); C11(821)	$4.67x10^{1}$	$2.24x10^{1}$
Warfarin	Yes (72%)	Yes (75%)	C1(945); C12(855); C2(689); C23(604)	4.43	$2.34x10^{-1}$
1	No (60%)	Yes (53%)	C11(497)	$1.74x10^{2}$	$8.05x10^{-1}$
2	Yes (56%)	No (98%)	NS	NS	NS
3	No (98%)	No (90%)	NS	NS	NS
4	No (74%)	No (61%)	NS	NS	NS
Ibuprofan	Yes (56%)	Yes (58%)	C4(830); C2(814); C1(768); C3(768)	$9.08x10^{1}$	$1.36x10^{1}$

NS =Non substrate. Percentages in parenthesis indicate confidence in prediction. Numbers in parenthesis under "sites" compares propensities for identified atoms as likely active sites in the 2D structures. A "yes" output suggests likelihood of being a substrate or inhibitor

Inh= qualitative estimation of general inhibitory action against CYP2C9; Substr= qualitative assessment of a molecule being the substrate of CYP2C9; Sites= specific sites of human CYP2C9 mediated oxidation; Km= Michaelis-Menten Km constants for predicted sites of CYP2C9; Vmax= Michaelis-Menten Vmax constants for predicted sites of CYP2C9

Table 4.10: Predictions on Kinetics of CYP2C19 Mediated Catalysis

Compound	Inh	Substr	Sites	**Km** (μM)	**Vmax** (nmol/min/nmol enzyme)
Cimetidine	Yes	Yes (54%)	C1(993); S7(984); C14(819); C11(748)	92.30	$7.51x10^{2}$
Warfarin	No	Yes (78%)	C1(984); C12(843); C2(822)	$1.39x10^{2}$	$5.29x10^{-1}$
1	No	No (61%)	NS	NS	NS
2	No	No (95%)	NS	NS	NS
3	No	No (99%)	NS	NS	NS
4	No	No (53%)	NS	NS	NS
Ibuprofan	No	Yes (50%)	C2(731); C4(721); C3(503); C1(503)	$1.43x10^{2}$	8.42

NS =Non substrate. Percentages in parenthesis indicate confidence in prediction. Numbers in parenthesis under "sites" compares propensities for identified atoms as likely active sites in the 2D structures. A "yes" output suggests likelihood of being a substrate or inhibitor

Inh= qualitative estimation of general inhibitory action against CYP2C19; Substr= qualitative assessment of a molecule being the substrate of CYP2C19; Sites= specific sites of human CYP2C19 mediated oxidation; Km= Michaelis-Menten Km constants for predicted sites of CYP2C19; Vmax= Michaelis-Menten Vmax constants for predicted sites of CYP2C19

Table 4.11: Predictions on Kinetics of CYP2D6 Mediated Catalysis

Compound	Inh	Substr	Sites	**Km** (μM)	**Vmax** (nmol/min/nmol enzyme)
Cimetidine	No (95%)	Yes (57%)	C1(980); S7(916); C14(869); 15(830); C11(771)	7.20	$2.96x10^{1}$
Warfarin	No (57%)	No (96%)	NS	NS	NS
1	No (95%)	No (71%)	NS	NS	NS
2	No (59%)	No (96%)	NS	NS	NS
3	No (95%)	No (96%)	NS	NS	NS
4	No (95%)	No (96%)	NS	NS	NS
Ibuprofan	No (95%)	Yes (58%)	C4(548); C2(539); C11(352)	$6.66x10^{1}$	6.95

NS =Non substrate. Percentages in parenthesis indicate confidence in prediction. Numbers in parenthesis under "sites" compares propensities for identified atoms as likely active sites in the 2D structures. A "yes" output suggests likelihood of being a substrate or inhibitor

Inh= qualitative estimation of general inhibitory action against CYP2D6; Substr= qualitative assessment of a molecule being the substrate of CYP2D6; Sites= specific sites of human CYP2D6 mediated oxidation; Km= Michaelis-Menten Km constants for predicted sites of CYP2D6; Vmax= Michaelis-Menten Vmax constants for predicted sites of CYP2D6

Table 4.12: Predictions on Kinetics of CYP3A4 Mediated Catalysis

Compound	Inh	Substr	Sites	Km (μM)	Vmax (nmol/min/nmol enzyme)
Cimetidine	Yes	Yes	S7(996); C1(975); C14(873); C11(649)	$2.37x10^2$	5.81
Warfarin	Yes	Yes	C1(703); C2(639); C12(410)	$1.79x10^2$	2.19
1	No	No	NS	NS	NS
2	Yes	No	NS	NS	NS
3	Yes	No	NS	NS	NS
4	No	Yes	C20(816); C19(691); C2(690); C16(613); C23(556); C5(540)	23.1	75.7
Ibuprofan	No	No	NS	NS	NS

NS =Non substrate. Percentages in parenthesis indicate confidence in prediction. Numbers in parenthesis under "sites" compares propensities for identified atoms as likely active sites in the 2D structures. A "yes" output suggests likelihood of being a substrate or inhibitor

Inh= qualitative estimation of general inhibitory action against CYP3A4; Substr= qualitative assessment of a molecule being the substrate of CYP3A4; Sites= specific sites of human CYP3A4 mediated oxidation; Km= Michaelis-Menten Km constants for predicted sites of CYP3A4; Vmax= Michaelis-Menten Vmax constants for predicted sites of CYP3A4

Table 4.13 Predictions on Phase II Conjugation with Isoforms of UDP-Glucoronosyl Transferases

Generic	UGT1A1	UGT1A3	UGT1A4	UGT1A6	UGT1A8	UGT1A9	UGT1A10	UGT2B7	UGT2B15
Cimetidine	No (62%)	No (96%)	No (67%)	No (98%)	No	Yes (69%)	No (98%)	No (53%)	No (99%)
Warfarin	Yes (58%)	Yes (47%)	No (98%)	No (98%)	No (59%)	Yes (80%)	Yes (90%)	Yes (65%)	Yes (72%)
1	No (92%)	Yes (97%)	No (90%)	Yes (53%)	Yes (83%)	Yes (93%)	Yes (48%)	Yes (63%)	Yes (91%)
2	Yes (61%)	Yes (87%)	No	No (98%)	Yes	No	No (91%)	No (57%)	No (95%)
3	No (92%)	Yes (87%)	No (98%)	Yes (58%)	No (96%)	No (78%)	No (91%)	Yes (82%)	No (95%)
4	No (88%)	No (96%)	No (84%)	No (98%)	No (62%)	No (91%)	No (91%)	No (95%)	No (68%)
Ibuprofan	No (92%)	Yes (97%)	No (80%)	Yes (58%)	No (96%)	Yes (93%)	No (98%)	Yes (97%)	No (99%)

Percentages in parenthesis indicate confidence in prediction. A “yes” output suggests likelihood of being a substrate for phase II conjugation.

UGT1A1- UGT2B15= qualitative model of a glucuronidation by UDP glucoronosyltransferase enzymes

4.28 Cumulative Risk Codes for Predicted ADME Properties

Table 4.14 is a summary of risks associated with all predicted physico-chemical, metabolism and toxicity models for drug-like properties of compounds. The Lipinsky rule of five and scores developed by software providers (ADMET) are used to identify compounds that are least likely to possess desired properties. Compound 1 was predicted not to have any associated risks. Compounds with risks codes on solubility (Sw) and lipophilicity (ow) were generally not considered for bioactivity (compound 4) as these compounds are likely to present permeability concerns and/or high lipid absorption.

Table 4.14 Compound Risks Codes Predictions for Drug-Like Properties Qualification

Generic	RuleOf5	Absn	ADMET
Cimetidine			Xr,Hp,C9,19,D6,
Warfarin			fu,ra,Hp,
1			
2	Hb,NO	Sz,HD,HA,ch,Pf	Sz,HD,HA,ch,Pf,Hp,
3		Pf	Pf,Xr,Hp
4	LP	Sz,ch,ow,Sw	Sz,ch,ow,Sw,fu,3A,
Ibuprofan			C9

RuleOf5 original Lipinski rule of 5 (Lipinski, *et al*., 1997) Absn= risks associated with absorption (simulations plus); ADMET= overall risks assessment from prediction of modules in simulations plus ADMET Predictor licensed software. Codes are defined as follows;

HD(b) = Hydrogen bond donors; HA or NO = hydrogen bond acceptors; ch= charge; ow= lipophilicity; pf= permeability, C9= high CYP2C9 clearance; C19= high CYP2C19 clearance; D6 = high CYP2D6 clearance; 3A= high CYP3A4 clearance; ra= acute toxicity in rat; Xr= carcinogenicity in rat; Hp = hepatotoxicity; Sz= size; fu= fraction unbound in human liver microsomes at 1mg/ml microsomal concentration; sw= native solubility; LP = logP

4.29 Antibacterial Activity of Selected Compound 1

Results presented in Figure 4.60 on the susceptibility screening of clinical isolates of selected bacteria revealed compound 1 to be active against the enteropathogenic bacteria previously screened using the crude methanol extract (see Figure 4.1). The zones of inhibition ranged from 25 mm-34 mm, with *S. dysenteriae* being the most susceptible enterobacteria. Compound 1 was also active against *B. cereus, S. typhi* and *E. coli*. All screenings were carried out at 100 µg/ml (456 µM) stock concentration.

The minimum inhibition (MIC) and bactericidal (MBC) concentrations presented in Figure 4.61 showed MIC of 57 µM for *B cereus, S. typhi* and *S. dysenteriae* while the MIC for *E. coli* was 114 µM. Bactericidal property of compound 1 observed for the pathogenic enterobacteria *S. dysenteriae* was 114 µM. The other susceptible enterobacteria were killed at 228 µM concentration of the test compound.

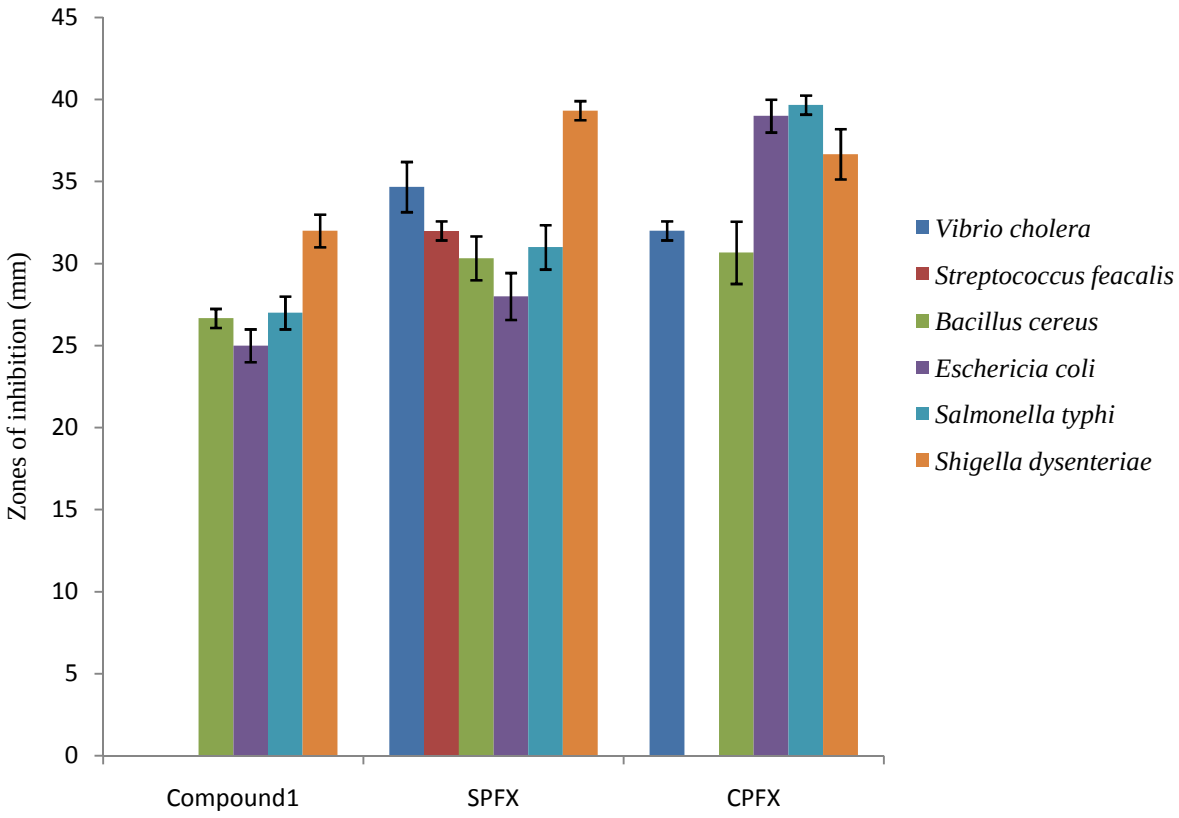

Figure 4.60: Zones of Inhibition of Organisms Susceptible to Compound 1

CPFX=ciprofloxacin; SPFX=sparfloxacin

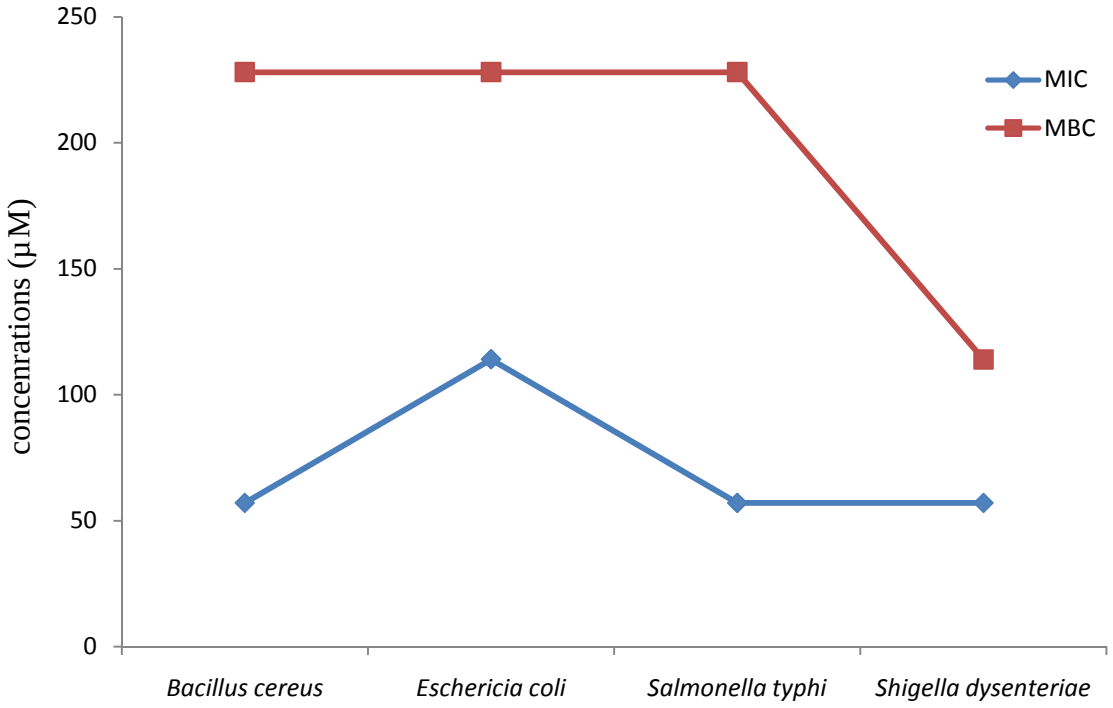

Figure 4.61: Minimum Inhibition and Bactericidal Concentrations of Compound 1 on Susceptible Organisms

CHAPTER FIVE

5.0 DISCUSSION

Application of modern techniques in traditional medicinal plants research have promoted and facilitated the ease of discovery of natural products based new chemical entities. Although research in natural products experienced a down turn for more than 20 years, however, of the 520 new drugs approved between 1983 and 1994, 39% were natural products or derived from natural products; between 60-80% of antibacterial and anticancer drugs were natural products derived (Harvey, 2000). The 2015 Nobel Prize for Physiology or medicine awarded for discoveries in natural products research (development of avermectin / ivermectin complexes and artemisinin) clearly shows the significance of natural products based drug discovery in modern day science (Newman, and Cragg, 2016).

Extracts of aerial parts of *Mirabilis jalapa* demonstrated antibacterial effects on the selected enterobacteria *S. typhi*, *E. coli*, *S. dysenteriae* and *B. cereus* (Figure 4.1). The methanol extract proved to be more active probably due to presence of increased amounts of active substances in the mixture. This suggests polar substances may be responsible for the antibacterial activities. As presented in Tables 4.1 and 4.2, the MIC and MBC recorded for the methanol extract was 2.5 mg/ml and 10 mg/ml respectively against susceptible organisms except for *S. dysenteriae* where no growth was observed at 5 mg/ml (MBC values). The growth of the organisms was also inhibited by the DCM extract but at higher concentrations when compared to the methanol extract. Interestingly, the extracts appeared to have more effect on the bacterium *S. dysenteriae* which is the causative agent of dysentery. Traditional claims for treatment of dysentery using macerations from aerial parts of *M. jalapa* have been reported (Rozina, 2016).

The findings of this research also corroborated earlier studies reported by Eneji *et al*., (2011) which showed the ethanolic extracts of *M. jalapa* leaves inhibited growth of *S. typhi* and *B. cereus*. Similar results were reported by Zachariah *et al*., (2012) who identified polar methanol fraction to be most effective amongst several extracts of *M. jalapa* tested for antibacterial properties. Gujjiah (2012) however reported petroleum ether and chloroform extracts to be active against selected bacterial and fungal organisms which are less implicated in diarrhoeal related enteric diseases. Chromatography of the methanol and DCM extracts led to isolation of four compounds. Structures of the isolated compounds 1, 2 and 3 from the methanol extract and compound 4 isolated from the DCM extract were elucidated using several spectroscopic techniques.

The UV-Vis (Figure 4.2) and FTIR (Figure 4.3) spectra for compound **1** were consistent in terms of the likely existence of an aromatic ring and presence of tertiary amide type linkage functional group respectively in the structure of the compound. As presented in Figures 4.6-4.8, the ^{13}C and DEPT NMR spectra identified four methylenes, three methines and five quaternary carbons in compound **1**. The HSQC analysis reveals the proton bearing carbons and their chemical shifts (Figures 4.11 and 4.12). Protons with chemical shifts 6.55 ppm appearing as a tall singlet in ^{1}H NMR (Figures 4.4) and integrating for 2H (H1 and H2) are attached to carbons 112.39 ppm (C10) and 116.24 ppm (C7), both of which appear in the aromatic region. The tall singlet may probably be due to existence of both protons in similar chemical environment and are neither in ortho or meta positions on the aromatic ring. Carbons C-10 and C-7 were also revealed as methine carbons in DEPT 90 (Figure 4.7). The third aliphatic methine carbon with $^{C}\delta$ 58.30 ppm (C10b) is shown to have proton with $^{H}\delta$ 4.72 (H3) appearing as a triplet. The splitting pattern is consistent for a proton neighbouring 2 germinal methylene protons

with *J* couplings 7.8Hz. The methylene carbons with $^{C}\delta$ (in ppm) 28.75 (C-1), 32.69 (C-2), 38.64 (C5) and 28.82 (C-6) all appeared as negative peaks in DEPT 135 spectrum (Figure 4.8) and showed large *J* couplings in the range 10.8-20 Hz which is consistent with couplings observed for germinal protons. The protons attached to carbons presented in the HSQC spectrum (Figures 4.11 and 4.12) were in agreement with the observed COSY for these protons (Figures 4.9 and 4.10). The 2-3 bond HMBC spectrum (Figures 4.13 and 4.14) showed the long range proton carbon correlations existing within same nuclear spin. Mass spectroscopic analysis also suggested the presence of nitrogen atom in the proposed structure of compound **1**. The high resolution EI-MS elemental analysis (Figure 4.16) gave the composition $C_{12}H_{13}O_3N$ with molecular mass of 219 which was validated on ESI-MS (positive mode) which gave a molecular ion peak at m/z 220 (Figure 4.15). Indeed, the $^{C}\delta$ 175ppm is characteristic of carbonyl shift and the odd numbered mass in both mass spectral analyses is evidence for the presence of odd numbered nitrogen atoms in the structure of the compound. The elucidated structure with degree of unsaturation 7 is consistent with the carbon and proton assignments deduced from ^{1}H, ^{13}C and 2D spectral analyses as described. The IUPAC name for the compound is 8,9-dihydroxy-1,5,6,10b-tetrahydropyrrolo[2,1-a]isoquinolin-3(2H)-one. The isomer of this compound was previously isolated from *Portulaca oleracea* and reported as oleracein E by Yang *et al.*, (2009). Another common name is trolline (PubChem open chemistry database: https://pubchem.ncbi.nlm.nih.gov). There are no reports however, documenting the isolation of this compound from the aerial parts of *Mirabilis jalapa*.

The spectroscopic data of compound 2 showed characteristic features of a sugar moiety present in the structure of the compound due to observed signals appearing in the regions 62.51 - 78.55 ppm in C-13 spectrum (Figures 4.19 and 4.20). Analyses on the

proton (Figures 4.17 and 4.18) and HSQC (Figures 4.26 and 4.27) spectra revealed the anomeric proton which appeared at $^{H}\delta$ 5.38 ppm, a doublet and integrating for 1H is attached to carbon C-1′′ ($^{C}\delta$ 103.66 ppm). The protons of CH_2-OH ($^{H}\delta$ 3.72; 3.55 ppm) system of the sugar moiety appeared upfield of the anomeric proton and correlates with C-6′′ **(**$^{C}\delta$ 62.51 ppm), seen as a methylene pair in HSQC. The assignment is consistent with DEPT 135 spectrum indicating this carbon (C-6′′**)** as a methylene (negative peak). HMBC spectrum showed protons with $^{H}\delta$ 7.92 correlated with C-4′ and C-6′; $^{H}\delta$ 6.91 correlated with C-3′, C-4′ and C-6′ while $^{H}\delta$ 7.58 correlated with C-2, C-2′ and C-3′. These correlations suggest the protons belonged to same spin system hence were assigned to the B ring of the flavonoid skeleton. The *J* coupling 1.6Hz observed for proton $^{H}\delta$ 7.92 is consistent for meta coupling with neighbouring protons. This pattern was also observed in the ^{1}H splitting pattern which appeared as a doublet. The proton with $^{H}\delta$ 7.58 showed doublet of doublet (dd) splitting pattern, which was assigned ortho to proton with $^{H}\delta$ 6.91 (*J* 12.6Hz) and meta to proton with $^{H}\delta$ 7.92 (*J* 2Hz). Similar coupling was observed for protons on the A ring of the structure and were assigned in meta positions to each other with *J* coupling constant 1.6Hz, (doublet). This relationship clearly demonstrated in the COSY spectrum presented in Figures 4.23-4.25 showed $^{H}\delta$ 7.57 correlated with protons with $^{H}\delta$ 7.92 and $^{H}\delta$ 6.91 (ring B) while proton with $^{H}\delta$ 6.37 correlated with proton with $^{H}\delta$ 6.18 (A ring). Observations made on HMBC spectrum (Figures 4.28-4.29) revealed the anomeric proton correlated with C-3 ($^{C}\delta$ 135 ppm) on the C ring of the aglycone moiety of the compound which most probably is point of attachment between the sugar and the aglycone of the compound (Zhang *et al.*, 2014). The methoxy protons ($^{H}\delta$ 3.94, s) correlated with C-3′ position (B ring). The chemical shifts observed for compound **2** were consistent with flavonoid carbon skeleton reported in literature (Zhang *et al.*, 2014; Salah *et al.*, 2015). The molecular ion

peak with m/z 479 (Figure 4.30) obtained from ESI-MS (positive mode) suggested a molecular mass of 478 for compound **2**. Based on spectroscopic analyses and data in literature, the name for compound **2** was proposed to be 5,7-dihydroxy-2-(4-hydroxy-3-methoxyphenyl)-3-[3,4,5-trihydroxy-6-(hydroxymethyl)oxan-2-yl]oxychromen-4-one, commonly known as Isorhamnetin. The compound isorhamnetin isolated from various plants have been reported notably from *Oenanthe javanica* (water dropwort) (Kim *et al.*, 2013).

UV/Vis and FTIR of compound **3** showed absorbance in the region 229 nm, 282 nm which are characteristic of benzene ring and 1600 cm^{-1} and 3400 cm^{-1} peaks which are finger prints for presence of carbonyl and amino group in the structure respectively (Figures 4.31 and 4.32). The proton NMR of compound **3** (Figures 4.33 and 4.34) revealed four protons in the aromatic region. Exactly 12 signals were observed in the C-13 NMR (Figure 4.35) comprising 6 methine carbons in DEPT 90 (Figure 4.36) and 1 methylene carbon observed in DEPT 135 (Figure 4.37). HSQC analysis (Figures 4.39 and 4.40) showed the proton bearing carbons in the aromatic region were in agreement with the COSY (Figure 4.38) correlations as assigned for the protons suggesting their existence in same spin system. Proton with chemical shift $^{H}\delta$ 7.11 correlated with $^{H}\delta$ 7.36 and $^{H}\delta$7.04. Similarly, proton with $^{H}\delta$ 7.19 correlated with $^{H}\delta$ 7.04. These protons were assigned to the benzene moiety of the structure. Protons in the aliphatic region also showed COSY correlation as described in Figure 4.38. The HMBC analysis (Figures 4.41 and 4.42) of the proposed structure showed long range proton-carbon correlations. The protons with $^{H}\delta$ 3.14, 3.52, 3.84 correlated with the carbonyl carbon $^{C}\delta$ 174.55 all of which appear in the aliphatic region suggesting the carbonyl associates with the aliphatic moiety of the structure. The mass of the compound as determined by EI-MS gave a m/z molecular ion peak of 204 and this was validated using ESI-MS

(positive mode) with molecular ion peak appearing at 205 (Figure 4.43). The elucidated structure is the amino acid tryptophan with α[D] optical rotation experiments indicating this compound to be the naturally occurring L-amino acid (see appendix III). The signals observed for this compound were consistent with reported spectral data (Saeidnia *et al*., 2011; Xu *et al*., 2015).

Spectroscopic analyses of compound **4** suggest strongly the compound to be common isolates of plant extracts β-sitosterol. Characteristic ^{1}H NMR signals 5.33 and 3.49 (Figure 4.44) attached to carbon with ^{C}δ 121.72 and 71.77 respectively as seen in HSQC (Figures 4.52 and 4.53) are commonly observed signals in β-sitosterol and the closely related β-stigmasterol which is often co-isolated alongside β-sitosterol (Pateh *et al.,* 2009). β-sitosterol is difficult to obtain in pure form thus weak peaks belonging to trace β-stigmasterol contaminants may appear in spectral data (Pateh *et al*., 2009; Pierre and Moses, 2015). The molecular mass (Figure 4.56) observed was 414 with characteristic fragment peaks appearing at m/z 381 and m/z 273 (Pateh *et al.,* 2009). Compound **4** is a common isolate from many plant species including *Mirabilis jalapa* while tryptophan (compound **3**) an amino acid is reported to be isolated from the aerial parts of this plant (Singh and Mittal, 2012).

SMILES notation of elucidated structures of isolated compounds trolline (compound **1**), isorhamnetin (compound **2**) tryptophan (compound **3**) and β-sitosterol (compound **4**) was used to create input file for Admet Predictor software which was used to generate descriptors for in silico prediction of some possible physico-chemical, metabolic and toxicity related properties useful in determining drug-like properties for chemical entities intended for oral route administration. The use of 2 and 3 dimensional (2D and 3D) display of chemical structures in predicting quantitative structure-activity relationships with the help of in silico models is fast gaining popularity and

acceptability in pharmaceutical and combinatorial chemistry research. The European cooperation in the Field of Scientific and Technical research (COST) action B15 launched in 1998 sought to address issues on the possibilities offered by computer assisted modeling in predicting the administration, distribution, metabolism, elimination and toxic (ADME-tox) properties of existing and new chemical entities (Boobis *et al.*, 2002). This approach was adopted in this study as a screening method to initially predict and then screen out compounds with predicted properties that indicate the compounds to least likely possess drug-like properties.

Predictions on solubility (Figure 4.57) and permeability (Figure 4.58) properties of the compounds revealed both compounds **1** and **3** were soluble in simulated fasted state gastric fluid (FaSGF); compound **1** was also predicted to be soluble in water while compound **3** was soluble also in fasted state intestinal fluid. Predictions on compound **2** indicated the likelihood for this compound to be more soluble in simulated Fed state intestinal fluid. The differences in the simulated fluids lie in the pH of the compartmentalized body fluid system and the degree to which the compounds would be ionized. This physical property is an important determinant in the degree of permeability of these compounds across cell membranes. Predicted pKa values for the compounds (see appendix I) further explains the observed solubility properties of the compound. Compound **1** predicted to have two ionizable groups with pKa 11.69 and 8.77 most likely would acquire protons and be ionized thus increasing solubility properties. A similar tendency was observed for compound **2** since pH of the gut decreases minimally in the fed state compared to the fasted state. This situation may enhance solubility properties of the compound (Avdeef, 2001). Conversely, permeability properties decreases with increased ionization thus increased solubility of the compounds. Prediction on permeability suggested compound **1** to have high jejunal

and MDCK permeabilities probably due to the existence of this compound in the less ionized state in the intestine since pH increases slightly compared to pH of the gastric fluid. Findings on solubility and permeability of compound **1** using Caco-2 cell monolayer showed this compound to be moderately permeable across biological membranes (Li-jia *et al.,* 2014). Compound 4 was predicted to have least solubility properties however, it was predicted to have highest jejunal permeability. Compound **2** with pKa values 13.66 and 7.99 as predicted correlated with observed low jejunal permeability. The Biopharmaceutics Classification System (BCS) developed by Amidon *et al.,* (1995) observed that drugs intended for administration orally, permeability of the drug through the gastrointestinal membrane and solubility of the target drug dose around site of absorption are key parameters for drug bioavailability (Savjani *et al.,* 2012). About 40% of problems encountered in drug discovery are associated with low solubility drug candidates (Dahan and Miller, 2012). Observations on predicted properties for compound **1** suggested the compound may not be absorbed through the stomach, it could however be absorbed favourably in the jejunum.

Interactions of drugs with plasma proteins play critical role in the overall therapeutic outcome of drugs. Alterations in plasma proteins inevitably affect dose formulations, clearance time and systemic distribution of drugs (Scheife, 1989; Roberts *et al.,* 2013). Compound **4** predicted to have high permeability was shown to interact with blood proteins at greater than 95% interaction. The compound also distribute in tissues (Figure 4.59). The propensity for compound **1** to have a reduced interaction with plasma proteins as predicted could be viewed as availability of the compound to interact with target sites. Compound **2** though predicted to have low tissue distribution is however about 80% bound to plasma proteins. Predictions on warfarin and ibuprofen were consistent with reported data in literature which are highly bound to plasma proteins

(Aarons, *et al.,* 1983; Mullakandov *et al.,* 2014; www. Drugbank.ca). Correlations between predicted and laboratory data on compounds provides some degree of reliability of descriptors developed for compounds which are test sets for models used in predicting physicochemical and biopharmaceutical properties of compounds. From the forgoing, it could be construed that observed physicochemical properties of compound **1** (trolline) favours its bioavailability and an increased tendency to interact with target sites. Compound **2** which may be retained within the gastrointestinal tract may however have an increased clearance time.

Drugs taken through the oral route are generally subjected to first pass effects which involves the liver, the major organ for drug biotransformation. This overtly places the liver as a potential indicator of toxicity and other adverse reactions associated with drug metabolism. Changes in body fluid concentrations of enzyme biomarkers and other indicators of liver damage provide information (in the short and long term) on toxicity related effects of administration of a chemical substance. Qualitative assessment on the possible toxic effects of isolated compounds on the liver suggested compound **2** possess the potential to be toxic as predictions indicate elevated levels of lactate dehydrogenase (LDH) and alanine amino trnasferase (ALT) enzymes. Compound **4** was also predicted to have the likelihood to cause an elevation in LDH and gamma glutamyl transferase (GGT) enzymes. Elevated levels of LDH enzyme indicates tissue cellular injury not necessarily restricted to the liver. However, elevations in other enzyme biomarkers like GGT and ALT could be linked to damage in hepatic cells. Compound **2** was also predicted to be a potential inhibitor of CYP1A2, CYP1C9 and CYP3A4 enzymes (Tables 4.8, 4.9, 4.12). Flavonoids have been reported to have high potency and selectivity in terms of CYP450 1A enzymes (Breinholt *et al.,* 2012; Liu *et al.,* 2013). QSAR methods show model prediction on flavones (a subclass of flavonoids) to be

CYP2C9 inhibitors (Jonsdoltir *et al.,* 2012). The enzyme CYP3A4 responsible for over 50% of xenobiotic metabolim has active sites considerably larger than other CYP isoforms thus increasing the versatility of this enzyme (Sevrioukova and Poulos, 2013). According to GALAS (Globally Adjusted According to similarity) model, potential CYP3A4 inhibitors are likely to have an increase in molecular size and incorporation of hydrophobic aliphatic or aromatic residues in their structure (Didziapetris *et al.,* 2010). The features of compound **2** in terms of structure may well define its property as a potential inhibitor of CYP3A4. Compound **1** was predicted to be a substrate of CYP2C9. This enzyme is the second highly expressed after CYP3A4 and is responsible for metabolic clearance of 15-20% of all drugs undergoing phase I metabolism (van Booven *et al.,* 2010). This enzyme is involved in the metabolism of polar acidic drugs and have been shown to be competitively inhibited by NSAIDS (Sridhar *et al.,* 2012) as demonstrated by predictions on ibuprofen molecule (with 58% confidence levels).

Similar pathways for phase II glucuronidation reaction were predicted for compounds **1** and **2** involving the isoforms UGT1A3 and UGT1A8, however compound **1** was shown to be more of a substrate for several isoforms of UGT enzymes (Table 4.13). In humans about 40-70% of drugs used clinically undergo glucuronidation (Wells *et al.,* 2004). The rapidity with which this reaction occurs by way of exposure to several CYP isoforms may compromise bioavailability of the compounds, drugs or their metabolites. Newly formed β-D-glucuronides exhibit increased water solubility and are easily eliminated in the urine or bile (Mckenzie *et al.,* 2008; Rowland, 2013). Predicted outcomes of metabolism of the compounds clearly indicated compound **4** a substrate of CYP3A4 but not glucuronidated thus a delayed clearance may be experienced as earlier suggested. It is also assumed compound **1** may easily be removed from circulation compared to compound **2**.

Compound **1** selected for antibacterial studies was based on summation of all predicted variables on ADME properties presented in Table 4.14. Compounds having the combined associated risk codes on molecular weight (mw), permeability (peff), solubility (sw), and lipophililcity (ow) were screened out while the amino acid tryptophan was ruled out for bioassay studies. Modeling ADME-Tox properties provides a gateway for high throughput screening of lead compounds which previously, were selected on the basis of potency (only). Assessing information on likely pharmacokinetic outcome of a lead compound fine tunes the chances of emergence of lead compounds that may scale through several stages of clinical trials. Compound **1** demonstrated antibacterial effects against *B. cereus, S. typhi E. coli* and *S. dysenteriae*. The MIC of 57 µM and MBC of 114 µM against *S. dysenteriae* showed compound **1** to be most effective against this organism. Compounds containing the pyrrolo [2, 1-a] isoquinoline skeleton as seen in the structure of compound **1** have been reported to have antibacterial properties. Compound **1** previously isolated from *Trollius chinensis* (Wang *et al.,* 2004) was reported to exhibit antibacterial activity against *Staphylococcus aureus, Staphylococcus pneumonia* and *Klebsiella pneumonia*. Earlier studies by Eneji *et al.,* (2011) suggested isoquinolines as possible active constituents of ethanol extracts tested to have antibacterial effects on *S. typhi* and *B. cereus*. The observed antibacterial activity of compound **1** may substantiate claims attributing *Mirabilis jalapa* to having dysentery and diarrhoeal healing properties (Shaik *et al.,* 2012; Zachariah *et al.,* 2012). This property may not be limited to presence of compound **1** in the selected extract. The observed increased activity of the compound when compared with tested crude extract concentrations on same organisms supports the argument that this compound is a significant bioactive constituent of the extract with respect to antibacterial properties of *Mirabilis jalapa*.

CHAPTER SIX

6.0 CONCLUSION AND RECOMMENDATIONS

6.1 Conclusion

The trado-medicinal properties of extractives of *Mirabilis jalapa* are known to many cultures across the world for the treatment of various ailments. In silico method used to evaluate pharmacokinetics and metabolism of the compounds selected for antibacterial experiments were based on solubility, permeability and non-carcinogenic related properties predicted for the compounds isolated from the plant. The selected compound trolline was demonstrated to be antibacterial activity against *B.cereus*, *E. coli*, *S. dysenteriae* and *S. typhi* (*in vitro*) at concentrations between 0.11-0.23 mM.

The findings of this research leans support strongly, to suggest the presence of bioactive compounds in the plant *Mirabilis jalapa* with potential antibacterial properties.

6.2 Recommendations

Based on the findings of this research, the following recommendations are made:

1. Cultivation of medicinal plants to preserve biodiversity and encourage availability of source material for isolation and characterization of molecules with novel carbon scaffolds.

2. Conduct experiments to assess mechanism of growth inhibition using bioactive compounds identified as well as possible toxicity effects on eukaryotic cell lines.

3. 3D QSAR and ligand-protein docking experiments to understand the relationship of the bioactive compounds with binding and/or receptor sites.

REFERENCES

Aarons, L., Grennan, D. M., Rajapakse, C., Brinkley, J., Siddiqui, M., Taylor, L., and Higham, C. (1983). Anti-inflammatory (ibuprofen) drug therapy in rheumatoid arthritis-rate of response and lack of time dependency of plasma pharmacokinetics. *British Journal of Clinical Pharmacology*, *15*(3), 387-388.

Admet predictor manual, (2015). Simulations plus Inc, Lancaster, California. Web site www.simulations-plus.com. Pages 69-79.

Ahmad, A., Husain, A., Mujeeb, M., Khan, S. A., Najmi, A. K., Siddique, N. A., Damanhouri, Z.A. and Anwar, F. (2013). A review on therapeutic potential of Nigella sativa: A miracle herb. *Asian Pacific Journal of Tropical Biomedicine*, *3*(5), 337-352.

Amidon, G.L., Lennernas, H., Shah, V.P., Crison, J.R. (1995). A theoretical basis for a biopharmaceutic drug classification: the correlation of in vitro drug product dissolution and in vivo bioavailability. *Journal of Pharmaceutical Research,12*, 413–420.

Avdeef, A. (2001). Physicochemical profiling (solubility, permeability and charge state). *Current Topics in Medicinal Chemistry*, *1*(4), 277-351.

Bent, S. (2008). Herbal medicine in the United States. Review of efficacy, safety and regulation. *Journal of General Internal Medicine*, *23*(6), 854-859.

Berry, L. M., Li, C. and Zhao, Z. (2011). Species differences in distribution and prediction of human V ss from preclinical data. *Drug Metabolism and Disposition, 39*(11), 2103-2116.

Bindseil, K. U., Jakupovic, J., Wolf, D., Lavayre, J., Leboul, J., and van der Pyl, D. (2001). Pure compound libraries; a new perspective for natural product based drug discovery. *Drug Discovery Today, 6*(16), 840-847.

Black, R. E., Morris, S. S., & Bryce, J. (2003). Where and why are 10 million children dying every year? *The Lancet*, *361*(9376), 2226-2234.

Boldi, A. M. (2004). Libraries from natural product-like scaffolds. *Current Opinion in Chemical Biology*, *8*(3), 281-286.

Boobis, A., Gundert-Remy, U., Kremers, P., Macheras, P., and Pelkonen, O. (2002). In silico prediction of ADME and pharmacokinetics: Report of an expert meeting organised by COST B15. *European Journal of Pharmaceutical Sciences*, *17*(4):183-193.

Borrelli, F., Ascione, V., Capasso, R., Izzo, A.A., Fattorusso, E. and Taglialatela, S.O. (2006). Spasmolytic effects of nonprenylated rotenoid constituents of *Boerhaavia diffusa* roots. *Journal of Natural Prod*ucts, *69*, 903-906

Boschi-Pinto, C., Velebit, L. and Shibuya, K. (2008). Estimating child mortality due to diarrhoea in developing countries. *Bulletin of the World Health Organization*, *86*(9), 710-717.

Brandon, E. F. A., Raap, C. D., Meijerman, I., Beijnen, J. H. and Schellens, J. H. M. (2003). An update on in vitro test methods in human hepatic drug biotransformation research: Pros and cons. *Toxicology and Applied Pharmacology, 189*(3), 233-246.

Breinholt, V.M., Offord, E.A., Brouwer, C., Nielsen, S.E., Brosen, K. and Friedberg, T. (2002). In vitro investigation of cytochrome P450-mediated metabolism of dietary flavonoids. *Journal of Food and Chemical Toxicology, 40*(5), 609–616.

Brennan, M. J. (2012). The clinical implications of cytochrome P450 interactions with opioids and strategies for pain management. *Journal of Pain and Symptom Management, 44*(6 SUPPL.), S15-S22.

Brunner, M. and Langer, O. (2006). Microdialysis versus other techniques for the clinical assessment of in-vivo tissue drug distribution. *The AAPS Journal*, 8(2), E2663-E271.

Butina, D., Segall, M. D., & Frankcombe, K. (2002). Predicting ADME properties in silico: methods and models. *Drug Discovery Today*, *7*(11), S83-S88.

Cammue, B. P., De Bolle, M. F., Terras, F. R., Proost, P., Van Damme, J., Rees, S. B., Vanderleyden, J. and Broekaert, W. F. (1992) Isolation and characterization of a novel class of plant antimicrobial peptides from *Mirabilis jalapa* L. seeds. *Journal of Biological Chemistry, 267*(4), 2228-2233.

Comerford, S. C. (1996). Medicinal plants of two Mayan healers from San Andŕes, Peten, Guatemala. *Economic Botany.* 50:327–336.

Crivori, P., Cruciani, G., Carrupt, P. A., and Testa, B. (2000). Predicting blood brain barrier permeation rom the three-dimensional molecular structure. *Journal of Medicinal Chemistry,* 43, 2204-2216.

Dahan, A., and Miller, J. M. (2012). The solubility–permeability interplay and its implications in formulation design and development for poorly soluble drugs. *The AAPS journal*, *14*(2), 244-251.

Didziapetris, R., Dapkunas, J., Sazonovas, A., and Japertas, P. (2010). Trainable structure–activity relationship model for virtual screening of CYP3A4 inhibition. *Journal of Computer-aided Molecular Design*, *24*(11), 891-906.

Eikel, D., Vavrek, M., Smith, S., Bason, C., Yeh, S., Korfmacher, W. A. and Henion, J. D. (2011). Liquid extraction surface analysis mass spectrometry (LESA-MS) as a novel profiling tool for drug distribution and metabolism analysis: The terfenadine example. *Rapid Communications in Mass Spectrometry, 25*(23), 3587-3596.

EMEA. (2005). Guidelines on quality of herbal medicinal products/ traditional medicinal products. EMEA/CVMP/81400 Review. European Agency for the evaluation of medicinal products (EMEA), London.

Encarnacion Dimayuga, R., Virgen, M. and Ochoa, N. (1998). Antimicrobial activity of medicinal plants from Baja California Sur (Mexico). *Pharmaceutical Biology*, *36*(1), 33-43.

Eneji, S. M., Inuwa, H. M., Ibrahim, S., Ibrahim, A. B. and Abdulfattah, A. (2011). In vitro assessment of bioactive components of *Mirabilis jalapa* ethanolic extract on clinical isolates of *Salmonella typhi* and *Bacillus cereus*. *African Journal of Biotechnology, 10*(71), 16006-16011.

EUCAST Discussion Document (2003). Determination of minimum inhi bitory concentrations (MICs) of antibacterial agents by broth dilution. *Clinical Microbiology and Infection*, 9(8), 1-7.

European Committee on Antimicrobial Susceptibility Testing. (2000). Terminology relating to methods for the determination of susceptibility of bacteria to antimicrobial agents. EUCAST Definitive Document E. Def 1.2. *Clinical Microbiology and Infection*, *6*, 503-508.

Guay, J., Bateman, K., Gordon, R., Mancini, J. and Riendeau, D. (2004). Carrageenan-induced paw edema in rat elicits a predominant prostaglandin E2 (PGE2) response in the central nervous system associated with the induction of microsomal PGE2 synthase-1. *Journal of Biological Chemistry*, *279*(23), 24866-24872.

Gujjaiah, D. S. (2012). Antibacterial and antifungal activities of *Mirabilis jalapa* of Indian origin. *Research and Reviews: A Journal of Biotechnology*, *2*(2).

Gupta, R. C. and Atul, B. V. (2000). Drug metabolism studies in animal models. *Indian Journal of Pharmacology*, 32, 562-566.

Harvey, A. L. (2000). Strategies for discovering drugs from previously unexplored natural products. *Drug discovery today*, *5*(7), 294-300.

Harvey, A. L. (2008). Natural products in drug discovery. *Drug Discovery Today, 13*(19), 894-901.

Hodges, K., and Gill, R. (2010). Infectious diarrhea: cellular and molecular mechanisms. *Gut Microbes*, *1*(1), 4-21.

Holdsworth, D. K. (1992). A preliminary study of medicinal plants of Easter Island, South Pacific. *International Journal of Pharmacognosy*, *30*(1), 27-32.

Holstein, A., Beil, W. and Kovacs, P. (2012). CYP2C metabolism of oral antidiabetic drugs - impact on pharmacokinetics, drug interactions and pharmacogenetic aspects. *Expert Opinion on Drug Metabolism and Toxicology, 8*(12), 1549-1563.

Ikawatip, Z. (2006). Cytotoxicity against tumor cell lines of a ribosome inactivating protein (RIP)-like protein isolated from leaves of *Mirabilis jalapa* L. *Malaysian Journal of Pharmaceutical Sciences*, *4*(1), 31-41.

Jacob, S. and Ahmed, A. E. (2003). Effect of route of administration on the disposition of acrylonitrile: Quantitative whole-body autoradiographic study in rats. *Pharmacological Research*, *48*(5):479-488.

Jónsdóttir, S. Ó., Ringsted, T., Nikolov, N. G., Dybdahl, M., Wedebye, E. B., and Niemelä, J. R. (2012). Identification of cytochrome P450 2D6 and 2C9 substrates and inhibitors by QSAR analysis. *Bioorganic and Medicinal Chemistry*, *20*(6), 2042-2053.

Kadiyala, I. and Tan, E. (2013). Formulation approaches in mitigating toxicity of orally administrated drugs. *Pharmaceutical Development and Technology*, *18*(2), 305-312.

Kapetanovic, I. M. (2008). Computer-aided drug discovery and development (CADDD): in silico-chemico-biological approach. *Chemico-Biological Interactions*, *171*(2), 165-176.

Kim, I. S., Kim, S. Y. and Yoo, H. H. (2012). Effects of an aqueous-ethanolic extract of ginger on cytochrome P450 enzyme-mediated drug metabolism. *Pharmazie*, *67*(12), 1007-1009.

Kim, I., Booth-Genthe, C. and Ambudkar, S. V. (2008). Relationship between drugs and functional activity of various mammalian P-glycoproteins (ABCB1). *Mini-Reviews in Medicinal Chemistry*, *8*(3), 193-200.

Kim, T. H., Ku, S. K., and Bae, J. S. (2013). Anti-inflammatory activities of isorhamnetin-3-O-galactoside against HMGB1-induced inflammatory responses in both HUVECs and CLP-induced septic mice. *Journal of Cellular Biochemistry*, *114*(2), 336-345.

Kowalska, J., Pszczoła, K., Wilimowska-Pelc, A., Lorenc-Kubis, I., Zuziak, E., Ługowski, M., Łęgowska, A., Kwiatkowska, A., Śleszyńska, M., Lesner, A., Walewska, A., Zabłotna, E., Rolka, K. and Wilusz, T. (2007). Trypsin inhibitors from the garden four o'clock (*Mirabilis jalapa*) and spinach (*Spinacia oleracea*) seeds: isolation, characterization and chemical synthesis. *Phytochemistry*, *68*(11), 1487–1496.

Krajcsi, P., Jani, M., Tóth, B., Erdo, F., Kis, E., Beéry, E. and Sziráki, I. (2012). Efflux transporters in the bloodbrain interfaces in vitro and in vivo methods and correlations. *Expert Opinion on Drug Metabolism and Toxicology*, *8*(4), 419-431.

Kunle, O. F., Egharevba, H. O. and Ahmadu, P. O. (2012). Standardization of herbal medicines - a review. *International Journal of Biodiversity and Conservation, 4*(3), 101-112.

Lahlou, M. (2013). The success of natural products in drug discovery. *Pharmacology and Pharmacy, 4*(3A), 17.

Leucuta, S. T. and Vlase, L. (2006). Pharmacokinetics and metabolic drug interactions. *Current Clinical Pharmacology.* 1:5-20.

Li-Jia, L. I. U., Xiu-Wen, W. U., Ru-Feng, W. A. N. G., Yu-Shuai, P. E. N. G., Xin, Y. A. N. G. and Jun-Xiu, L. I. U. (2014). Absorption properties and mechanism of trolline and veratric acid and their implication to an evaluation of the effective components of the flowers of Trollius chinensis. *Chinese Journal of Natural Medicines, 12*(9), 700-704.

Lim, T. K. (2014). *Mirabilis jalapa*. In: *Edible Medicinal and Non Medicinal Plants* (pp. 497-513). Springer Netherlands.

Lin, J. H. (1995). Species similarities and differences in pharmacokinetics. *Drug Metabolism and Disposition, 23*(10), 1008-1021.

Lin, J. H. and Lu, A. Y. H. (1997). Role of pharmacokinetics and metabolism in drug discovery and development. *Pharmacological Reviews, 49*(4), 403-449.

Lin, J. H., Chiba, M., Balani, S. K., Chen, I., Kwei, G. Y., Vastag, K. J. and Nishime, J. A. (1996). Species differences in the pharmacokinetics and metabolism of indinavir, a potent human immunodeficiency virus protease inhibitor. *Drug Metabolism and Disposition, 24*(10), 1111-1120.

Liu, J., Sridhar, J. and Foroozesh, M. (2013). Cytochrome P450 family 1 inhibitors and structure-activity relationships. *Molecules, 18*(12), 14470-14495.

Mackenzie, P. I., Anne, R., Joanna, T., Bo R. J., John, O. M. and Robyn, M. (2008). "Identification of UDP glycosyl transferase 3A1 as a UDP N-acetylglucosaminyl transferase. *Journal of Biological Chemistry,* 283(52), 36205-36210.

Meera, R., Devi, P., Muthumani, P., Kameswari, B., and Eswarapriya, B. (2010). In vitro antimicrobial activity of various extracts of *Mirabilis jalapa* leaves. *International Journal of Chemical Sciences, 8*(1), 559-564.

Mehrotra, N., Lal, J., Puri, S. K., Madhusudanan, K. P., and Gupta, R. C. (2007). In vitro and in vivo pharmacokinetic studies of bulaquine (analogue of primaquine), a novel antirelapse antimalarial, in rat, rabbit and monkey—highlighting species similarities and differences. *Biopharmaceutics and Drug Disposition, 28*(5), 209-227.

Moriguchi, I., Hirono, S., Liu, Q., Nakagome, I.and Matsushita, Y. (1992). Simple method of calculating octanol/water partition coefficient. *Chemical and Pharmaceutical Bulletin, 40*(1), 127-130.

Mullokandov, E., Ahn, J., Szalkiewicz, A., and Babayeva, M. (2014). Protein binding drug-drug interaction between warfarin and tizoxanide in human plasma. *Austin Journal of Pharmacology and Therapeutics*, *2*(7), 3.

Muthumani, M., Devi, P., Meera, R., Kameswari, B., and Eswarapriya, B. (2010). In vitro antimicrobial activity of various extracts of *Mirabilis jalapa* leaves. *Internet Journal of Microbiology*, *7*(2):120-124.

Nath, L. R, Manjunath, K. P., Savadi, R. V. and Akki, K. S. (2010). Anti-inflammatory activity of *Mirabilis jalapa* linn. Leaves. *Journal of Basic Clinical Pharmacy. 1*(2): 93-96.

National Center for Biotechnology Information. PubChem Compound Database; CID=31703, https://pubchem.ncbi.nlm.nih.gov/compound/31703 (accessed Jan. 18, 2016).

Navaneethan, U. and Giannella, R. A. (2008). Mechanisms of infectious diarrhea. *Nature clinical practice Gastroenterology and Hepatology*, *5*(11), 637-647.

Newman, D. J. and Cragg, G. M. (2016). Natural products as sources of new drugs from 1981 to 2014. *Journal of Natural Products*, 79, 629−661.

Okeke, I. N., Aboderin, O. A., Byarugaba, D. K., Ojo, K. K., and Opintan, J. A. (2007). Growing problem of multidrug-resistant enteric pathogens in Africa. *Emerging Infectious* Diseases, *13*(11), 1640-1646.

Oladunmoye, M. K. (2007). Comparative evaluation of antimicrobial activities of leaf extract of *Mirabilis jalapa* and microbial toxins on some pathogenic bacteria. *Trends Medical Research, 2*(2), 108-112.

Oladunmoye M (2012). Antioxidant, free radical scavenging capacity and antimicrobial activities of *Mirabilis jalapa*. *Journal of Medicinal Plant Research*, *6*(15):2909–2913.

Pateh, U. U., Haruna, A. K., Garba, M., Iliya, I., Sule, I. M., Abubakar, M. S. and Ambi, A. A. (2009). Isolation of stigmasterol, β-sitosterol and 2-hydroxyhexadecanoic acid methyl ester from the rhizomes of Stylochiton lancifolius Pyer and Kotchy (Araceae). *Nigerian Journal of Pharmaceutical Sciences*, *7*(1), 19-25.

Pedersen, H. A., Stine, K. S, and Carsten, C. (2010). "Cinnamoylphenethylamine 1H-NMR chemical shifts: a concise reference for ubiquitous compounds." *Natural Product Communications 5*(8), 1259-1262.

Peng, S., Zhou, Q., Cai, Z., and Zhang, Z. (2009). Phytoremediation of petroleum contaminated soils by *Mirabilis Jalapa* L. in a greenhouse plot experiment. *Journal of Hazardous Materials*, *168*(2), 1490-1496.

Petri, W. A., Miller, M., Binder, H. J., Levine, M. M., Dillingham, R., and Guerrant, R. L. (2008). Enteric infections, diarrhea, and their impact on function and development. *The Journal of Clinical Investigation*, *118*(4), 1277-1290.

Pierre, L. L. and Moses, M. N. (2015). Isolation and Characterisation of Stigmasterol and B-Sitosterol from Odontonema Strictum (Acanthaceae). *Journal of Innovations in Pharmaceuticals and Biological Sciences*, *2*(1), 88-96.

Qiao, X., Ye, M., Xiang, C., Wang, Q., Liu, C., Miao, W., and Guo, D. (2012). Analytical strategy to reveal the in vivo process of multi-component herbal medicine: a pharmacokinetic study of licorice using liquid chromatography coupled with triple quadrupole mass spectrometry. *Journal of Chromatography A*, *1258*, 84-93.

Roberts, J. A., Pea, F., and Lipman, J. (2013). The clinical relevance of plasma protein binding changes. *Clinical Pharmacokinetics*, *52*(1), 1-8.

Rowland, A., Miners, J. O., and Mackenzie, P. I. (2013). The UDP-glucuronosyl transferases: their role in drug metabolism and detoxification. *The International Journal of Biochemistry and Cell Biology*, *45*(6), 1121-1132.

Rozina, R. (2016). Pharmacological and biological activities of *Mirabilis jalapa* L. *International Journal of Pharmacological Research*, *6*(5), 160-168.

Saeidnia, S., Gohari, A. R., Malmir, M., Moradi-Afrapoli, F. and Ajani, Y. (2011). Tryptophan and sterols from Salvia limbata. *Journal of Medicinal Plants, 1*(37), 41-47.

Salah, N. B., Casabianca, H., Jannet, H. B., Chenavas, S., Sanglar, C., Fildier, A. and Bouzouita, N. (2015). Phytochemical and biological investigation of two Diplotaxis species growing in Tunisia: *D. virgata* and *D. erucoides. Molecules*, *20*(10), 18128-18143.

Savjani, K. T., Gajjar, A. K., and Savjani, J. K. (2012). Drug solubility: importance and enhancement techniques. *ISRN Pharmaceutics*, *2012*.

Scheife, R. T. (1989). Protein binding: what does it mean? *Annals of Pharmacotherapy*, *23*(7-8), S27-S31.

Sevrioukova, I. F. and Poulos, T. L. (2013). Understanding the mechanism of cytochrome P450 3A4: recent advances and remaining problems. *Dalton Transactions*, *42*(9), 3116-3126.

Shaik, S., Rajendra, Y. and Jaya Chandra Reddy, P. (2012). Phytochemical and pharmaclogical studies of *Mirabilis jalapa* Linn. *International Journal of Pharmacy and Technology*, *4*(2), 2075-2084.

Singh, M. and Mittal, S. K. (2012). Mirabilis Jalapa - a review. *International Journal of Pharmaceutical, Medical and Applied Sciences, 1*(3):22-43.

Singh, M., Kumar, V., Singh, I., Gauttam, V. and Kalia, A. N. (2010). Anti-inflammatory activity of aqueous extract of *Mirabilis jalapa* Linn. leaves. *Pharmacognosy Research*, *2*(6), 364.

Solon, E. G. (2012). Use of radioactive compounds and autoradiography to determine drug tissue distribution. *Chemical Research in Toxicology*, *25*(3), 543-555.

Sridhar, J., Liu, J., Foroozesh, M., and Klein Stevens, C. L. (2012). Inhibition of cytochrome p450 enzymes by quinones and anthraquinones. *Chemical Research in Toxicology*, *25*(2), 357-365.

Tao, D., Zeng, Y., Cao, H., and Guan, Y. (2010). Traditional chinese medicine composition for treating swine influenza, preparation method and use thereof. *U.S. Patent Application 13/377,862*.

Van Booven, D., Marsh, S., McLeod, H., Carrillo, M. W., Sangkuhl, K., Klein, T. E., & Altman, R. B. (2010). Cytochrome P450 2C9-CYP2C9. *Pharmacogenetics and Genomics*, *20*(4), 277.

van de Kerkhof, E. G., Ungell, A. L., Sjöberg, A. K., de Jager, M. H., Hilgendorf, C., de Graaf, I. A. and Groothuis, G. M. (2006). Innovative methods to study human intestinal drug metabolism in vitro: precision-cut slices compared with ussing chamber preparations. *Drug Metabolism and Disposition. 34*(11), 1893-902.

van De Waterbeemd, H. and Gifford, E. (2003). ADMET in silico modelling: towards prediction paradise? *Nature Reviews Drug Discovery*, *2*(3), 192-204.

Wang, R. F., Yang, X. W., Ma, C. M., Cai, S. Q., Li, J. N., and Shoyama, Y. (2004). A bioactive alkaloid from the flowers of *Trollius chinensis*. *Heterocycles*, *63*(6), 1443-1448.

Wang, Y.F, Chen, J.J., Yang, Y., Zheng, Y.T., Tang, S.Z. and Luo, S.D. (2002). New rotenoids from roots of *Mirabilis jalapa. Helvetica Chimica Acta*, *85*(8):2342–2348.

Wells, P. G., Mackenzie, P. I., Chowdhury, J. R., Guillemette, C., Gregory, P. A., Ishii, Y. and Ritter, J. K. (2004). Glucuronidation and the UDP-glucuronosyl transferases in health and disease. *Drug Metabolism and Disposition*, *32*(3), 281-290.

World Health Organisation, (2002). WHO traditional medicine strategy 2002-2005.

www.drugbank.ca. Accessed October 26, 2015.

Xu, J. J., Qing, C., Lv, Y. P., Liu, Y. M., Liu, Y., and Chen, Y. G. (2010). Cytotoxic rotenoids from *Mirabilis jalapa*. *Chemistry of Natural Compounds*, *46*(5), 792-794.

Xu, X. B., Tang, F., Guo, X. F., Wang, J., Yao, X., Sun, J., and Xun, H. (2015). Isolation, Identification and Determination of Six Nucleosides and Two Amino Acids from Bamboo Shoots of Gramineae Phyllostachys prominens (WY Xiong). *Tropical Journal of Pharmaceutical Research*, *14*(12), 2239-2246.

Yamashita, F. and Hashida, M. (2004). In silico approaches for predicting ADME properties of drugs. *Drug Metabolism and Pharmacokinetics*, *19*(5), 327-338.

Yang, S.W., Ubillas, R.., McAlpine, J., Stafford A, Ecker, DM, Talbot, M.K. and Rogers, B. (2001) Three new phenolic compounds from a manipulated plant cell culture M. jalapa. *Journal of Natural Products, 64*(3), 313–317.

Yang, Z., Liu, C., Xiang, L., and Zheng, Y. (2009). Phenolic alkaloids as a new class of antioxidants in Portulaca oleracea. *Phytotherapy Research*, *23*(7), 1032-1035.

Yi-Fen, W., Ji-Jun, C., Yan, Y., Yong-Tang, Z., Shao-Zong, T., and Shi-De, L. (2002). New rotenoids from roots of *Mirabilis jalapa*. *Helvetica Chimica Acta*, *85*(8), 2342-2348.

Zachariah, S. M., Viswanad, V., Aleykutty, N. A., Jaykar, B., and Halima, O. A. (2012). Free radical scavenging and antibacterial activity of *Mirabilis jalapa* Linn using in vitro models. *Asian Journal of Pharmaceutical and Clinical Research*, 5(3), 115-120.

Zhang, T., Zhu, Y. and Gunasatne, C. (2003). Simultaneous determination of metabolites from multiple Cytochrome P450 probe substrates by Gradient liquid chromatography with UV detection. *Current Separations, 20*(3), 87-91.

Zhang, Y., Wang, D., Yang, L., Zhou, D., and Zhang, J. (2014). Purification and characterization of flavonoids from the leaves of *Zanthoxylum bungeanum* and correlation between their structure and antioxidant activity. *PloS one*, *9*(8), e105725.

Zhou, J., Chan, L., and Zhou, S. (2012b). Trigonelline: a plant alkaloid with therapeutic potential for diabetes and central nervous system disease. *Current Medicinal Chemistry*, *19*(21), 3523-3531.

Zhou, J., Zhou, S. and Zeng, S. (2013), Experimental diabetes treated with trigonelline: effect on β cell and pancreatic oxidative parameters. *Fundamental and Clinical Pharmacology,* 27, 279–287. doi: 10.1111/j.1472.

.

APPENDICES

Appendix I: Predicted pKa Values and Lipophilicity of Isolated Compounds

Compound	pKa	MlogP	SlogP
Cimetidine	13.23; 11.16; 10.75	-0.4	0.57
Warfarin	5.06	2.33	3.28
Compound 1	11.69; 8.77	1.56	0.53
Compound 2	13.66; 13.14; 12.73; 12.20; 9.76; 9.05; 7.90	-1.86	-0.23
Compound 3	13.97; 2.56	-2.15	-1.4
Compound 4	13.41	6.79	9.49
Ibuprofan	4.54	2.82	3.65

pKa = (ionization constants of mainly acidic nature; Simulations Plus model)
MlogP = (Moriguchi model of octanol-water partition coefficient, log P (Moriguchi et al; 1992))
SlogP = (octanol-water partition coefficient, log P; Simulations Plus model)

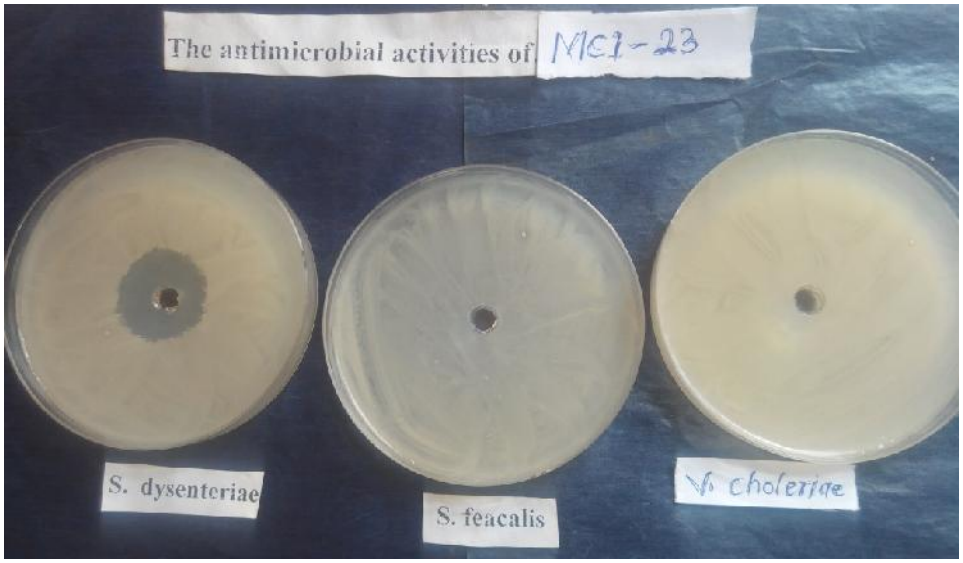

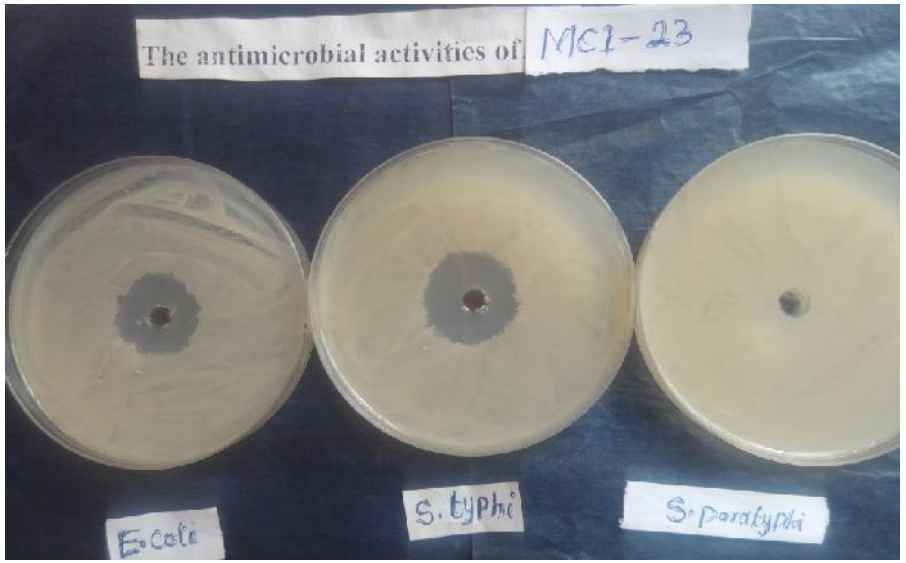

Appendix II: Culture Plates Showing Zones of Inhibition for Compound 2(trolline) Against Susceptible Bacterial Cells

[Data Information]
Creation Date 5/6/2015 11:18 AM

[Measurement Information]
Instrument Name POLARIMETER
Model Name P-2000
Serial No. A060061232
Polarizer Glan-Taylor Prism
Faraday Cell Quartz

Accessory RSC-200
Accessory S/N B044761260

Light Source WI
Monitor wavelength 589 nm
D.I.T. 5 sec
No. of cycle 1
Cycle interval 0 sec
Temp. Monitor Cell
Temp. Corr. Factor None
Aperture(S) 8.0mm
Aperture(L) Auto
Mode Optical Rotation
Factor 1

No.	Sample Name	Measurement Date	PMT Voltage[V]	Temperature[C]	Optical Rotation Monitor	Optical Rotation[deg]	Comment
1	Blank	5/6/2015 11:16 AM	223	26.95	-0.2854		
2	BUT-6927	5/6/2015 11:17 AM	222	27.10	-0.2973	-0.0119	MASUD/Prof.Iqbal/10mm/1ml
3	BUT-6927	5/6/2015 11:17 AM	226	27.23	-0.2945	-0.0091	MASUD/Prof.Iqbal/10mm/1ml
4	BUT-6927	5/6/2015 11:17 AM	224	27.31	-0.2918	-0.0064	MASUD/Prof.Iqbal/10mm/1ml
5	BUT-6927	5/6/2015 11:18 AM	228	27.37	-0.2910	-0.0056	MASUD/Prof.Iqbal/10mm/1ml
6	BUT-6927	5/6/2015 11:18 AM	226	27.44	-0.2913	-0.0059	MASUD/Prof.Iqbal/10mm/1ml
7	BUT-6927	5/6/2015 11:18 AM	228	27.49	-0.2937	-0.0083	MASUD/Prof.Iqbal/10mm/1ml

Appendix III: α[D] Optical Rotation Results for Compound 3